9950-762

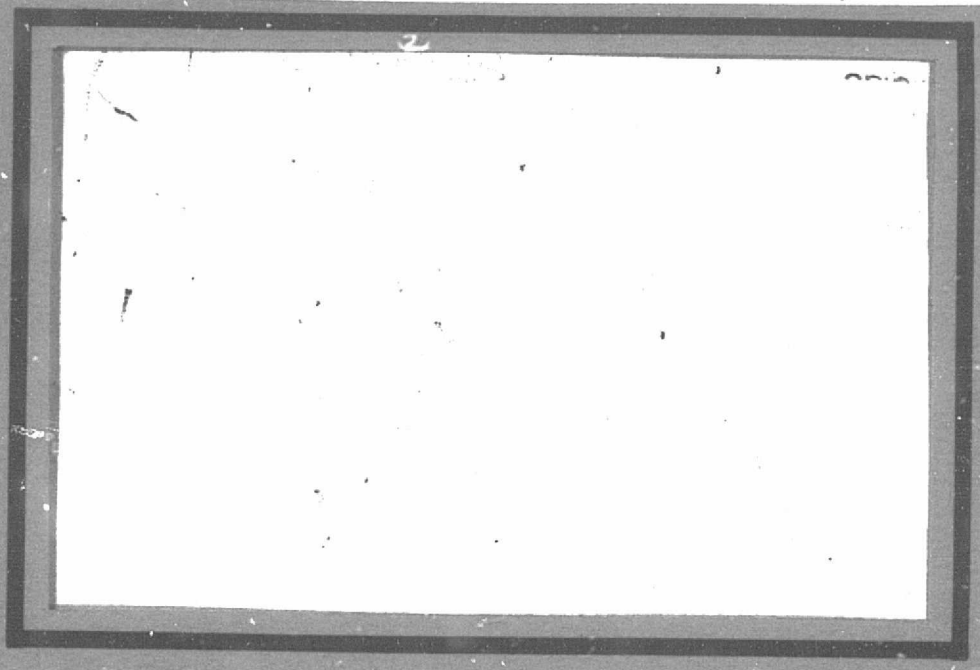

Virginia Polytechnic Institute and State University

Electrical Engineering

BLACKSBURG, VIRGINIA 24061

MILLIMETER WAVE SATELLITE

COMMUNICATION STUDIES

Results of the 1981 Propagation Modeling Effort

Report Number SATCOM-82-4

W. L. Stutzman
A. Tsolakis
W. K. Dishman
December 1982
JPL Contract 955954

Satellite Communications Group
Electrical Engineering Department
Virginia Polytechnic Institute and State University
Blacksburg, Virginia 24061

This work was performed for the Jet Propulsion Laboratory, California Institute of Technology, sponsored by the National Aeronautics and Space Administration under Contract NAS7-100.

1. Report No.	2. Government Accession No.	3. Recipient's Catalog No.
4. Title and Subtitle MILLIMETER WAVE SATELLITE COMMUNICATION STUDIES - Results of the 1981 Propagation Modeling Effort		5. Report Date December 1982 6. Performing Organization Code SATCOM-82-4
7. Author(s) W. L. Stutzman, A. Tsolakis, W. K. Dishman		8. Performing Organization Report No.
9. Performing Organization Name and Address VPI&SU Department of Electrical Engineering Blacksburg, VA 24061		10. Work Unit No. 11. Contract or Grant No. JPL Contract 955954 13. Type of Report and Period Covered
12. Sponsoring Agency Name and Address Jet Propulsion Laboratory Attn: Dr. Ernest Smith Mail Stop 161-228 4800 Oak Grove Dr. Pasadena, CA 91109		14. Sponsoring Agency Code

15. Supplementary Notes

16. Abstract

This report is a supplement to the 1981 year final report under the same project. It presents the details of the theoretical modeling associated with rain effects on millimeter wave propagation. Three areas of work are discussed. A simple model for prediction of rain attenuation is developed and evaluated. A method for computing scattering from single rain drops is presented. A complete multiple scattering model is described which permits accurate calculation of the effects on dual polarized signals passing through rain.

17. Key Words (Selected by Author(s))	18. Distribution Statement
Millimeter waves, Depolarization, Attenuation, Rain, Multiple scattering.	Unlimited

19. Security Classif. (of this report)	20. Security Classif. (of this page)	21. No. of Pages	22. Price*
U	U	160	

*For sale by the National Technical Information Service, Springfield, Virginia 22151.

TABLE OF CONTENTS

Chapter 1

INTRODUCTION

This report augments the annual report for 1981 that describes the work performed by the Virginia Tech Satellite Communications Group under Jet Propulsion Laboratory Contract No. 955954. This report details the modeling phase of the overall effort. A separate report was necessary because of the already excessive length of the annual report.

This year's effort in modeling consisted of five tasks. These tasks and a brief report on the progress made in each follow.

1. Simple Attenuation Model. The development of the simple attenuation model is complete. It consists of an exponentially shaped spatial rain rate distribution. Many comparisons to measured data and to other models have been made. See Chapter 3 for a more complete discussion.

2. Attenuation Exceedance Testing. This effort is the prediction of rain attenuation exceedance statistics. The procedure is to couple a rain rate exceedance model (such as that recommended by CCIR) with the simple attenuation model which

predicts slant path attenuation for a given point rain rate. Results of this technique are also found in Chapter 3.

3. Isolation versus Attenuation. After the spatial rain rate distribution is established it can be used together with a complete depolarization computational model to calculate isolation (as a function of attenuation). This particular task is incomplete because of the extensive effort required on the development of the spatial rain rate distribution (Task A) and the development of the multiple scattering model (Task E), both of which must precede this task.

4. Single Particle Scattering Computations. In order to make complete depolarization calculations for rain media the single rain drop scattering coefficients must be evaluated at the frequency of interest. This task was completed by developing and testing a computer program for calculation of oblate spheroidal rain drops. It uses the Fredholm integral equation method. Unfortunately, the calculations are very complicated and involve considerable computer time. Complete details are presented in Chapter 4.

5. Multiple Scattering Model. The derivation and initial testing of a general rain depolarizacion model which includes multiple scattering effects has been completed under this task. Chapter 5 discusses this effort in detail. In Chapter 2 the multiple scattering model is placed into perspective relative to other computing capabilities.

Chapter 2

MODELING CAPABILITIES

In the past several years three levels of rain propagation computing capabilities have been developed. It may be helpful to summarize this capability before proceeding into the details of the recent findings.

1. SAM - Simple Attenuation Model. This model is intended for use in predicting rain attenuation encountered on earth-space communication links. Given the earth terminal location, attenuation versus point rain rate is easily calculated. Further, input of the rain rate exceedance (such as the appropriate global rain rate region adopted by CCIR) permits prediction of attenuation exceedance (percent time during the year a given attenuation level is exceeded) on a worldwide basis. Although computing capability over the frequency range of 1 to 1000 GHz exists, only the 11 to 35 GHz band has been tested.

2. RPP - Rain Propagation Prediction Model. This is a first-order multiple scattering model developed for computation of isolation and phase as well as

attenuation as a function of point rain fall rate on an earth-space link. The program can be used for instantaneous or average computations by entering the appropriate spatial rain rate profile in a piecewise (ten level) uniform manner. The restriction on the capacity of the method is that computations are restricted to frequencies for which single rain drop scattering coefficients are available. Currently the program operates at frequencies of 11, 14, 20, and 30 GHz.

3. Multiple Scattering Model. This program operates in essentially the same manner as RPP with the same inputs and outputs. The algorithm is, however, more general in that all orders of multiple scattering are included. The recent computer program version of this technique has shown that numercial results are very similar to those of the RPP first-order multiple scattering program for frequencies of 30 GHz or under. Differences are expected to occur for higher frequencies. The multiple scattering computer program is not only more general than RPP but is also computationally more efficient.

The modeling capabilities are illustrated in the block diagram of Fig. 1. Since the multiple scattering model is

MODELING CAPABILITIES

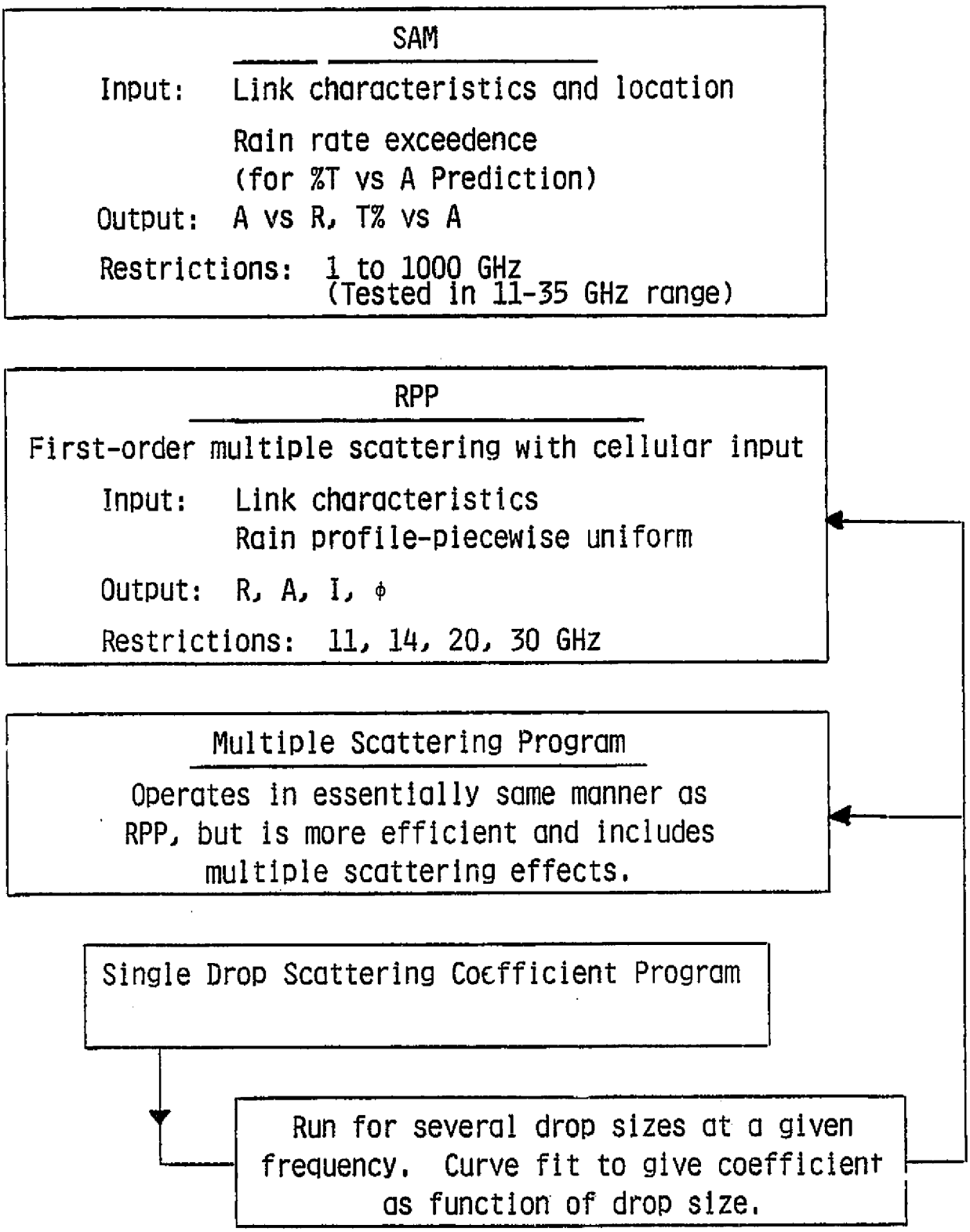

Figure 1. Summary of rain propagation modeling capabilities at Virginia Tech.

more general and is computationally more efficient than RPP, the multiple scattering model is recommended for future depolarization calculations.

Chapter 3

THE SIMPLE ATTENUATION MODEL

This chapter is similar to the paper in the Nov/Dec 1982 special issue of Radio Science on the NASA Propagation Program. More details can be found in the interim report "Estimation of Rain Attenuation on Earth-Space Millimeter Wave Communication Links," by W. K. Dishman and W. L. Stutzman published May 1982.

3.1 INTRODUCTION

As earth-satellite communications increase, economic considerations become more important. One method of reducing system cost is to operate with lower signal power margin. Accurate calculation of predicted signal power budgets permit systems to operate with a narrower margin for fading. Central to such calculations for links operating above 10 GHz is the accurate modeling of rain fading [Crane, 1977; Ippolito, 1981]. Initial attenuation prediction attempts involved extrapolation of measurements to other locations, frequencies, and elevation angles. The complex nature and regional variability of rain make this approach highly inaccurate. Over the past several years research activity has been very vigorous with many models being proposed in an

attempt to improve predictions. A wealth of literature exists and the reader is referred to several review papers [Rogers, 1976; Crane, 1977; Lane and Stutzman, 1980b; Brussaard, 1981; Ippolito et al., 1982].

There are some areas of attenuation modeling which are incomplete due to the lack of sufficient physical data. There is also some disagreement among researchers about how the problem should be attacked. These not withstanding, research investigations over the past several years have, indeed, moved closer together in approach. As pointed out by Brussard [1981], rain propagation research has the goal of providing information useful for communication system design. With this is mind the following have been identified by Fedi [1981a] as being desirable features of a prediction method:

1. Simple. The model should be easy to apply to communication system calculations. The unnecessary introduction of new parameters and mathematical complexity is to be avoided.

2. Physically sound. As much as possible, the model should be checked against directly observed physical data, such as spatial rain behavior.

3. Data Tested. The model should be tested against measured data from many different regions. Emphasis should be given to the data at low percentages

of time that are of most interest to system designers.

4. Flexible. As more data becomes available and a deeper understanding is obtained, model refinements surely follow. The model should be structured to accept modifications.

Herein a prediction method that incorporates all of the features mentioned above is presented. In spite of converging thought, it would be presumptuous to report that this work represents the prevailing trends of all researchers. However, even though differences are present in current models, the opportunity is taken to include many commonly accepted elements into a single model. Complete details on this investigation are given by Dishman and Stutzman [1982].

In Section 3.2 of this report fundamental concepts of attenuation modeling are discussed. In Section 3.3 we deal with the difficult problem of describing the spatial distribution of rain and we propose an exponential rain rate profile. The complete attenuation model is presented in Section 3.4 and it is evaluated by comparison to measured data from many experiments around the world and to predictions from other models.

3.2 FUNDAMENTAL CONCEPTS IN ATTENUATION MODELING

All attenuation models are "semi-empirical" in nature in that they employ attenuation data in the development of the model. This is done, however, to various degrees and we shall classify attenuation models as using either an empirical approach, a rain-cell approach, or a rain profile approach. The empirical approach develops an expression for attenuation directly from measured attenuation. Models based on a completely empirical approach are usually easy to apply, but do not relate directly to rain parameters. The methods of Lin [1979] and the CCIR [1981b] are examples of empirical models. Models based on a rain cell approach include the physically realistic idea of a randomly located "cell". The rain-cell models of Misme and Waldteufel [1980] and Lane and Stutzman [1980a, 1980b] require computer programs for evaluation. Models based on a rain profile employ an effective rain rate spatial distribution and are generally easy to use.

The decision of which approach to select for attenuation prediction is guided by the desirable features of a model discussed in Section 3.1. In particular, the model must be simple and physically sound. Empirical models are usually easy to use, but lack the necessary physical foundations, which in turn, leads to questions concerning the range of applicability. On the other hand, rain-cell models are more physically acceptable, but are generally more complex. It

has been found [Lane and Stutzman, 1980a, 1980b] that a rain-cell model which is stochastic in nature, allowing for the rain cell position to be random, is unnecessary and that a space-fixed rain profile is sufficient for prediction of average attenuation. Thus, we select the rain profile model approach, which contains both the elements of being physically sound and simple.

Now, the rain attenuation modeling problem using the rain profile approach can be divided into three different areas [Fedi, 1981a]: (1) The relationship between specific attenuation and rain rate; (2) The statistics of point rainfall intensity; and (3) The spatial distribution of rainfall. The first two areas are relatively well understood and have received much attention in the literature. A brief discussion of these topics will be presented in this section along with a discussion of the path integral concept. The spatial distribution of rainfall will be treated separately in the next section.

3.2.1 Specific Attenuation

The relationship between specific attenuation and rain rate is approximated by the familiar power law relationship

$$\alpha(R) = a\, R^{b} \qquad [dB/km] \qquad (1)$$

where a and b depend upon frequency and the microstructure of rain. The theoretical basis for this relationship has

been given by Olsen et al.[1978]. The main parameters associated with the microstructure of rain are the shape, size distribution, and temperature of the raindrops.

Raindrops are usually assumed to be either spherical, oblate spheroidal, or of the shape described by Pruppacher and Pitter [1971]. Use of the latter two shapes allows one to include the effects of wave polarization, drop canting angle, and slant-path elevation angle in the calculation of specific attenuation. Attenuation values computed assuming spherical drops generally lie between the extremes of values computed for vertical and horizontal linear polarization assuming distorted drop shapes. Because the errors between attenuation values computed using spherical drops and those computed using distorted drop shapes are typically 10% or less in the frequency range of interest [Crane, 1977; Olsen et al., 1978], specific attenuation values calculated for spherical drops will produce adequate results.

Various drop size distributions have been considered in the calculation of specific attenuation. These include the distributions of Laws and Parsons [1943], Marshal and Palmer [1948], and Joss et al.[1968]. While there is little difference in the values of attenuation computed using these distributions for frequencies below 30 GHz, the Laws and Parsons distribution is preferred because of the tendency of the other distributions to overestimate attenuation at the higher frequencies [Crane, 1977; Olsen et al., 1978; Upton et al., 1980; Ippolito, 1981].

The temperature of the raindrops is perhaps the most critical parameter. The assumed temperature has little effect above 15 GHz, but specific attenuation values are very sensitive to temperature variations in the 11-14 GHz band [Olsen et al., 1978; Upton et al., 1980; Thompson et al., 1980]. Values of a and b are generally available for temperatures of 0° C and 20° C. While 20° C is a reasonable assumption for terrestrial link attenuation prediction [Damosso et al., 1980], it is probably not representative of the temperature for earth-space paths [Thompson et al., 1980]. Attempts have been made to include the temperature variation of specific attenuation with altitude [Misme and Waldteuful, 1980], but this introduces a complexity into the calculation of attenuation that has little effect upon the results. For most climates, the assumption of 0° C drop temperature should give good results [Olsen et al., 1978].

Based upon the previous assumptions about the fine structure of rainfall, we believe that the use of spherical drops, the Laws and Parsons drop size distribution, and 0° C rain temperature will give reasonably accurate values of specific attenuation. A convenient source of computing the coefficients a and b for any frequency of interest are the

following equations taken from Olsen et al. [1978]:

$$a(f) = \begin{cases} 4.21 \times 10^{-5} f^{2.42} & 2.9 \leq f < 54 \text{ GHz} \\ 4.09 \times 10^{-2} f^{0.699} & 54 \leq f \leq 180 \text{ GHz} \end{cases} \quad (2)$$

$$b(f) = \begin{cases} 1.41 f^{-0.0779} & 8.5 \leq f < 25 \text{ GHz} \\ 2.63 f^{-0.272} & 25 \leq f < 164 \text{ GHz} \end{cases} \quad (3)$$

Should more precise values of a and b be desired, the tabulated values given in [Olsen et al., 1978] should be used. To include the effects of polarization and elevation angle, refer to the tabulated values recommended by the CCIR [1981c] or to the regression equations given by Thompson et al. [1980] and Damosso [1981].

3.2.2 Point Rainfall Intensity Distribution

A critical parameter in the estimation of attenuation exceedance is the point rain rate distribution. As pointed ou by Crane [1977], cumulative rain rate distributions may show considerable variability from year to year. For this reason care must be taken when estimating the average distribution at a site. An excellent review of procedures for

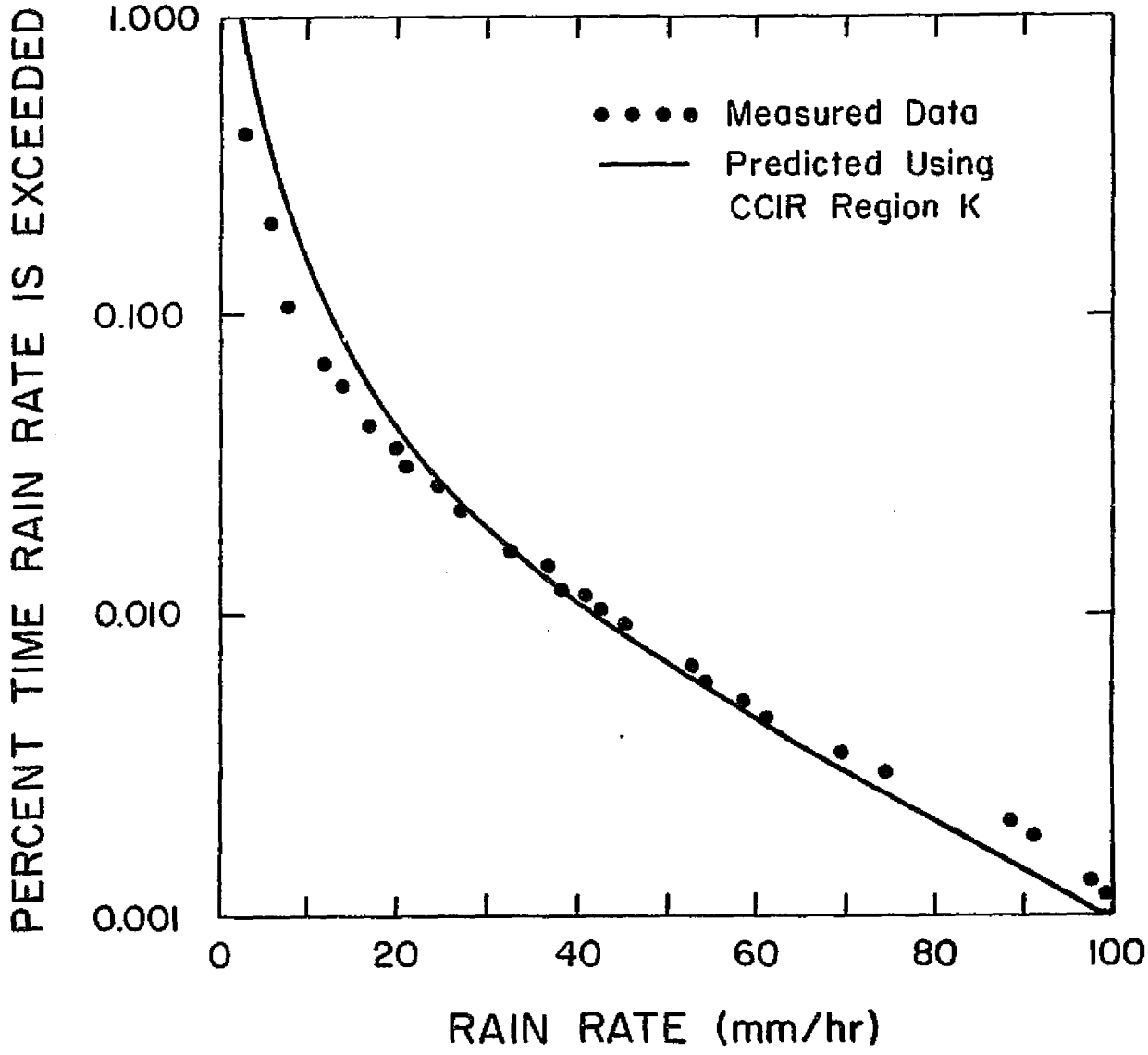

Figure 1. Cumulative distribution of rainfall intensity at Blacksburg, VA as measured for the period June 1976 to June 1979 (dots) and as estimated for rain climate zone K using the CCIR distribution [CCIR, 1981a].

estimating the rain intensity distribution is given by Fedi [1981a]. For use in attenuation estimates, data obtained from local sources are preferred. However, when adequate local data is not available, the distributions can be estimated from the rain climate region maps recommended by the CCIR [1981a]. These maps present cumulative rainfall distributions for 14 different regions of the world. A comparison between three years of measured data from Blacksburg, VA, and the corresponding CCIR region is shown in Fig. 1. The measurements were taken with a tipping bucket type rain gauge which usually provides a good approximation to the instantaneous rain rate. In general we have obtained good results using the CCIR rain region model [Dishman and Stutzman, 1982].

3.2.3 The Path Integral

If the rain rate profile, $R(\ell)$, were known along the extent of the propagation path, L, it would be a simple matter to calculate the total attenuation by integrating over the incremental (or specific) attenuation:

$$A(R_o) = \int_0^L \alpha[R(\ell)]\, d\ell \qquad (4)$$

In this equation we have indicated that total attenuation is a function of the point rain rate at the $\ell=0$ end of the path, or $R_o = R(\ell=0)$. This is done to emphasize the real-

ities of the problem. Rarely is $R(\ell)$ known, whereas point rain rate is directly measured and is available in historical data form. Thus, A is expressed in terms of R_o. As mentioned earlier, one step in the modeling process is to obtain a spatial rain rate profile. Once this is done (4) can be used to make predictions. Since the profile $R(\ell)$ is an average one, the calculated attenuation will be also.

Several methods have been proposed to utilize the path integral, but without explicitly developing a rain profile $R(\ell)$. These methods include using an effective path length L_e (where $A = \alpha (R_o) L_e$), a path averaged rain rate (where $A = a R_{ave} L$), or a path average factor $r = R_{ave}/R_o$. Although good results have been obtained in some cases, each of these approaches involve some approximation which limits its usefulness [Kheirallah et al., 1980; Dishman and Stutzman, 1982]. Attenuation prediction for arbitrary situations follows directly from the path integral (4) and this is discussed in the next section.

3.3 SPATIAL RAINFALL DISTRIBUTION

The most difficult parameter of an attenuation model to characterize is the spatial distribution of rain. Generally, precipitation systems are combinations of both stratiform and convective rain structures. Radar measurements indicate that most precipitation is characterized by large areas of low rates with a number of smaller regions of high

rain rates [Crane, 1977]. It is the presence of these imbedded rain "cells" that makes the spatial distribution of rain difficult to describe. Because rain rate statistics are usually only available for point rain rates, it is necessary to develop an "effective" spatial rain distribution model (or rain profile) that relates the rainfall along a path to the rainfall at a point. A rain profile is not applicable to single event analysis; it is useful for communication system design situations that involve long term performance. In other words, the wide variations in rain cells (observed for short time periods) tend to average out over long time periods, and a rain profile is useful in statistical predictions.

The rain profile for use in attenuation prediction must include both the horizontal and vertical spatial variations of rain as discussed in this section. Ideally, spatial variations should be determined with direct measurements of rain behavior, such as with rain gauge networks and radar. But there are not enough direct observations available to completely develop a model. The large indirect-measurement data base of attenuation on earth-space links must also be used [Fedi, 1981b]. Direct measurements are used in this section to establish a rain cell model which is exponential in shape. In the next section it is shown that the results agree with inferences from indirect measurements as well.

We will adopt the customary assumption that this effective distribution is the same in all geographic regions of interest. It is noted, however, that in regions where orographic features play a strong role or where rainfall is dominated by a particular form of precipitation (e.g. typhoons, hurricanes) this assumption may not hold.

3.3.1 Vertical Variation of Rain

Radar observations have shown that the vertical structure of precipitation is characterized by two different regions. The upper region consists of a mixture of ice and snow and does not contribute significantly to attenuation at frequencies below 60 GHz [CCIR, 1981a]. The lower region is mostly rain and is the primary source of attenuation. The transition height between the two regions corresponds approximately to the height of the 0° C isotherm.

Goldhirsh and Katz [1979] have presented median reflectivity factor profiles obtained from radar observations of summer rain cells at Wallops Island, VA. These profiles indicate that reflectivity is essentially constant up to a certain height and drops off rapidly above this height. Similar observations have been reported by other researchers [CCIR, 1981a]. This leads to the assumption of uniform rain structure from the ground up to an "effective" rain height H_e, as shown in Fig. 2. The contribution to attenuation by particles above the effective rain height will be neglected.

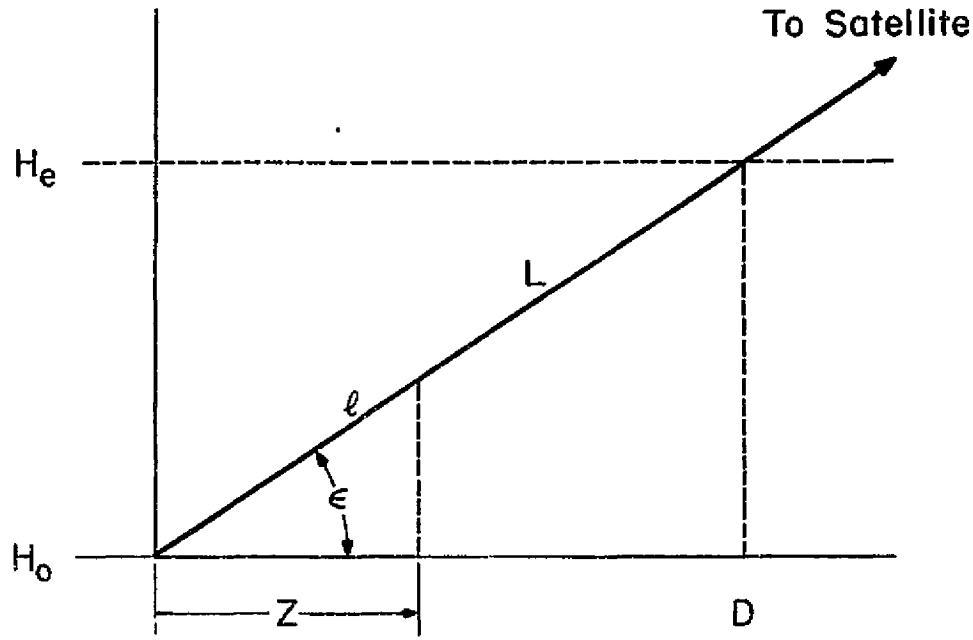

Figure 2. Vertical profile containing the propagation path. H_e is the effective rain height. The earth station is located at the z=0 point and is of height H_o above sea level.

The radar reflectivity profiles given by Goldhirsh and Katz [1979] show that the rain height is approximately constant and equal to the height of the 0° C isotherm for low rain rates. This is consistent with other observations of stratiform rain. As rain rate increases, however, the rain height indicated by the reflectivity profiles also increases. This increase is due to the structure of convective rain cells in which liquid water may be carried well above the 0° C isotherm level by updrafts. The data of Goldhirsh and Katz indicates that on the average the rain height may extend approximately 1 km above the 0° C isotherm height for rain rates in excess of 100mm/hr. A reasonable model for the effective rain height therefore consists of using the 0° C isotherm height for low rain rates and adding a rain rate dependent term to the 0° C isotherm height for higher rain rates. We propose the following simple relationship for the "effective" rain height H_e in km:

$$H_e = \begin{cases} H_i & R_o \leq 10 \text{ mm/hr} \\ H_i + \log\left(\frac{R_o}{10}\right) & R_o > 10 \text{ mm/hr} \end{cases} \qquad (5)$$

where R_o is the point rain rate in mm/hr and H_i is the 0° C isotherm height in km. The breakpoint of 10 mm/hr was chosen because it corresponds to the approximate value of the maximum rain rate associated with stratiform rain.

The 0° C isotherm height H_i varies with latitude and with the season of the year. Zonally averaged values of H_i versus latitude for the four seasons are given by Oort and Rasmussen [1971]. Based upon this data, Crane [1978] approximated the average height of H_i by

$$H_i = \begin{cases} 4.8 & |\Lambda| \leq 30° \\ 7.8 - 0.1|\Lambda| & |\Lambda| > 30° \end{cases} \tag{6}$$

where Λ is the latitude in degrees. As stated by Crane, this expression is an approximation to the observed mean seasonal values that lies midway between the summer and spring or fall values. The effective rain height H_e is shown in Fig. 3 as a function of latitude and rain rate. These curves were obtained using (6) in (5).

3.3.2 Horizontal Variation of Rain

Convective cells imbedded in stratiform rain render the distribution of rain nonuniform in the horizontal direction. Direct methods of observing rain cell structure include rain gauge networks and radar, and possibly the synthetic storm method. Radar observations yield the best information about the rain structure, but have not yet been used widely in determining the path-averaged to point rainfall relation-

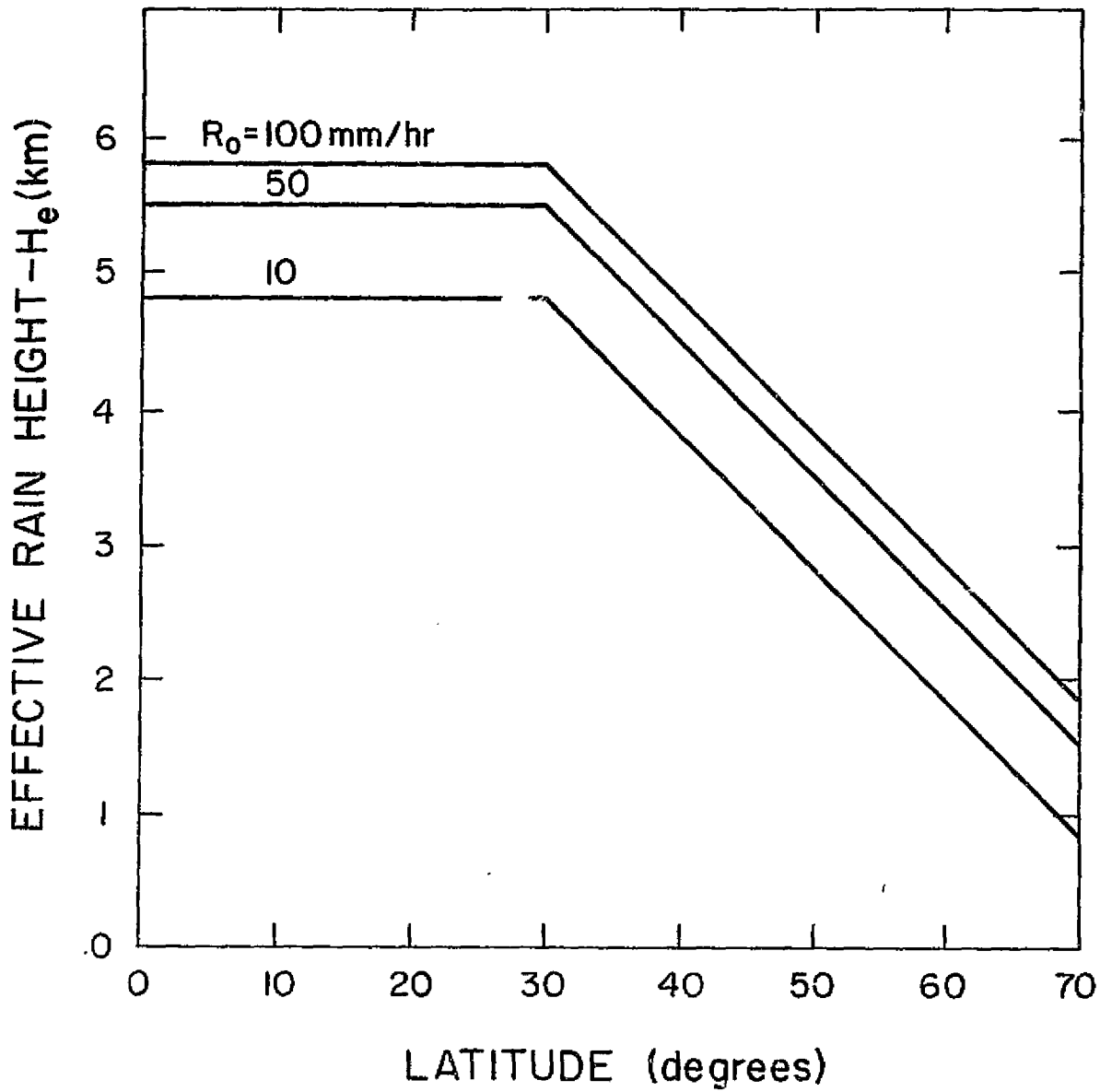

Figure 3. Variation of the effective rain height H_e with latitude and point rainfall rate, R_o.

ship. There have been a limited number of rain gauge networks operated around the world. Sims and Jones [1975] analysed data obtained from the 1946 Thunderstorm Project with lines of rain gauges in Florida and from a network of gauges in Illinois during the summer of 1970. Freeny and Gabbe [1969] reported on the results of a dense rain gauge network operated for six months in New Jersey. Harden et al.[1977] and Valentin [1977] operated rain gauge networks in conjunction with radio links in England and West Germany, respectively. The synthetic storm method, as employed by Drufuca [1974] and others [Harden et al., 1974; Kheirallah et al., 1980; Watson et al., 1977] uses the translational velocity of a storm over a rain gauge to convert point rainfall statistics to spatial distributions. Although this method is somewhat difficult to apply at an arbitrary site, it does provide useful information for developing a general relationship for the spatial rain distribution.

The point-to-path rainfall relation can be indirectly characterized from terrestrial link attenuation data. The most widely used method is the effective path length method, which was mentioned in Section 3.2.3. The exclusive use of these methods for determining spatial characteristics of rain should be avoided because of the non-linear relationship between specific attenuation and rain rate. However, when used in conjunction with data from rain gauge networks, attenuation data is very valuable.

The data of Sims and Jones [1975] and of Harden et al.[1977] both suggest that the point and path-averaged rain rates are the same up to rates of 10 to 14 mm/hr. Similar results were reported by Kheirallah et al.[1980] based upon synthetic storm studies at three locations in Canada. For rain rates in excess of 10 mm/hr, the path-averaged rain rate decreases as point rain rates increase and as path lengths increase. Several researchers [Valentin, 1977; Barsis and Samson, 1976] have presented curves derived from rain gauge data that illustrate the point-to-path rain relationship.

As pointed out by Fedi [1981a] and Kheirallah et al.[1980], the use of path-averaged rain rate in the specific attenuation relationship is not directly applicable due to the influence of the exponent in (1). Crane [1980] attempted to overcome this problem by fitting a power-law relation to the rain gauge data from Europe and the United States, then differentiating these data to obtain the path profile of the rain. The resulting data were fitted with a series of exponential functions that could be used in the path integral relation (4). Kheirallah et al.[1980] point out that the Crane model overestimates the path averaged rain rates for low values of point rain rate.

The piecewise uniform path profile model [Persinger et al., 1980] gives good results but has only two rain rate values allowed along the path. The piecewise exponential

path profile of the global model [Crane, 1980] also gives good results but is unnecessarily complicated and does not include uniform rain rates for low point rain rate values. Combining these ideas together with a goal of simplicity we propose the following exponential-shaped effective path profile for rain rate:

$$R(z) = \begin{cases} R_o & R_o \leq 10 \text{ mm/hr} \\ R_o \, e^{-\gamma \ln(R_o/10) z} & R_o > 10 \text{ mm/hr} \end{cases} \quad . \quad (7)$$

R_o is the point rainfall intensity, z is the horizontal distance along the path, and γ is a parameter controlling the rate of decay of the profile.

The path-averaged rain rate for a path of length D is found from (7) as

$$R_{ave} = \frac{1}{D} \int_0^D R(z)dz = \begin{cases} R_o & R_o \leq 10 \text{ mm/hr} \\ R_o \dfrac{1 - e^{-\gamma \ln(R_o/10) D}}{\gamma \ln(R_o/10) D} & R_o > 10 \text{ mm/hr} \end{cases} \quad (8)$$

This relation was compared to measured values of path rain rate obtained from the literature [Sims and Jones, 1975; and

Valentin, 1977; Freeny and Gabbe, 1969; Harden et al., 1977] and to values derived using the synthetic storm model [Kheirallah et al., 1980] in order to establish the value of the parameter γ. This study was bounded by values of γ between 1/10 and 1/30, with 1/22 giving a best fit. A plot of the normalized rain profile of (7) versus distance is shown in Fig. 4 for $\gamma = 1/22$ and several values of rain rate.

3.3.3 Summary of the Proposed Rain Rate Profile

Equations (5)-(7) describe the proposed spatial distributions in the vertical and horizontal planes. Because the rain is assumed to be uniform in the vertical direction up to H_e, the rain profile $R(\ell)$ along the slant path (see Fig. 2) can be derived using the simple trigometric relationship $z = \ell \cos\varepsilon$ in (7), giving

$$R(\ell) = \begin{cases} R_o & R_o \leq 10 \text{ mm/hr} \\ R_o \, e^{-\gamma \ln(R_o/10)\ell \cos\varepsilon} & R_o > 10 \text{ mm/hr} \end{cases} \qquad (9)$$

for $\ell \leq L$, where

$$L = \frac{H_e - H_o}{\sin\varepsilon} \qquad (10)$$

This expression is likely to be valid for elevation angles above about 10^o. For lower elevation angles a value of L as suggested by the CCIR [1981b] could be used, although very

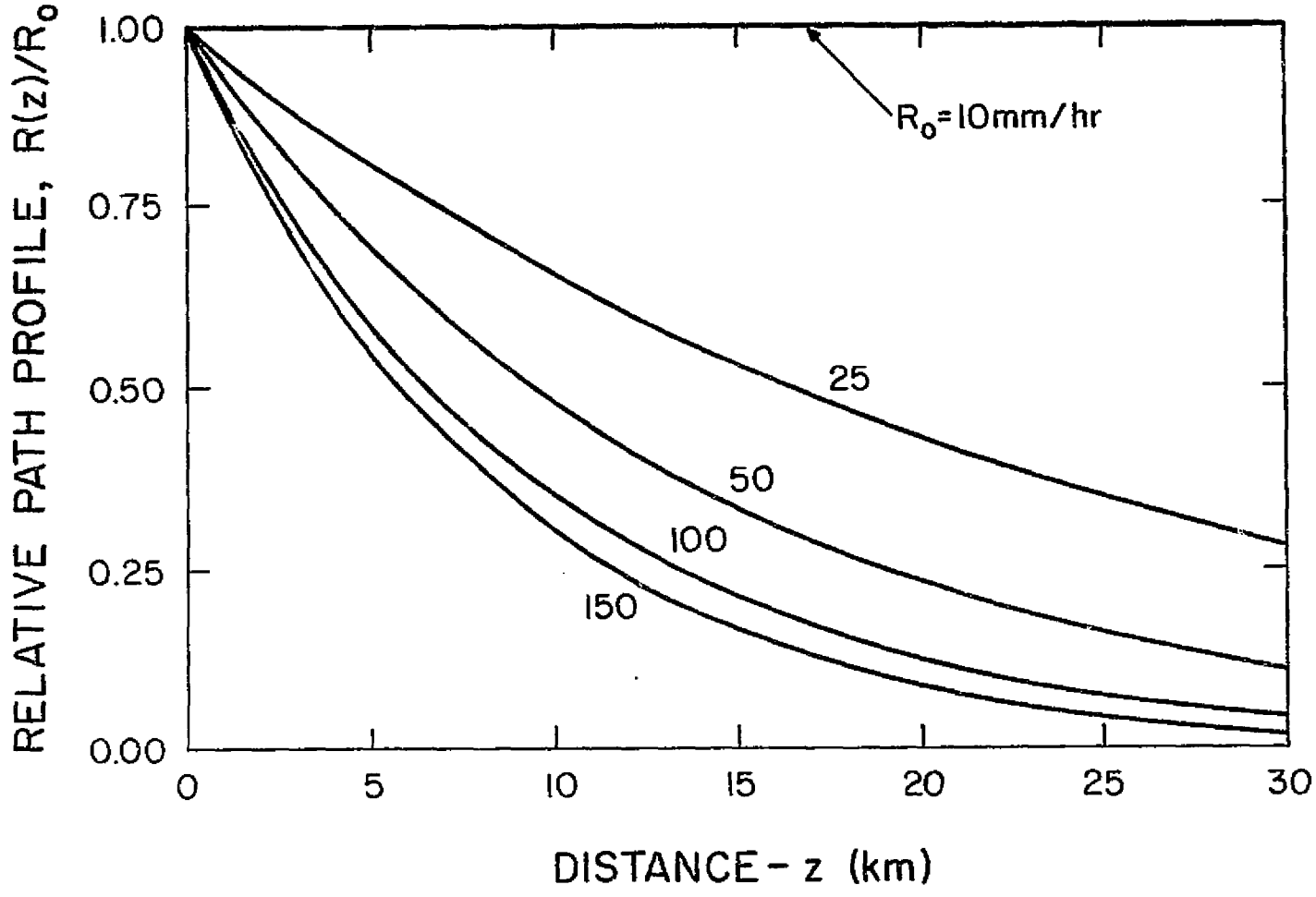

Figure 4. Normalized rain profile as a function of horizontal distance and point rainfall rate from (7) with $\gamma=1/22$.

low elevation angle satellite data and terrestrial data have not been compared to this model. H_o is the altitude of the earth station location and H_e is defined by (5) and (6). This expression will be used in the next section to derive the corresponding total attenuation model.

3.4 THE SIMPLE ATTENUATION MODEL AND ITS PERFORMANCE

The total attenuation due to a point rainfall rate R_o is easily computed using the effective rain profile from (9) in the path integral (4). Evaluating the integral gives

$$A(R_o) = \begin{cases} a R_o^{\,b} L & R_o \leq 10 \text{ mm/hr} \\ a R_o^{\,b} \dfrac{1 - e^{-\gamma b \ln(R_o/10) L \cos\epsilon}}{\gamma b \ln(R_o/10) \cos\epsilon} & R_o > 10 \text{ mm/hr} \end{cases} \tag{11}$$

where the path length L is given by (10).

The simple attenuation model (SAM) given by (11) is a function of the point rainfall intensity only; it is not a function of the percentage of time that rain rate is exceeded. This decoupling of the attenuation model and the rain rate statistics allows evaluation of the model parameters independent of the errors associated with the rain rate statistics.

Many propagation experiments using satellite beacons have been conducted in North America, Europe, and Japan. An extensive collection of the rain rate, attenuation, and isolation statistics associated with these experiments has been assembled at VPI&SU to form a data base for use in developing and testing propagation models. The attenuation versus rain rate data (based on equal probability levels) from this data base were compared to the predictions calculated from (11). The best average agreement was found when $\gamma = 1/22$. This is the same value found when comparing the path-averaged rain rate to directly measured rain gauge data (see Section 3.3.2). Thus, both direct and indirect data agree with the model of (11) when $\gamma = 1/22$ is used. This adds confidence that the spatial rain rate variation of Section 3.3 is an accurate model. A plot of typical A vs R_o data is shown in Fig. 5. The data were obtained from three years of measurements in Blacksburg, VA using the CTS (11.7 GHz) and COMSTAR (19 and 28 GHz) beacons. Also shown in Fig. 5 is the attenuation calculated using (11) with $\gamma = 1/22$.

Estimates of attenuation statistics are found by combining the attenuation versus rain rate model with a rainfall distribution (see Section 3.2.2). An example of this procedure is given in Fig. 6. The predicted attenuation distributions were calculated using the CCIR rain rate distribution for the Blacksburg region (see Fig 4) together with the SAM predictions of attenuation as a function of rain rate.

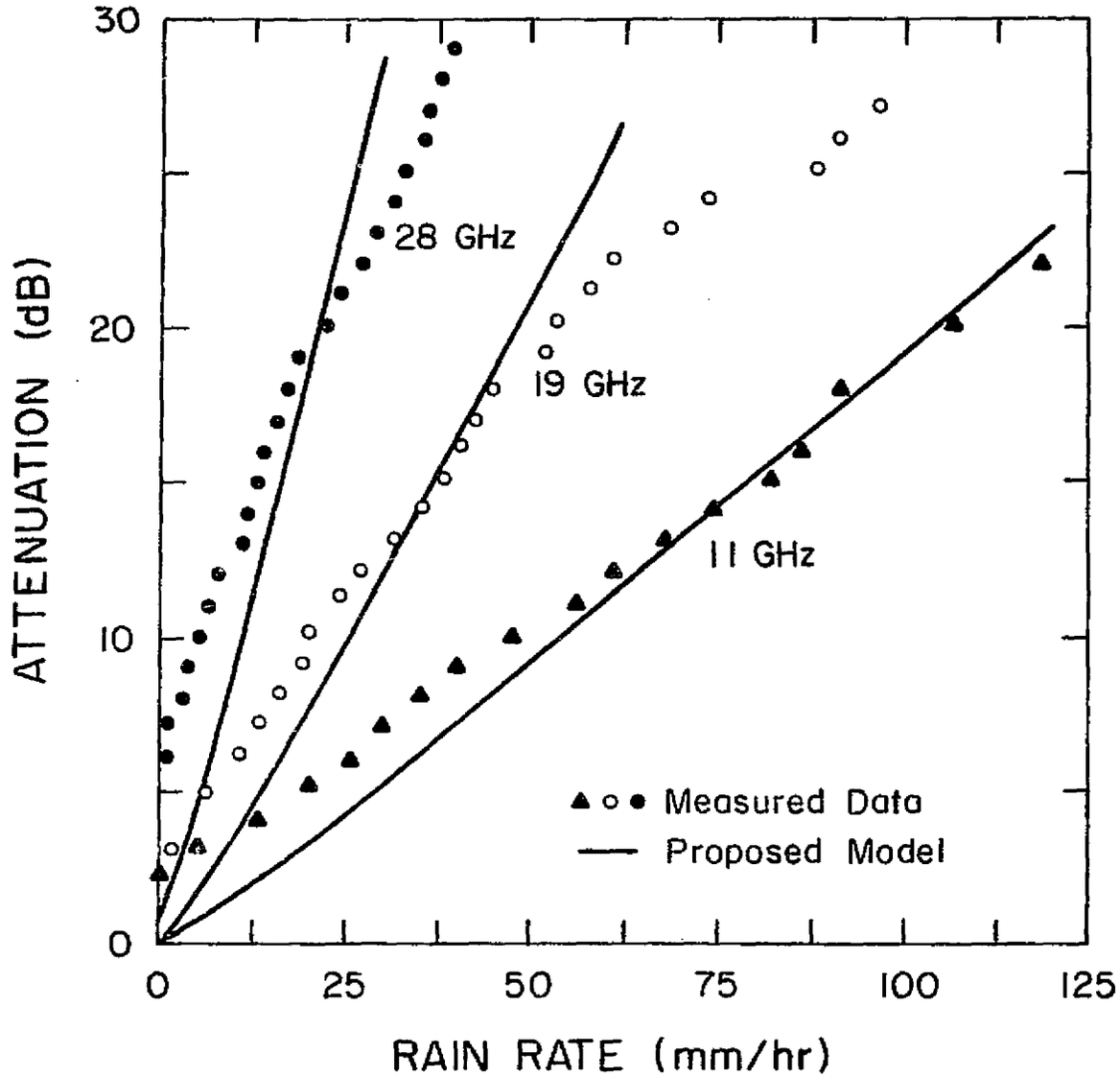

Figure 5. Attenuation vs. rain rate data from the following experiments in Blacksburg, VA: CTS (11.7 GHz, 33 degree elevation angle, circular polarization, June 1976 to June 1979), COMSTAR (19.4 and 28.56 GHz, 45 degree elevation angle, vertical polarization, July 1977 to August 1980). The solid lines are the estimates for each experimental data set using the proposed model.

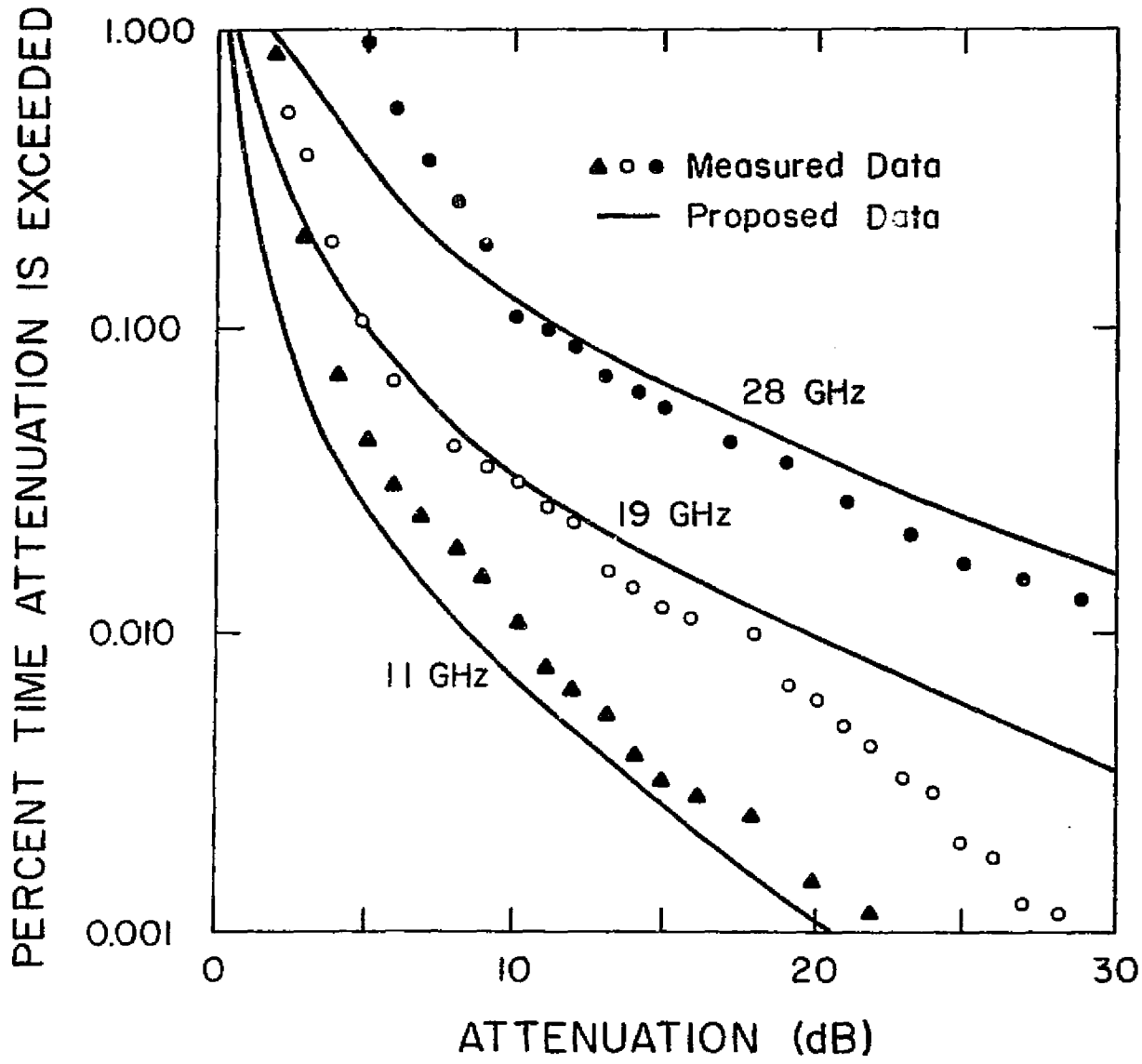

Figure 6. Cumulative attenuation distribution for Blacksburg, VA. The points are measured data using the CTS (11.7 GHz, June 1976 to June 1979) and COMSTAR (19.04 and 28.56 GHz, July 1977 to August 1980) beacons. The solid lines are the estimates using the proposed model and the cumulative rain rate distribution for CCIR rain climate region K.

To do this we make the customary assumption that the probability of the attenuation exceeding a certain values is the same as the probability of the point rainfall intensity exceeding the point rainfall rate used to predict the attenuation. Also plotted in Fig. 4 are the measured attenuation distributions obtained from three years of observations in Blacksburg.

The complete VPI&SU data base which consists of attenuation measurements from 47 experiments is presented in Table 1 [Dishman and Stutzman, 1982]. The experiments represent 17 different sites in the U.S., Europe, and Japan ranging in latitude from 28 to 52° N, varying in frequency from 11.5 to 34.5 GHz, and having elevation angles from 10.7 to 57°. Of the 47 experiments, 18 represented two or more years of data (24 months or more as indicated in parentheses with the time interval). The attenuation values given in Table 1 for the 1% down to the 0.001% level of occurence were taken from the literature cited.

In Fig. 7 a scatter plot of the percent deviation values of the simple attenuation model predictions for each of the 47 data sets is plotted together with the mean and standard deviation limits. Good agreement is obtained with the model. The relatively high percent deviations for high percentages of time arise from the fact that the attenuations are low and small deviations appear as high percentages. This is overcome by using an absolute deviation in dB as

TABLE 1 Data Sets: Experiment Characteristics and Attenuation Values

Code	Location	Frequency Polarization*	Elevation Angle (degrees)	Time Interval†	Measured Attenuation for Given Percentage of Time							Source
					1.0%	0.3%	0.1%	0.03%	0.01%	0.003%	0.001%	
A28	Kashima, Japan	11.5 C	46.5	May 1977–April 1978(12)	1.0	1.5	2.4	4.3	6.2	10.0	·	[*Fujono*, 1979]
A73	Blacksburg, Virginia (main)‡	11.6 C	10.7	July 1980–June 1981(12)	1.2	3.6	6.0	12.7	16.2	20.2	22.9	[*Towner et al.*, this issue]
A74	Blacksburg, Virginia (remote)‡	11.6 C	10.7	July 1980–June 1981(12)	···	2.3	4.4	8.7	13.9	17.4	20.1	[*Towner et al.*, this issue]
A48	Fucino, Italy	11.6 C	33.0	Jan. 1978–Dec. 1980(36)	··	···	···	2.9	4.8	8.0	11.5	[*Mauri and Paraboni*, 1981]
A49	Lario, Italy	11.6 C	32.0	Jan. 1978–Dec. 1980(36)	···	··	2.6	4.5	8.2	12.9	··	[*Mauri and Paraboni*, 1981]
A40	Spino D'Adda, Italy	11.6 C	32.0	Oct. 1978–Sept. 1980(24)	··	··	2.8	4.4	6.8	10.0	11.9	[*Mauri and Paraboni*, 1981]
A65	Slough, United Kingdom	11.6 C	29.5	Sept. 1977–Aug. 1980(36)	···	··	···	···	3.0	5.8	9.6	[*Davies et al.*, 1981]
A32	Gometz-la-Ville, France	11.6 C	32.0	Nov. 1977–Nov. 1978(13)	1.2	1.8	2.4	3.4	4.6	6.3	7.7	[*Misme and Waldteufel*, 1980]
A21	Leeheim, West Germany	11.6 C	28.8	Jan. 1979–Dec. 1979(12)	···	··	···	3.0	7.0	13.0	18.0	[*Rucker*, 1980]
A61	Kashima, Japan	11.7 V	37.7	Aug. 1978–July 1979(12)	···	1.0	2.0	4.8	6.2	8.6	···	[*Fukuchi et al.*, 1981]
A20	Blacksburg, Virginia	11.7 C	33.0	June 1976–June 1979(31)	··	2.7	3.7	6.3	10.3	16.0	23.1	
A34	Austin, Texas	11.7 C	49.0	June 1976–June 1979(37)	···	1.2	2.8	7.1	13.5	21.7	··	[*Vogel*, 1980]
A19	Waltham, Massachusetts	11.7 C	24.0	June 1977–May 1979(24)	···	1.1	2.0	4.8	9.7	15.1	··	[*Nackoney*, 1979]
A51	Crawford Hill, New Jersey	11.7 C	27.0	May 1976–April 1979(36)	···	···	3.3	6.9	12.4	21.5	···	[*CCIR*, 1979]
A72	Greenbelt, Maryland	11.7 C	29.0	July 1976–June 1979(36)	···	0.9	1.8	4.9	11.9	21.5	28.7	[*CCIR*, 1979]
A66	Gometz-la-Ville, France	11.8 C	33.6	Jan. 1979–Nov. 1979(11)	···	1.5	2.3	3.4	5.1	7.4	10.4	[*Ramat*, 1981]
A64	Slough, United Kingdom	11.8 C	30.3	July 1978–Aug. 1980(26)	···	··	···	···	4.2	7.5	15.9	[*Davies et al.*, 1981]
A58	Martlesham Heath, United Kingdom	11.8 C	29.9	July 1978–June 1980(24)	···	··	···	···	3.8	5.4	7.4	[*Thirlwell and Howell*, 1981]
A22	Leeheim, West Germany	11.8 C	32.5	Jan. 1979–Dec. 1979(12)	··	···	···	3.1	5.5	9.4	14.2	[*Rucker*, 1980]
B19	Blacksburg, Virginia	19.04 V	45.0§	July 1977–Aug. 1980(34)	2.0	3.4	5.1	10.0	16.9	23.8	···	[*Andrews et al.*, this issue]
B23	Crawford Hill, New Jersey	19.04 V	18.5	July 1976–June 1978(24)	2.5	6.8	11.5	25.0	···	·	·	[*Arnold et al.*, 1981]
B10	Crawford Hill, New Jersey	19.04 V	38.6	May 1977–May 1978(12)	···	3.4	6.0	12.8	21.5	·	··	[*Arnold et al.*, 1980]
B26	Palmetto, Georgia	19.04 V	29.9	June 1976–July 1977(12)	··	5.4	11.0	25.0	··	·	·	[*Lin et al.*, 1980]
B27	Palmetto, Georgia	19.04 V	49.5	Aug. 1977–Aug. 1978(12)	···	··	9.7	21.3	···	·	···	[*Lin et al.*, 1980]
B24	Grant Park, Illinois	19.04 V	27.3	July 1976–June 1977(12)	···	···	9.7	25.4	···	·	···	[*Lin et al.*, 1980]
B25	Grant Park, Illinois	19.04 V	41.8	Aug. 1977–Aug. 1978(12)	···	···	10.0	22.4	···	··	···	[*Lin et al.*, 1980]
B32	Clarksburg, Maryland	19.04 V	21.0	July 1976–Aug. 1977(13)	···	3.9	8.8	16.2	22.5	··	·	[*Kumar*, 1981]
B34	Clarksburg, Maryland	19.04 V	41.0	Aug. 1977–Aug. 1978(12)	···	··	5.7	12.9	25.0	··	···	[*Kumar*, 1981]
B36	Clarksburg, Maryland	19.04 V	43.5	Aug. 1978–Aug. 1980(25)	···	5.0	9.6	16.1	···	··	···	[*Kumar*, 1981]
B31	Waltham, Massachusetts	19.04 V	38.2	Jan. 1979–Dec. 1979(12)	2.1	3.9	7.5	13.1	18.7	·	···	[*Tang and Davidson*, 1981]
B30	Tampa, Florida	19.04 V	57.0	Jan. 1979–Dec. 1979(12)	1.8	10.6	···	···	···	···	···	[*Tang and Davidson*, 1981]
B21	Austin, Texas	19.04 V	52.0	Oct. 1978–Aug. 1980(23)	1.0	2.5	6.5	17.0	24.0	·	··	[*Vogel*, this issue]
B38	Kashima, Japan	19.50 C	48.0	April 1978–March 1980(24)	1.5	3.0	5.4	9.4	16.2	···	···	[*Fukuchi et al.*, 1981]
C31	Blacksburg, Virginia	28.56 V	45.0§	March 1977–Aug. 1980(41)	5.5	8.1	11.5	19.5	27.9	··	···	[*Andrews et al.*, this issue]
C12	Crawford Hill, New Jersey	28.56 V	38.6	May 1977–May 1978(12),	3.2	7.5	13.5	28.1	44.0	··	··	[*Arnold et al.*, 1980]
C24	Palmetto, Georgia	28.56 V	29.9	June 1976–July 1977(12)	···	8.0	21.8	···	···	·	···	[*Lin et al.*, 1980]
C25	Palmetto, Georgia	28.56 V	49.5	Aug. 1977–Aug. 1978(12)	···	8.8	19.2	···	···	···	···	[*Lin et al.*, 1980]
C22	Grant Park, Illinois	28.56 V	27.3	July 1976–June 1977(12)	···	8.0	17.6	···	···	···	···	[*Lin et al.*, 1980]
C23	Grant Park, Illinois	28.56 V	41.8	Aug. 1977–Aug. 1978(12)	···	8.2	20.0	···	···	···	···	[*Lin et al.*, 1980]
C28	Clarksburg, Maryland	28.56 V	21.0	July 1976–Aug. 1977(13)	3.4	5.3	15.9	27.5	··	···	···	[*Kumar*, 1981]
C29	Clarksburg, Maryland	28.56 V	41.0	Aug. 1977–Aug. 1978(12)	···	10.2	13.6	24.7	·	·	···	[*Kumar*, 1981]
C30	Clarksburg, Maryland	28.56 V	43.5	Aug. 1978–Aug. 1980(25)	4.5	9.8	17.5	26.7	·	·	···	[*Kumar*, 1981]
C27	Waltham, Massachusetts	28.56 V	38.2	Jan. 1979–Dec. 1979(12)	4.1	23.5	18.9	···	·	·	···	[*Tang and Davidson*, 1981]
C26	Tampa, Florida	28.56 V	57.0	Jan. 1979–Dec. 1979(12)	4.4	6.0	···	···	···	·	··	[*Tang and Davidson*, 1981]
C21	Austin, Texas	28.56 V	52.0	Oct. 1978–Aug. 1980(23)	1.5	7.3	15.0	32.0	·	·	··	[*Vogel*, this issue]
C20	Wallops Island, Virginia	28.56 V	43.5§	April 1977–Aug. 1980(36)	···	10.4	15.5	···	·	·	·	[*Goldhirsh*, 1980]
C17	Kashima, Japan	34.5 C	46.5	May 1977–April 1978(12)	4.7	·	20.0	···	·	·	···	[*Fujono*, 1979]

* C is circular; V is linear vertical.

† Actual months of operation given in parentheses.

‡ Diversity experiment (7.3 km separation).

§ Average value.

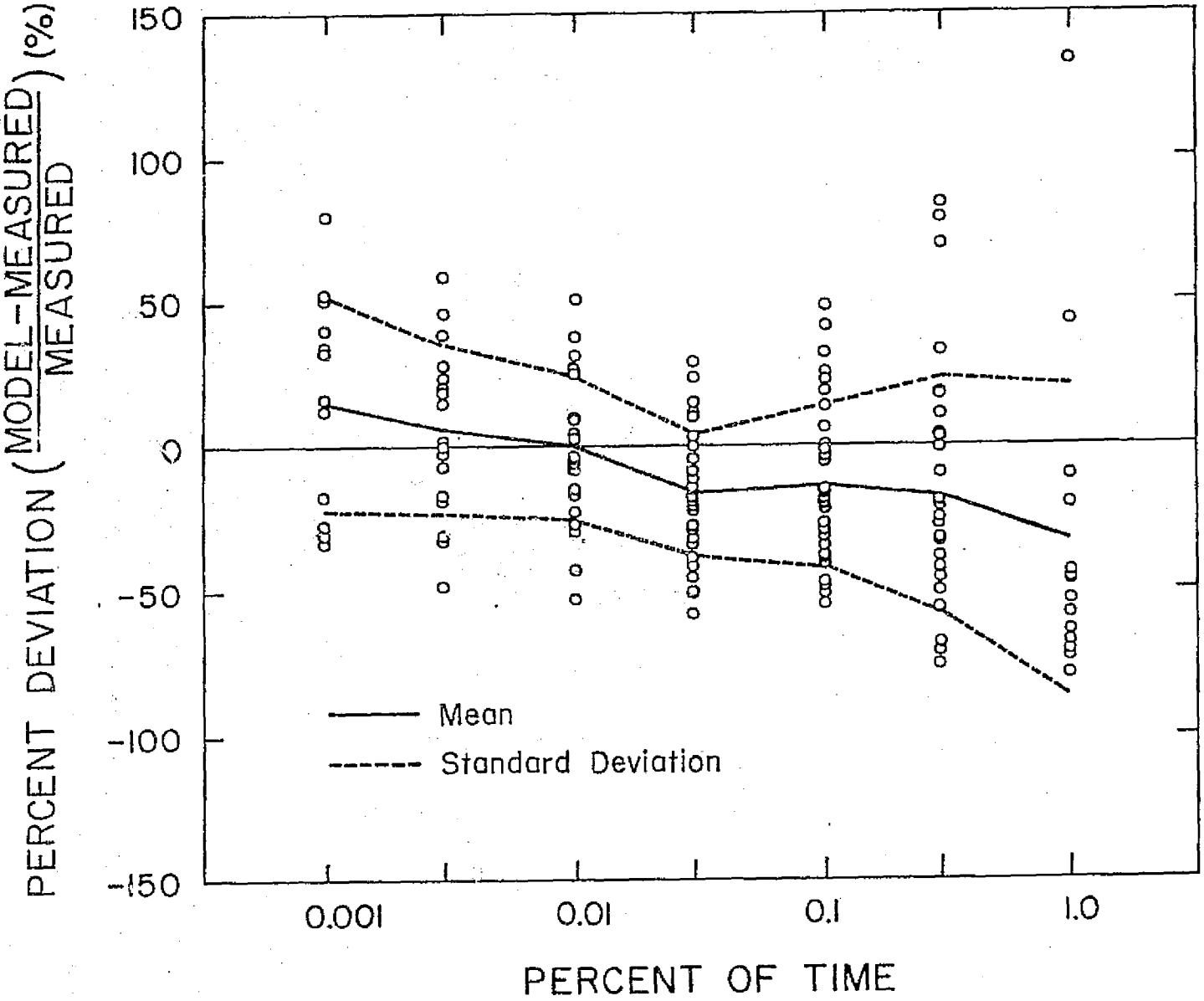

Figure 7. Scatter plot of relative deviations of the simple attenuation model from the data of Table 1.

presented in Table 2. Another measure of the quality of fit for a model is that recently proposed by the CCIR [1981a]. In this method, data from many radio link experiments are tabulated at fixed probability levels, such as 1.0, 0.1, 0.01, and 0.001% of the year. A test variable is computed from the logarithm of the ratio of predicted to measured attenuation. To suppress measurement inaccuracies, the test variable is set to zero if the measured and predicted values differ by less than 1 dB. The figure of merit, D, is computed for each probability level from the mean and standard deviation of the test variables. According to the CCIR, the best prediction method produces the smallest D values. This evaluation method represents an important first step toward developing a standard model evaluation method. The results of deviation in dB and the D values are shown in Table 2 for the simple attenuation model (SAM).

An important consideration in the evaluation of an attenuation model is whether or not the model offers an improvement over existing models. With this in mind, the performance of the proposed model was compared to the global model [Crane, 1980] and the CCIR [1981b] model. These models were chosen because they represent different approaches to the modeling problem. The global model is a rain profile model based on rain gauge measurements. The recently introduced CCIR model is an empirical model derived from terrestrial and slant-path attenuation data. There is a "maritime" and

TABLE 2. Summary of Deviations Between Measured Attenuation From Data Sets of Table 1 and Model Predictions

Percent Time	Simple Attenuation Model			Global Model			CCIR Model (Maritime)		
	Mean	Standard Deviation	*D*	Mean	Standard Deviation	*D*	Mean	Standard Deviation	*D*
1.0	−1.2 dB	1.4 dB		−0.9 dB	1.6 dB		0.1 dB	1.3 dB	
1.0	−33.5%	53.9%	111.7%	−22.0%	64.0%	116.1%	21.8%	69.3%	53.6%
0.1	1.3 dB	3.3 dB		0.6 dB	4.0 dB		−0.4 dB	2.6 dB	
0.1	−14.3%	28.1%	43.7%	5.1%	34.3%	32.7%	6.6%	30.2%	30.2%
0.01	0 dB	3.3 dB		2.9 dB	5.1 dB		−0.8 dB	3.4 dB	
0.01	−0.6%	25.0%	31.1%	23.2%	31.8%	36.9%	0.4%	26.9%	31.0%
0.001	0.9 dB	5.2 dB		4.9 dB	5.3 dB		0.6 dB	8.2 dB	
0.001	15.1%	37.2%	42.1%	45.8%	47.7%	59.8%	8.9%	44.9%	60.9%

a more complicated "continental" version of the CCIR model. We use the maritime CCIR model for all calculations since its results are superior to those found when including the different procedure for continental regions. The CCIR model for percentages of time from 0.001 to 0.1% are found in [CCIR, 1981b] and for 0.001 to 1% [CCIR, 1981d].

Attenuation values predicted using the global and CCIR models are given in Table 2 for the 47 experiments. The specific attenuation coefficients used were obtained from the sources recommended by each model. The CCIR rain climate regions were used to determine rainfall statistics for each model to eliminate the effects of variations in rainfall distribution models. Results are shown for the 1, 0.1, 0.01, and 0.001 percentages of time, but similar values occur for intermediate values. The comparison in Table 2 indicates that on the whole all three models provide good agreement to data. At high percentages of time (1 and 0.1%) the CCIR model yields the lowest mean and standard deviations in dB as well as D values. For the important low percentages of time (0.01 and 0.001%) the SAM and CCIR models give very good fits to the data. The global model is slightly inferior at all levels. The SAM model has the lowest percent standard deviation at all levels. Comparison on the basis of the D value should be made with caution. Much lower D values result from underprediction than from overpredictions by the same amount, especially at low attenua-

tions (high percentages of time). Thus, the D values associated with underpredictions at high percentages of time in Table 2 are disproportionately high.

3.5 CONCLUSIONS

In this chapter the simple attenuation model (SAM) was introduced for use in estimating rain-induced attenuation along an earth-space path. The model is both conceptually and computationally simple. It is a rain profile model that uses an effective spatial rain distribution which is uniform for low rain rates and has an exponential shaped horizontal rain profile for high rain rates. The spatial distribution function was derived from direct observations of rain using rain gauge data and verified indirectly by comparison to slant-path attenuation data from many experiments. Model estimates of attenuation as a function of point rainfall rate are easily computed with SAM using the physical parameters of the earth station location (elevation angle, latitude, and altitude) and the frequency of operation. To produce attenuation exceedance estimates, the model is combined with a model of the point rainfall intensity distribution for the geographic region of interest.

Attenuation data for various percentages of time were presented for 47 experiments throughout the world. See Table 1. Comparisons were made to this data base with predicted values from the SAM, global, and CCIR (maritime)

models using CCIR rain climate regions rainfall statistics. See Table 2. The SAM model performed well in the important region of low percentages of time (0.01 and 0.001%) and the lowest percent standard deviation at all percent time values tested. Furthermore, the SAM model is easy to use and is modular in construction. It is basically an attenuation versus point rainfall rate model that is coupled with rain rate exceedance to produce an attenuation exceedance prediction. This allows for separate inclusion of rain rate statistics that affect the accuracy of attenuation exceedance prediction.

3.6 REFERENCES

Andrews, J. H., C. Ozbay, T. Pratt, C. W. Bostian, E. A. Manus, J. M. Gaines, R. E Marshall, W. L. Stutzman, and P. H. Wiley (1982), Results of the COMSTAR Experiment, Radio Science, 17(6), pp. 1349-1359, Nov./Dec. 1982.

Arnold, H. W., D. C. Cox, H. H. Hoffman, and R. P. Leck (1980), Characteristics of rain and ice depolarization for a 19- and 28-GHz propagation path from a COMSTAR satellite, IEEE Trans. on Ant. and Prop., AP-28, 22-27.

Arnold, H. W., D. C. Cox, and A. J. Rustako (1981), Rain attenuation at 10-30 GHz along earth-space paths: elevation angle, seasonal, and diurnal effects, IEEE Trans. on Comm., COM-29, 716-721.

Barsis, A. P., and C. A. Samson (1976), Performance estimation for 15-GHz microwave links as a function of rain attenuation, IEEE Trans. on Comm., COM-24(4), 462-470.

Brussaard, G. 91981), Prediction of attenuation due to rainfall on earth-space links, Radio Science, 16(5), 745-760.

CCIR (1979), USA Attenuation by rainfall at 11.7 GHz from CTS observations, CCIR Study Group Report 564-1, Doc. USSG 5/25T.

CCIR (1981a) Radiometeorological Data, Draft Report 563-1 (MOD F), Doc. 5/5049-E.

CCIR (1981b) Propagation Data Required for Space Telecommunication Systems, Draft Revision of Report 564-1 (MOD F), Doc. 5/5046-E.

CCIR (1981c) Attenuation by Precipitation and other Atmospheric Particles, Draft Report 721 (MOD F), Doc. 5/5026-E.

CCIR (1981d) Propagation Data for Broadcasting From Satellites, Draft Report 565-1 (MOD F), Doc. 5041-E.

Crane, R. K. (1977), Prediction of the effects of rain on satellite communication systems, Proc. IEEE, 65(3), 456-474.

Crane, R. K. (1978), A global model for rain attenuation prediction, EASCON Record (Arlington, VA), 391-395.

Crane, R. K. (1980), Prediction of attenuation by rain, IEEE Trans. on Comm., COM-28(9), 1717-1733.

Damosso, E., G. DeRenzis, F. Fedi, and P. Migliorini (1980), A systematic comparison of rain attenuation prediction methods for terrestrial paths, presented at URSI Open-Symposium of Effects of the Lower Atmosphere on Radio Frequencies Above 1 GHz (Lennoxville, Canada) Paper 2.11.

Damosso, E. (1981), Dependence of specific rain-attenuation and phase shift on electrical, meteorological and geometrical parameters, CSELT Rapporti Tecnici, 6(3).

Davies, P. G., M. J. Courthold, and E. C. MacKenzie (1981), Measurements of circularly-polarized transmissions from the OTS and SIRIO satellites in the 11 GHz band, IEE Conf. on Ant. and Prop., Publ. No. 195, P5. 2, 76-80.

Dishman, W. K., and W. L. Stutzman (1982), Estimation of rain attenuation on earth-space millimeter wave communication links, Interim Report under JPL Contract 955954, Virginia Tech, EE Dept., Blacksburg.

Drafuca, G. (1974), Rain attenuation statistics for frequencies above 10 GHz from raingauge aboservations, J. Tech. Atmospheriques, 8, 399-411.

Fedi, F. (1981a), Prediction of attenuation due to rainfall on terrestial links, Radio Science, 16(5), 731-743.

Fedi, F. (1981b), Normalization procedures and prediction techniques for rain attenuation on terrestrial and

earth-space radio links, IEE Conf. Publ. No. 195 (Antennas and Propagation) Part 2, 173-179.

Freeny, A. E., and J. D. Gabbe (1969), A statistical description of intense rainfall, BSTJ, 48(6), 1789-1850.

Fugono, N. (1979), Summary of millimeter wave propagation experiments using Japan's first geostationary satellite "Kiku-2", Ann. Telecommun., 34, 299-318.

Fukuchi, H., M. Fujita, K. Nakamura, Y. Furuhama, and Y. Otsu (1981), Rain attenuation characteristics on quasi-millimeter waves using Japanese geostationary satellites CS and BSE, IEE Conf. Ant. and Prop., Publ. no. 195, Pt. 2, 41-45.

Goldhirsh, J. (1980), Cumulative slant path fade statistics associated with the COMSTAR beacon at 28.56 GHz for Wallops Island, Va. over a three year period, The Johns Hopkins University-Applied Physics Labortory Report S1R80U-048.

Goldhirsh, J., and I. Katz (1979), Useful experimental results for earth-satellite rain attenuation modeling, IEEE Trans. on Ant. and Prop., AP-27(3), 413-415.

Harden, B. N., J. R. Norbury, and W. J. K. White (1974), Model of intense convective rain cells for estimating attenuation on terrestrial millimeter wave radio links, Electronics Letters, 10(23), 483-484.

Harden, B. N., J. R. Norbury, and W. J. K. White (1977), Measurements of rainfall for studies of millimetric radio attenuation, Microwaves, Optics, and Acoustics, 1(6), 197-202.

Ippolito, L. J. (1981), Radio propagation for space communications systems, Proc. IEEE, 69(6), 697-727.

Ippolito, J. R., R. Kaul, and R. Wallace (1982), Propagation Effects Handbook for Satellite Systems Design. Second Edition, NASA Reference Publication 1082.

Joss, J., J. C. Thams, and A. Waldvogel (1968), The variation of raindrop size distributions at Locarno, Proc. Int. Conf. on Cloud Physics, 369-373.

Kheirallah, H. N., B. Segal, and R. L. Olsen (1980), Application of synthetic storm data to evaluate simpler techniques for predicting rain attenaution statistics, Ann. Telecommunic., 35(11-12), 456-462.

Kumar, P. N. (1981), Precipitation attenuation studies on 19/29-GHz COMSTAR beacon signals and 12-GHz radiometric measurements, 20th URSI General Assembly Meeting, Washington, D.C.

Lane, S. O., and W. L. Stutzman (1980a), Spatial rain rate distribution modeling for earth-space link propagation calculations, presented at URSI/IEEE AP-S International Symposium, Quebec, Canada.

Lane, S. O., and W. L. Stutzman (1980b), A Gaussian Rain Cell Model for Prediction of Rain Effects on Millimeter Wave Propagation, Virginia Tech Report SATCOM-80-3 under NASA Contract NAS5-22577, EE Dept., Blacksburg, VA.

Laws, J. O., and D. A. Parsons (1943), The relation of raindrop-size to intensity, Trans. Amer. Geophys. Union, 24, 452-460.

Lin, S. H. (1979), Empirical rain attenuation model for earth-space paths, IEEE Trans. Comm., COM-27(5), 812-817.

Lin, S. H., H. J. Bergmann, and M. V.Pursley (1980), Rain attenuation on earth-space paths - summary of 10-year experiments and studies, BSTJ, 39, 183-228.

Marshall, J. S., and W. M. Palmer (1948), The distribution of raindrops with size, J. Meteor., 5, 165-166.

Marui, M. and A. Paraboni (1981), Attenuation statistics at 11.6 GHz from satellite SIRIO after three years activity in Italy, Report from Institute di Elettrotecnica ed Elettronia del Politecnico di Milano.

Misme, P., and P. Waldteufel (1980), A model for attenuation by preciptation on a microwave earth-space link, Radio Science 15(3), 655-665.

Nackoney, O. G. (1979), CTS 11.7 GHz propagation measurements third year's data and final report, GTE (Waltham, Mass.) TR 79-471.3.

Olsen, R. L., D. V. Rogers, and D. B. Hodge (1978), The a R^b relation in the calculation of rain attenuation, IEEE Trans. on Ant. and Prop., AP-26(2), 318-329.

Oort, A. H., and E. M. Rasmusson (1971), Atmospheric Circulation Statistics, NOAA Professinal Paper 5, U.S. Dept. of Commerce.

Persinger, R. R., W. L. Stutzman, R. E. Castle, and C. W. Bostian (1980), Millimeter wave attenuation prediction using a piecewise uniform rain rate model, IEEE Trans. on Ant. and Prop., AP-28(2), 149-153.

Pruppacher, H. R., and R. L. Pitter (1971), A semi-empirical determination of the shape of cloud and raindrops, J. Atmos. Sci., 28, 86-94.

Ramat, P. (1981), Propagation oblique dans les bandes de frequencies des 11 et 14 GHz, Anne. de Telecomms., 36, 8-14.

Rogers, R. R. (1976), Statistical rainstorm models: Their theoretial and physical foundations, IEEE Trans. on Ant. and Prop., AP-24(4), 318-329..

Rucker, F. (1980), Simultaneous propagation measurements in the 12-GHz band on the SIRIO and OTS satellite links, URSI Open Symposium on Effects on the Lower Atmosphere on Radio Propagation at Frequencies Above 1 GHz, Paper 4.1, Lennoxville, Canada.

Sims, A., and D. Jones (1975), Frequencies of short-period rainfall rates along lines, J. App. Meteor., 14, 170-174.

Tang, D. D. and D. Davidson (1981), COMSTAR 19/19 GHz propagation experiment, II. 1979-1980, GTE Report TR 81-471.1.

Thompson, P. T., A. W. Dissanayake, and P. A. Watson (1980), The frequency dependence of microwave propagation through rainfall, AGARD Conf. on Prop. Effects in Earth-Space Paths (London), No. 284, Paper. 5.

Towner, G. C., R. E. Marshall, W. L. Stutzman, C. W. Bostian, T. Pratt, E. A. Manus, and P. H. Wiley (1982), Initial results from the VPI&SU SIRIO diversity experiment, Radio Science, 17(6), pp. 1489-1494.

Upton, S. A. J., B. G. Evans, and A. R. Holt (1980), Variations with model parameters of earth/space attenuation derived from radiometer and radar measurements, URSI Commission F Open Symposium on Effects of the Lower Atmosphere on Radio Frequencies Above 1 GHz (Lennoxville, Canada), Paper. 1.6.

Valentin, R. (1977), Attenuation and depolarization caused by rain at frequencies above 10 GHz, Proc. URSI Commission F Open Symposium (La Baule, France), 273-278.

Vogel, W. J. (1980), CTS attenuation and cross polarization measurements at 11.7 GHz, U. of Texas Final Report under Contract NAS5-22576.

Vogel, W. J. (1981), Presentation at January 1981 NASA Experimenters Meeting, Boulder, Colorado.

Watson, P. A., G. Papaionnou, and J. C. Neves (1977), Attenuation and cross-polarisation measurements at 36 GHz on a terrestrial path, Proc. URSI Commission F Open Symposium (LaBaule, France), 283-287.

Chapter 4

SINGLE PARTICLE SCATTERING COMPUTATIONS

In order to study radio wave or light wave propagation through an ensemble of scatterers, the scattering properties of individual scatterers must first be determined. Knowing the scattering properties of the individual scatterers, the effects of the ensemble of the scatterers on the propagating wave can be studied.

In this chapter, we will present the general formulation for a plane wave scattered by a single scatterer. Since the exact solution to this problem exists only when the scatterer is a sphere (Mie-solution), approximations to the general formulation will be given. After establishing calculation procedures for scattering by a single scatterer, scattering by an ensemble of scatterers will be discussed in Chapter 5.

4.1 THE SINGLE-SCATTERER PROBLEM AND SOLUTION METHODS

Let us consider a scatterer enclosed in volume V′ have permittivity and permeability μ_o. The medium in which the scatterer is embedded is vacuum, with parameters ε_o, μ_o (see Fig. 1). $\vec{E}_o$ is the incident plane wave upon the scatterer. The total electric field $\vec{E}(\vec{r})$ obeys the Fredholm

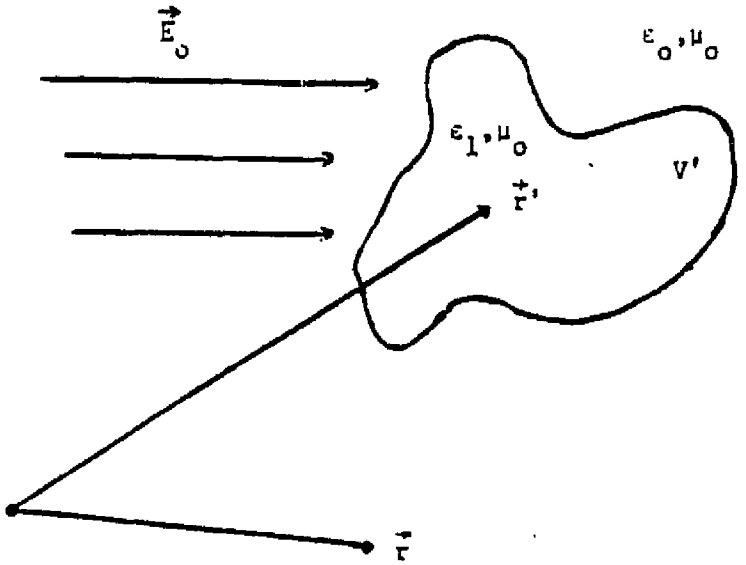

Figure 1. Geometry for scattering of a plane wave by a single particle.

integral equation [1].

$$\vec{\bar{E}}(\vec{r}) = \vec{\bar{E}}_o + (\vec{\nabla}\vec{\nabla}\cdot + k_o^2) \frac{1}{4\pi\varepsilon_o} \int_{V'} (\varepsilon - \varepsilon_o)\, \vec{\bar{E}}(\vec{r}')\, \psi(\vec{r}, \vec{r}')\, dV' \quad , \tag{1}$$

where

$$\psi(\vec{r}, \vec{r}') = \exp\{-jk_o\, |\vec{r} - \vec{r}'|\}/|\vec{r} - \vec{r}'| \tag{2a}$$

and k_o is the free space wave number

$$k_o^2 = \omega_o^2\, \mu_o\, \varepsilon_o \quad . \tag{2b}$$

Equation (1) has an exact solution only when the scatterer is a sphere (Mie-Theory). A detailed derivation for the scattered field by a sphere is presented in Ref. [2]. For arbitrary scatterers, different approximations exist to equation (1). In most practical situations, and especially in propagation through precipitation, we are interested in the scattered field in the far zone. At a large distance r from the scatterer the scalar Green's function $\psi(\vec{r}, \vec{r}')$ may be approximated as

$$\psi(\vec{r}, \vec{r}') \sim \exp\{-jk_o(\vec{r} - \hat{r}\cdot\vec{r}')\}/r \quad , \tag{3a}$$

where

$$r = |\vec{r}| \tag{3b}$$

and

$$\hat{r} = \frac{\vec{r}}{|\vec{r}|} \quad . \tag{3c}$$

Under this approximation the total field in the far zone may be written as

$$\vec{E}(\vec{r}) = \vec{E}_o + \frac{k_o^2 e^{-jk_o r}}{4\pi\epsilon_o r} \int_{V'} (\epsilon - \epsilon_o)\, \vec{E}(\vec{r}') \cdot (\bar{I} - \hat{r}\hat{r})\, e^{jk_o \hat{r} \cdot \vec{r}'}\, dV' \quad , \tag{4a}$$

where $\bar{I}$ is the unit dyadic. The field scattered by the scatterer in the far zone is given by

$$\vec{E}_s(\vec{r}) = \frac{k_o^2 e^{-jk_o r}}{4\pi\epsilon_o r} \int_{V'} (\epsilon - \epsilon_o)\, \vec{E}(\vec{r}') \cdot (\bar{I} - \hat{r}\hat{r})\, e^{jk_o \vec{r} \cdot \vec{r}'}\, dV' \quad . \tag{4b}$$

Depending on the scatterer size relative to wavelength and its dielectric constant, different approximations can be made to equation (4). In the following, three important approximations will be discussed: Rayleigh scattering, Rayleigh-Gans scattering and the WKB approximation.

a) Rayleigh Scattering [3]:

When the dimensions of the scatterer are very small relative to wavelength, in other words when $k_o|\vec{r}'| << 1$, the exponential within the integrand of (4) may be replaced by unity. Then,

$$\vec{E}(\vec{r}) = \frac{k_o^2 e^{-jk_o r}}{4\pi\varepsilon_o r} \{\vec{p} - (\vec{p} \cdot \hat{r})\hat{r}\} \quad , \tag{5a}$$

where

$$\vec{p} = \varepsilon_o \int_{V'} (\varepsilon_r - 1)\, \vec{E}(r')\, dV' \quad . \tag{5b}$$

The scatterer in this case radiates as an electric dipole of moment $\vec{p}$.

Equation (5) holds under two assumptions [4]. Let ℓ be the maximum dimension of the scatterer. Then, $k_o\ell$ must be much less than unity ($k_o \ell << 1$), and $|k \varepsilon_r \ell| << 1$. The first assumption, i.e., $k_o \ell << 1$, justifies the derivation of (5) and also indicates that the scatterer may be regarded as placed in a uniform external field. The assumption that $|k \varepsilon_r \ell| << 1$ implies that the field inside the scatterer follows the external field instantaneously, so that the phase changes are of no consequence.

The problem is thus reduced to a static one. We have to determine the internal field of the scatterer induced by a uniform electrostatic external field. By using (5b), the

dipole moment of the scatterer can be calculated from the internal field. In Ref. [5], the dipole moments of an oblate and prolate spheroid are calculated under the Rayleigh scattering assumptions. These results are used to calculate the scattering matrix of an ice-needle (prolate spheroid with eccentricity equal to one), and an ice plate (oblate spheroid with unity eccentricity).

b) Rayleigh-Gans Scattering:

The index of refraction of the scatterer is given by $\eta = \sqrt{\epsilon_r}$, where ϵ_r is the relative permittivity of the scatterer. In Rayleigh scattering, no specific assumptions about η were made. When η is approximately equal to unity, the scatterer is called diaphanaous [4]. For a diaphanous scatterer with $k_o \ell |\eta^2 - 1| << 1$, the Rayleigh-Gans [6] or Born [7] approximation holds.

In the Rayleigh-Gans approximation the field $\vec{E}(\vec{r})$ inside the scatterer is approximated with the incident field $\vec{E}_o$. Under this assumption, the far-zone scattered field $\vec{E}_s(\vec{r})$ from (4) becomes

$$\vec{E}_s(\vec{r}) = \frac{k_o^2 e^{-jk_o r}}{4\pi\epsilon_o r} \int_{V'} (\epsilon - \epsilon_o) \left(\vec{E}_o - (\vec{E}_o \cdot \hat{r})\hat{r}\right) e^{+jk_o \hat{r} \cdot \vec{r}'} dV' \qquad (6)$$

For a homogeneous diaphanous sphere (see Fig. 2) the scat-

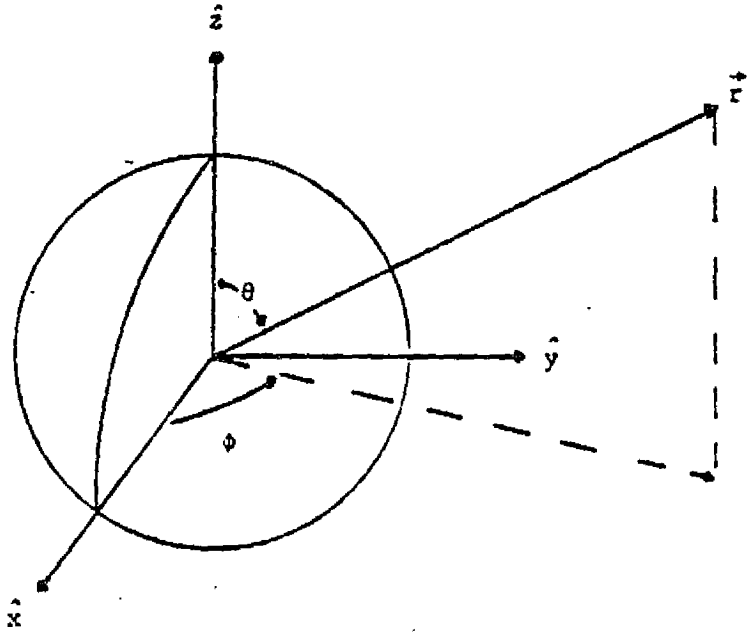

Figure 2. Geometry for scattering by a diaphanous sphere.

tered field takes the form

$$\vec{E}_s(\vec{r}) = k_o^2 \frac{e^{-jk_o r}}{4\pi\epsilon_o r} (\epsilon - \epsilon_o) \{\vec{E}_o - (\vec{E}_o \cdot \hat{r})\hat{r}\}$$

$$\int_0^{2\pi} d\phi' \int_0^{\pi} \sin\theta' \, d\theta' \int_0^{a} r'^2 \exp\{2j\, k_o \sin(\theta/2) \cos\theta'\} \, dr' \qquad (7a)$$

$$= \frac{k_o^2 e^{-jk_o r}}{\epsilon_o r} (\epsilon - \epsilon_o) \{\vec{E}_o - (\vec{E}_o \quad \hat{r})\hat{r}\} \left[\frac{\sin(2\, k_o \sin(\theta/2)a)}{2\, k_o \sin(\theta/2)}\right.$$

$$\left. - \frac{a \cos(2\, k_o \sin(\theta/2)a)}{(2\, k_o \sin(\theta/2))^2}\right] \quad , \qquad (7b)$$

where a is the radius of the sphere and θ is the angle between $\vec{r}$ and the z-axis, assuming that the origin is the center of the sphere. For more complicated shapes of scatterers the volume integral in (7a) cannot be calculated analytically and numerical solutions must be used. Exact evaluation of the volume integral can be done for ellipsoids [4].

c) High Frequency Scattering; The WKD Method:

The WKB approximation is applicable to cases where the Rayleigh or the Rayleigh-Gans approximations cannot be

applied. Specifically the WKB approximation holds when

$$|\eta^2 - 1|\, k_o \ell \gg 1 \quad \text{and} \quad |\eta^2 - 1| < 1 \quad . \tag{8}$$

In the WKB approximation and the field $\vec{E}(\vec{r})$ inside the volume V′ is approximated by a plane wave propagating in the same direction as the incident field, with propagation constant equal to

$$k^2 = \omega^2 \mu_o \epsilon_o = (\eta k_o)^2 \tag{9}$$

Under these assumptions equation (4) takes the form

$$\vec{E}(\vec{r}) \approx k_o^2 \frac{e^{-jk_o r}}{4\pi\epsilon_o r} \int_{V'} \frac{2(\epsilon - e_o)}{\eta + 1} \vec{E}_o\, e^{-j[k_o z_1 + k_o \eta(z' - z_1)]} \times e^{jk_o \hat{r} \cdot \vec{r}'}\, dV' \tag{10}$$

The incident plane wave is assumed to be propagating in the z-direction. z_1 is the value of z′ associated with $\vec{r}'$ for points lying on the surface of the scatterer as shown in Fig.3. The factor $\frac{2}{\eta + 1}$ is the normal incident transmission coefficient from a vacuum to the medium of the scatterer. The WKB approximation is part of a general mathematical method developed by Wentzel Kramers, and Brillouin [8]. According to the WKB method the field inside the scatterer

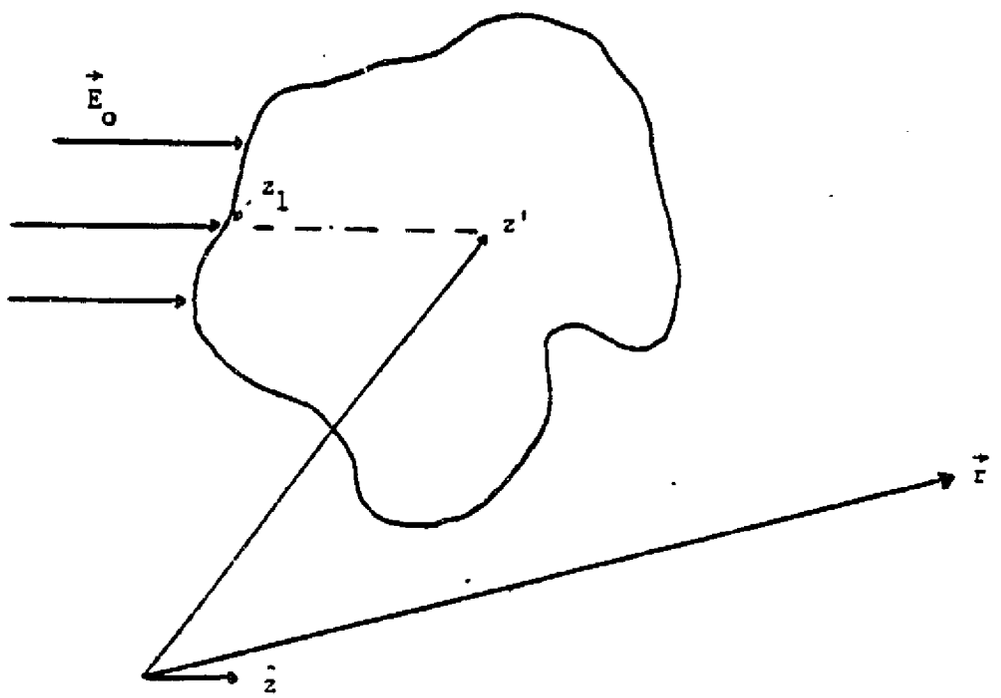

Figure 3. Geometry in calculating the scattered field by WKB approximation.

is expanded in the series

$$\vec{E}(\vec{r}) = e^{-jk_o f(\vec{r})} \{\vec{E}_o + \frac{\vec{E}_1}{k_o} + \frac{\vec{E}_2}{k_o^2} + \ldots \} \quad . \tag{11}$$

Using the above equation in conjunction with (2) and collecting together like powers of k_o, a set of equations can be obtained for $f(\vec{r})$, $\vec{E}_o$, $\vec{E}_1$, $\vec{E}_2$, ... , etc.. For high frequencies, $k_o(n^2 - 1)\ell >> 1$. In this case $\vec{E}(\vec{r})$ can be approximated by

$$\vec{E}(\vec{r}) = e^{-jk_o f(\vec{r})} \vec{E}_o \quad , \tag{12}$$

and equation (10) is obtained.

The three approximations discussed so far are valid only in specific cases when certain assumptions hold. However, in many scattering problems it is necessary to calculate the scattered field when none of the aforementioned approximations hold. For these specific problems exact analytical results do not exist. Most of the work in this area is based on numerical techniques and the use of fast computational machines. In the next few paragraphs we will summarize the most commonly used methods to calculate the scattered field by a dielectric body with complex permittivity. The majority of these methods have been used to calculate

the scattering coefficients of a spheroidal or ellipsoidal scatterer.

i) Point-Matching Technique:

In the point-matching solution the incident field, the scattered field, and the field inside the scatterer are expanded in terms of spherical wave functions. The infinite modal summations of the expansions are truncated at some model index (M, N), and boundary conditions are applied to the same number of points as the number of unknown expansion coefficients. The coefficients are then calculated by inverting a square M*N matrix that is formulated by the boundary conditions at M*N points.

The method described above has been used by Oguchi [9]. Morrison and Cross [10] also used the point-matching technique with a least squares fit. In the latter case the number of boundary points is larger than the number of unknown coefficients and the fields are matched at these points in the sense of least squares. The least squares fit technique coverges much faster than the one used by Oguchi.

ii) Spheroidal Wave Function Expansions:

The scattering properties of a spheroidal scatterer are obtained by expanding the fields in spheroidal vector wave functions and truncating the infinite summation of the expansion to a finite sum. The unknown coefficients of the

expansion functions are evaluated by applying boundary conditions. Usually, spheroidal wave function expansion methods require the boundary conditions to be applied to fewer points than the point matching technique, especially when the scatterer is a spheroid. This method has been applied by Oguchi [11].

iii) Waterman's T Matrix Formulation (Extended Boundary Condition):

This technique has been used extensively for scattering by perfectly conducting bodies. Recently, the technique has been applied to dielectrics. The scattered field is expressed in terms of electric and magnetic surface currents. These currents are expanded in terms of M_{rnm} , N_{rnm} [12] spherical harmonics. Boundary conditions are applied on an inscribed sphere inside the scatterer. By truncating the infinite expansion of the currents, the expansion coefficients can be obtained by matrix inversion.

iv) Fredholm Integral Equation Method:

This method was introduced by Holt, Uzunoglou and Evans [13]. Starting with the integral equation for scattering of (1), it is shown that the Fourier transform of the field inside the scatterer is the solution of two coupled integral equations. The integrations are reduced by numerical quadrature methods to matrix equations, whose solution can be

easily obtained. It is important to notice that the scattering amplitude obtained by this method satisfies the Schwinger variational principle, and thus the method is stable.

Of these numerical methods the most favorable are Waterman's method and the Fredholm Integral Equation method, since both converge rapidly over a wide range of scatterer sizes. It should be noted though that the latter needs a large amount of computer storage when the shape of the scatterer is complicated.

4.2 THE FREDHOLM INTEGRAL EQUATION METHOD APPLIED TO RAINDROPS

An extensive derivation of the method is described in [13]. The details of the derivation have been verified, but in this section we shall present a summary useful for performing calculations. Example calculations are performed for rain. The size of raindrops is of the order of the wavelength in the microwave region and Rayleigh or Rayleigh-Gans approximations do not hold.

The field scattered by a dielectric body of relative dielectric constant $\varepsilon_r(\vec{r})$ and volume V obeys the equation

$$\underline{\underline{E}}\,(\vec{r}) = \underline{\underline{J}}_i \exp(i\,\vec{k}_i \cdot \vec{r}) + \int_V \underline{\underline{G}}\,(\vec{r}, \vec{r}')\quad \gamma(\vec{r}')\,\underline{\underline{E}}\,(\vec{r}')d\vec{r}' \qquad (13a)$$

where

$$\underline{\underline{G}}(\vec{r}, \vec{r}') = \left[\underline{\underline{1}} + \frac{1}{k_o^2}\,\underline{\nabla}\,\underline{\nabla}\right] \frac{\exp(i\,k_o|\vec{r} - \vec{r}'|)}{4\pi\,|\vec{r} - \vec{r}'|} \tag{13b}$$

$$\gamma(\vec{r}) = k_o^2[\varepsilon_r(\vec{r}) - 1] \tag{13c}$$

k_o is the free space propagation constant, $\underline{\underline{1}}$ is the unit dyadic, $\vec{k}_i$ is the direction of propagation of the incident wave and

$$\underline{\underline{J}}_i = \underline{\underline{1}} - \vec{k}_i\,\vec{k}_i \tag{14}$$

In the far-field of the scatterer ($\vec{r} \to \infty$) the scattered field in the direction $\hat{k}_s$ is given in terms of the scattering tensor $\underline{\underline{f}}(\vec{k}_s, \vec{k}_i)$ as (see Fig. 4)

$$\underline{\underline{E}}_s(\vec{r}) = \frac{\exp(i\,k_o\,r)}{r}\,\underline{\underline{f}}(\vec{k}_s, \vec{k}_i) \tag{15a}$$

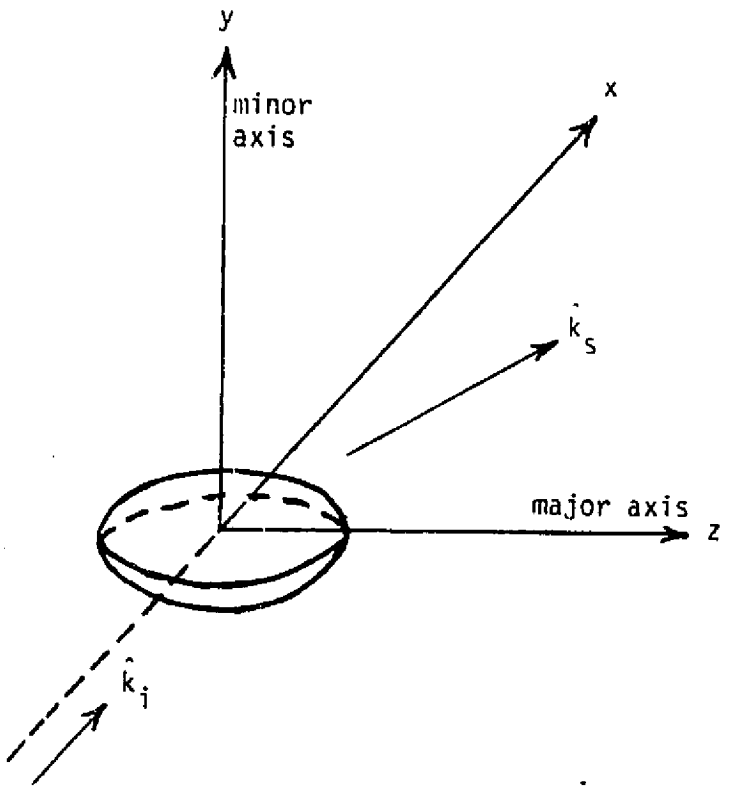

Figure 4. Geometry for electromagnetic scattering from a single spheroidal particle.

where

$$\underline{\underline{f}}(\vec{k}_s, \vec{k}_i) = \frac{1}{4\pi} \underline{\underline{J}}_s \cdot \int_v \exp(-\vec{k}_s \cdot \vec{r}) \quad \gamma(\vec{r}) \; \underline{\underline{E}}\,(\vec{r}) d\vec{r} \,. \tag{15b}$$

Let $\underline{\underline{C}}(\vec{k})$ be the Fourier transform of $\underline{\underline{E}}(\vec{r})$ with respect to $\vec{r}$. Then $\underline{\underline{f}}(\vec{k}_s, \vec{k}_i)$ can be expressed in terms of $\underline{\underline{C}}(\vec{k})$ as

$$\underline{\underline{f}}(\vec{k}_s, \vec{k}_i) = \frac{1}{4\pi} \; \underline{\underline{J}}_s \cdot \int d\, k_2 \; V(\vec{k}_s, \vec{k}_2) \; \underline{\underline{C}}(\vec{k}_2) \tag{16a}$$

where

$$V(\vec{k}_1, \vec{k}_2) = \int_v \gamma(\vec{r}) \exp\left[-i(\vec{k}_1 - \vec{k}_2) \cdot \vec{r}\right] d\vec{r} \tag{16b}$$

$\underline{\underline{C}}(\vec{k})$ obeys the integral equation

$$\int d\, \vec{k}_2 \; \underline{\underline{K}}\; (\vec{k}_1, \vec{k}_2) \cdot \underline{\underline{C}}\; (\vec{k}_2) = \underline{\underline{J}}_i \; V(\vec{k}_1, \vec{k}_i) \tag{17}$$

where

$$\underline{\underline{K}}(\vec{k}_1, \vec{k}_2) = \underline{\underline{1}} w(\vec{k}_1, \vec{k}_2) - \underline{\underline{Z}}(\vec{k}_1, \vec{k}_2) \tag{18a}$$

$$w(\vec{k}_1, \vec{k}_2) = \int_v \exp[-i(\vec{k}_1 - \vec{k}_2) \cdot \vec{r}] \, \gamma(\vec{r}) \quad \varepsilon(\vec{r}) \, d\vec{r} \qquad (18b)$$

and

$$\underline{\underline{Z}}(\vec{k}_1, \vec{k}_2) = \frac{1}{8\pi^3 \, k_o^{\,2}} \lim_{\varepsilon \to 0^+} \int \frac{p^2 \, d\, p}{p^2 - k_o^{\,2} - i\,\varepsilon} \left[\underline{\underline{1}} - \hat{p}\,\hat{p}\right] V(\vec{k}_1, \vec{p}) \; V(\vec{p}, \vec{k}_2) \qquad (18c)$$

Evaluating the integrals of (15b) and (17) by numerical quadrature we get:

$$\underline{\underline{f}}(\vec{k}_s, \vec{k}_i) = \underline{\underline{J}}_s \cdot \sum_{\ell=1}^{n} w_\ell \; \underline{\underline{C}}(\vec{k}_\ell) \; V(\vec{k}_s, \vec{k}_\ell) \qquad (19)$$

where

$$\sum_{\ell=1}^{n} w_\ell \; \underline{\underline{K}}(\vec{k}_j, \vec{k}_\ell) \cdot \underline{\underline{C}}(\vec{k}_\ell) = \underline{\underline{J}}_i \; V(\vec{k}_j, \vec{k}_i) \qquad j=1,\ldots,n \qquad (20)$$

Equation (20) can be used to solve for $\underline{\underline{C}}(\vec{k}_\ell)\, w_\ell$ by matrix inversion; and then placing these values into (19), the scattering tensor of the dielectric scatterer can be calculated.

A spheroidal dielectric scatterer obeys the equation

$$\frac{x^2}{a^2} + \frac{y^2}{b^2} + \frac{z^2}{c^2} = 1 \qquad (21a)$$

with

$$b = a \tag{21b}$$

Assuming that $\varepsilon_r(\vec{r})$ is constant and equal to ε_r, $V(\vec{k}_1, \vec{k}_2)$ for the spheroid becomes

$$V(\vec{k}_1, \vec{k}_2) = 4\pi abc\ \gamma\ j_1(X)/X \tag{22}$$

with

$$X = |\vec{k}_1 - \vec{k}_2| \tag{23}$$

and

$$\vec{k}_i = k_i\ (a \sin\ \theta_i \cos\ \phi_i,\ b \sin\ \theta_i \sin\ \phi_i,\ c \cos\ \theta_i) \tag{24}$$

$j_n(x)$ is the spherical Bessel function given by

$$j_n(x) = \left(\frac{\pi}{2x}\right)^{1/2} \underline{J}\ (n + 1/2) \tag{25}$$

Also the tensor $\underline{\underline{K}}(\vec{k}_1, \vec{k}_2)$ for spheroidal shaped scatterers takes the matrix form:

$$\underline{\underline{K}}(\vec{k}_1, \vec{k}_2) = \varepsilon_r\ \underline{\underline{I}}\ V(\vec{k}_1, \vec{k}_2) - \underline{\underline{Z}}(\vec{k}_1, \vec{k}_2) \tag{26}$$

where $\underline{\underline{I}}$ is a 3x3 unit matrix and

$$\underline{\underline{Z}}(\vec{k}_1, \vec{k}_2) = \frac{i\,8\pi\, a^4 c^2 \gamma^2}{k_o} \int_0^1 dx \frac{1}{y^2} \sum_{\substack{n=0 \\ n+m=\text{even}}}^{\infty} \sum_{m=0}^{\infty} (2m+3)\,(2n+3)$$

$$\frac{j_{n+1}(k_1)}{k_1} \frac{j_{m+1}(k_2)}{k_2} j_{m>+1}(k_o y)\, h_{m<+1}(k_o y) \qquad (27)$$

$$\sum_{s=0}^{n} \sum_{t=0}^{m} \frac{(s+1)\,(n-s)!}{(n+s+2)!} \frac{(t+1)\,(m-t)!}{(m+t+2)!} \frac{P_{n+1}^{s+1}(\chi)\, P_{m+1}^{t+1}(\chi)}{(1-x^2)} \frac{P_{n+1}^{s+1}(\chi_1)\, P_{m+1}^{t+1}(\chi_2)\, \underline{\underline{Q}}_{st}(x)}{[(1-x_1^2)(1-x_2^2)]^{1/2}}$$

with

$$y = [a^2 \cos^2 \phi + b^2 \sin^2 \phi]\,(1-x^2) + c^2 x^2 \qquad (28)$$

$$x = \cos\theta \quad , \quad y = \sin\theta \qquad (29)$$

$$\chi = cx[a^2 + (c^2 - a^2)\, x^2]^{-1/2} \qquad (30)$$

$$\chi_i = cx[a^2 + (c^2 - a^2)x^2]^{-1/2} \qquad i=1,2 \qquad (31)$$

and

$$\underline{\underline{Q}}_{st}(x) = \begin{pmatrix} I_1(s,t)-y^2\, I_6(s,t) & -y^2\, I_5(s,t) & -xy\, I_3(s,t) \\ -y^2\, I_5(s,t) & I_1(s,t)-y^2\, I_4(s,t) & -xy\, I_2(s,t) \\ -xy\, I_3(s,t) & -xy\, I_2(s,t) & y^2\, I_1(s,t) \end{pmatrix} \tag{32}$$

Notice that the matrix $\underline{\underline{Q}}_{st}(x)$ is symmetric and from (26) it is obvious that $\underline{\underline{K}}(\vec{k}_1, \vec{k}_2)$ is symmetric. The elements of the $\underline{\underline{Q}}_{st}(x)$ matrix are given below. For s+t even

$$I_1(s,t) = G(\phi_1, \phi_2) \qquad I_2 = I_3 = 0 \ .$$

$$\begin{Bmatrix} I_4(s,t) \\ I_5(s,t) \\ I_6(s,t) \end{Bmatrix} = G(\phi_1, \phi_2) \begin{Bmatrix} \sin^2(\bar{\phi}) \\ \sin\bar{\phi}\cos\bar{\phi} \\ \cos^2\bar{\phi} \end{Bmatrix} + \pi\, \delta_{st} \begin{Bmatrix} \cos(s\phi_{12}+\phi_1) \\ -\sin(s\phi_{12}+2\phi_1) \\ -\cos(s\phi_{12}+2\phi_1) \end{Bmatrix} \tag{33}$$

and for s+t odd

$$I_1(s,t) = I_4(s,t) = I_5(s,t) = I_6(s,t) = 0$$

$$\begin{Bmatrix} I_2(s,t) \\ \\ I_3(s,t) \end{Bmatrix} = G(\phi_1, \phi_2) \begin{Bmatrix} \sin \bar{\phi} \\ \\ \cos \bar{\phi} \end{Bmatrix} \tag{34}$$

where

$$G(\phi_1, \phi_2) = 2 \sum_m^1 < [\cos \phi_{12}] \tag{35}$$

$C_m^r(x)$ is the Gegenbauer polynomial

$$\phi_{12} = \phi_1 - \phi_2 \tag{36}$$

and

$$\bar{\phi} = \begin{cases} \phi_1 & s \geq t \\ \\ \phi_2 & s < t \end{cases} \tag{37}$$

In the version of (37) presented by Holt et al. the equal sign was missing in the inequality n > m.

ϕ_1, ϕ_2 are the angles of wavevectors $\vec{k}_1$, $\vec{k}_2$, respectively. See (24). In (27) $p_n^{\ell}(x)$ is the associated Legendre function and $h_h(x)$ is given by

$$h_n(x) = \left(\frac{\pi}{2x}\right)^{1/2} H^{(1)}_{n+1/2}(x) \qquad (38)$$

where $H_{n+1/2}(x)$ is the Hankel function. After finding $K(\vec{k}_j, \vec{k}_\ell)$ where $j=1, 2, \ldots, n$ $\ell = 1,2,\ldots,n$ and $V(\vec{k}_j, \vec{k}_i)$ we can solve (20) for $[\underline{\underline{C}}(\vec{k}_1, \underline{\underline{C}}(\vec{k}_2) \ldots, \underline{\underline{C}}(\vec{k}_n)]^T$. The scattering matrix $\underline{\underline{f}}(\vec{k}_s, \vec{k}_i)$ can be computed then from (19).

In calculating the element of the $\underline{\underline{Z}}(\vec{k}_1, \vec{k}_2)$ matrix the spherical Bessel and Neumann functions must be calculated as well as the associated Legendre functions and Gegenbauer polynomials. The integration in (27) required to evaluate the $\underline{\underline{Z}}(\vec{k}_1, \vec{k}_2)$ matrix was performed using a seven point Clenshaw-Curtis quadrature. The infinite summation was truncated to N terms. It was found that convergence occurred for small raindrops when N = 5 and for large raindrops when N=13. Note that these values of N were also used by Holt et al. The wave vectors $\vec{k}_1$, $\vec{k}_2$ are composed of ($x_1 = \cos\ \theta_1$, ϕ_1) and ($x_2 = \cos\ \theta_2$, ϕ_2) respectively. In (20) we chose the x pivots to be n_x with x varying between $-1 \leq x \leq 1$. The n_x pivots are equally spaced in the above interval. The pivots are equally spaced in the interval $0 \leq \phi \leq \pi$.

A Fortran computer program (called COEFF) was written. In Section 6.2 the COEFF program is described and a statement listing is presented.

Finally in this section we present the results from an example computation for raindrops using the COEFF program and compare those results to published values. Let

$$f'(0) = \mathbf{ff}\ (k_o\,\hat{x},\ k_o\,\hat{x}) \cdot \hat{z} \tag{39}$$

$$f''(0) = \mathbf{ff}\ (k_o\,\hat{x},\ k_o\,\hat{x}) \cdot \hat{y} \tag{40}$$

$f'(0)$ and $f''(0)$ are the forward scattering coefficients for incident field polarizations along the major and minor drop axes, respectively. The values $f'(0)$, $f''(0)$ were calculated for a spheroidal raindrop with a = 0.125443 cm, c = 0.172355 cm and $\varepsilon_r^2 = n_o = 7.884 + j\ 2.184$ at frequency of 11 GHz. These values were compared with one's of Holt. (See Table 1) For the above calculations the pivots n_x, n_ϕ were both equal to 5 and N=9. The execution time was 10.5 minutes. Execution time increases significantly with increasing N, n_x, and n_ϕ. Keeping n_x, n_ϕ constant, CPU execution time is proportional to N^2. For larger values of a, N must be increased which causes a large increase in execution time.

	Values computed using COEFF	Values from Holt et al
f'(0)	0.2479 + j 0.0204	0.2473 + j 0.02045
f"(0)	0.03517 + j 0.02379	0.03513 + j 0.02383

Table 1

Comparison of Scattering Coefficient Values for a Raindrop at 11 GHz.

4.3 THE SINGLE-PARTICLE SCATTERING TENSOR

We have seen that single-particle scattering coefficients can be calculated by one of a variety of analytical or numerical methods. These results are then to be used in computing the scattering effects of an ensemble of particles in precipitation media. This is facilitated by casting the single-particle problem into a tensor form. In this section we discuss the single-particle tensor in preparation for use in the multiple scattering algorithm for rain in Chapter 5.

For an incident plane wave propagating in the z-direction with electric field $\vec{E}_o$, the far zone scattered field of (4) has electric field components perpendicular to the direction of scattering and can be expressed as

$$\vec{E}_s(\vec{r}) = \frac{e^{-jkr}}{r} \bar{f}(\vec{r})\, \vec{E}_o \quad , \tag{41}$$

where $\bar{f}(\vec{r})$ is the scattering tensor of the scatterer. For example, in the case of Rayleigh-Gans scattering it follows from (6) that the scattering tensor is given by

$$\bar{f}(\vec{r}) = \frac{k_o^2}{4\pi\epsilon_o} \int_{V'} (\epsilon - \epsilon_o)\, (\bar{I} - \hat{r}\hat{r})\, e^{+jk_o \hat{r} \cdot \vec{r}'}\, dV' \tag{42}$$

Equation (41) may be written in a matrix form as

$$\begin{bmatrix} E_{x_s} \\ E_{y_s} \end{bmatrix} = \frac{e^{-jkr}}{r} \underline{f}(r) \begin{bmatrix} E_{ox} \\ E_{oy} \end{bmatrix} , \qquad (43)$$

where $\underline{f}(\vec{r})$ is a 2x2 matrix corresponding to the scattering tensor

$$\underline{f}(\vec{r}) = \begin{bmatrix} f_{11} & f_{12} \\ f_{21} & f_{22} \end{bmatrix} \qquad (44)$$

4.4 REFERENCES

1. J. Stratton, Electromagnetic Theory McGraw Hill Book Co., New York, 1941.

2. M. Kerker, The Scattering of Light, Academic Press, New York 1969.

3. Lord Rayleigh, Phil Mag., vol. 44, p. 28, 1897.

4. D. S. Jones, The Theory of Electromagnetism, MacMillan Company, New York, 1964.

5. W. L. Stutzman, W. P. Overstreet, C. W. Bostian, A. Tsolakis and E. A. Manus, "Ice Depolarization on Satellite Radio Paths," Final Report for Intelsat Contract, INTEL-123, VPI&SU EE Dept., April 1981.

6. R. Gans, Ann. Phys., vol. 37, p. 881, 1912.

7. A. Ishimaru, Wave Propagation and Scattering in Random Media, Academic Press, New York, 1978.

8. L. I. Schi-f, Quantum Mechanics, McGraw-Hill Co., New York, 1955.

9. T. Oguchi, "Attenuation of electromagnetic wave due to rain with disturted raindrops," J. Radio Res. Labs., vol. 33, pp. 467-485, 1960.

10. J. A. Morrison and T. S. Chu, "Perturbation calculations of rain-induced differential attenuation and differential phase shift at microwave frequencies," vol. 52, pp. 1907-1913, Dec. 1973.

11. T. Oguchi and Y. Hosoya, "Differential attenuation and differential phase shift of radio waves due to rain: Calculations at microwave and millimeter wave regions," J. de Rech. Atm.,vol. 8, pp. 121-128, 1974.

12. P. M. Morse and H. Feshback, Methods of Theoretical Physics, McGraw-Hill, New York, 1953.

13. A. R. Holt, N. K. Uzunoglou, and B. G. Evans, "An integral equation solution to the scattering of electromagnetic radiation by dielectric spheroids and ellipsoids," IEEE Trans. Ant. Prop., vol. AP-26, pp. 706-712, 1978.

Chapter 5

MULTIPLE SCATTERING COMPUTATIONS

5.1 Introduction

Scattering problems involving more than one scatterer are complicated and, in general, analytical solutions do not exist. It is necessary to make certain simplifying assumptions. Typically it is assumed that the scatterers are randomly distributed, are infinite in number, and are in the far zone of each other. In this paper a general approach to scattering from particulate media which includes multiple scattering is presented. The results are applied to the problem of millimeter wave propagation through rain. An excellent review of the role of multiple scattering in radiowave propagation through precipitation is given by Olsen [1982].

Scattering by random distributions of scatterers was first studied by Rayleigh [1871], who used a single-scattering approximation and identical, aligned scatterers. A detailed derivation of Rayleigh's results is available [Van de Hulst,1957]. The single-scattering approximation does not hold when the density of scatterers is large or the propagating wave frequency is high. Improved accuracy over that using single-scattering is possible using first-order multiple scattering or complete multiple scattering.

In this chapter equations are derived for the average vector electric field $\langle \vec{E}(\vec{r}) \rangle$ in the presence of a random distribution of scatterers using, first, lower order scattering

approximations and, second, the multiple scattering approach. In Section 5.2 the single-scattering approximation is used to derive expressions for the coherent electric field in an ensemble of scatterers with random distributions of location, size, shape, and orientation. These results are used to treat the ensemble of scatterers in which particle scattering only occurs once but the incident wave on each particle has included the effects of previous particles; this is first-order multiple scattering. In Section 3 complete multiple scattering is considered in which the field incident on a particle can arise, in part, from fields scattered from any other particles. The Foldy-Twersky scattering procedure is used to derive an integral equation for the vector coherent field in an ensemble of particles. In Section 4 multiple scattering results are applied to the rain propagation problem. Some typical calculations are performed.

5.2 Lower Order Scattering

Scattering from discrete media that does not include all orders of multiple scattering has been studied from various approaches by many investigators. An excellent review was prepared by Ishimaru [1977]. In this section we discuss two of these which have been applied to the rain propagation problem.

Single scattering

Under the single-scattering approximation, the electric field is scattered only once by the scatterers. Let us consider specifically the slab of scatterers of thickness L shown in Fig. 1, with a plane wave incident upon it. Each scatterer (say the p^{th} one) can have a random position $\vec{r}_p$, size as measured by the equivolumetric radius a_p, shape as represented by the shape parameter s_p, and orientation angle represented by θ_p. The field at point $\vec{r}$, where the receiving antenna is located, is the incident field plus the field scattered by particles in the active region of the slab; the active region is the central few Fresnel zones. Summing over the contributions from N particles in the active region, we obtain

$$\vec{E}(\vec{r}) = \vec{E}^i + \sum_{p=1}^{N} \frac{e^{-j\, k_o (x_p^2 + y_p^2)/2\, r_p}}{r_p} \bar{f}_p(\vec{r}) \cdot \vec{E}^i(\vec{r}) \quad , \quad (1)$$

where $\bar{f}_p(\vec{r})$ is the scattering tensor of the p^{th} scatterer and $r_p = |\vec{r}_p|$.

In order to compute the average field at point $\vec{r}$ we assume that the scatterers are randomly distributed in position, size, shape, and orientation angle, and that all of them have the same particle distribution

$$\frac{n(\vec{\omega}_p)}{N} \quad , \quad (2)$$

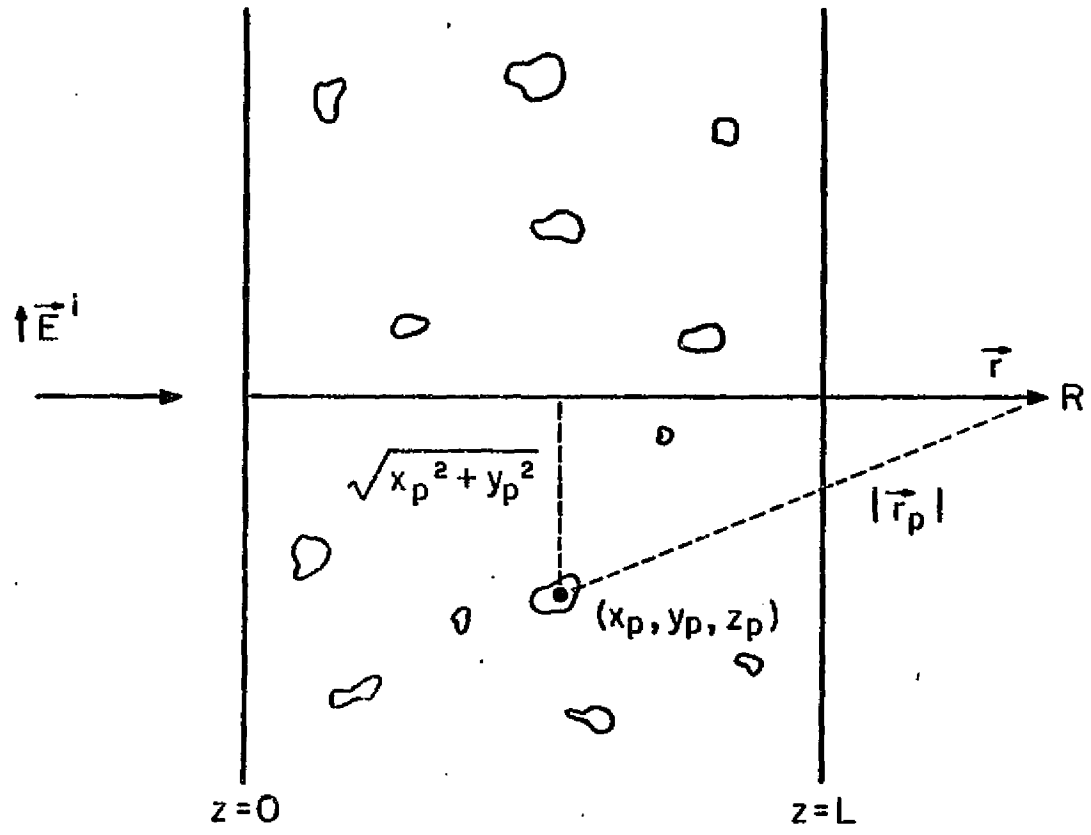

Figure 1. A plane wave propagating through a slab of scatterers.

where $\vec{\omega}_p$ represents the random parameters of position $\vec{r}_p$, size a_p, shape s_p, and orientation angle θ_p. $n(\vec{\omega}_p)$ is the number of scatterers per unit volume for particles in class $\vec{\omega}_p$.

Equation (1) is averaged using the distribution given in (2):

$$\langle \vec{E}(\vec{r}) \rangle = \left[\bar{\bar{I}} + \int_{r',\omega} \bar{\bar{f}}(r') \frac{e^{-jk_o(x'^2 + y'^2)/2r'}}{r'} n(r',\omega) dr' d\omega \right] \cdot \vec{E}^i \qquad (3)$$

Here, $dr' = dx'dy'dz'$ is the elemental volume of space, and ω encompasses the distribution parameters for the particle size, shape, and orientation, $\omega = (a, s, \theta)$.

Since major contributions arise from particles in the first few Fresnel zones, r' is nearly independent of x', and y' in in the integral appearing in (3). We can make then the substitutions

$$x_1 = \sqrt{\frac{jk_o}{2r'}}\, x' \quad , \quad y_1 = \sqrt{\frac{jk_o}{2r'}}\, y' \quad , \quad z_1 = z' \qquad (4)$$

giving

$$\langle \vec{E}(\vec{r}) \rangle = \left[\bar{\bar{I}} + \frac{2}{jk_o} \int_{\omega} d\omega \int_{z_1} dz_1 \int_{-\infty}^{\infty} dx_1 \int_{-\infty}^{\infty} dy_1\, e^{-(x_1^2 + y_1^2)}\, \bar{\bar{f}}\, n(r_1, \omega) \right] \cdot \vec{E}^i(\vec{r}) \quad . \qquad (5)$$

Using the relationship

$$\int_{-\infty}^{\infty} e^{-u^2}\, du = \sqrt{\pi} \quad , \tag{6}$$

and assuming that $n(r_1, \omega)$ varies only in the direction of propagation z, (5) gives

$$\langle \vec{E}(\vec{r}) \rangle = \left[\bar{I} + \frac{2\pi}{jk_o} \int \bar{f}\, n(z_1, \omega)\, dz_1 d\omega \right] \cdot \vec{E}^i(\vec{r})$$

$$\equiv [\bar{I} - j\bar{k}] \cdot \vec{E}^i(\vec{r}) \tag{7}$$

where

$$\bar{k} = \frac{2\pi}{k_o} \int \bar{f}\, n(z_1, \omega)\, dz_1 d\omega \quad . \tag{8}$$

If the elements of the tensor $\bar{k}$ are small, the quantity $\bar{I} - j\bar{k}$ may be approximated by an exponential. This step is further motivated by our knowledge that the exponential form includes multiple scattering effects as it will be shown in Section 5.3. Within the framework of this approximation (7) can be written in the matrix form as

$$\langle \underline{E}(\vec{r}) \rangle = e^{-j\underline{k}}\, \underline{E}^i(\vec{r}) \tag{9}$$

Here, $\langle \underline{E}(\vec{r}) \rangle$ is the column matrix corresponding to the vector $\langle \vec{E}(\vec{r}) \rangle$. Similarly, $\underline{E}^i(\vec{r})$ is the column matrix associated with $\vec{E}^i(\vec{r})$ and $\underline{k}$ the matrix corresponding to the tensor $\bar{k}$.

The coherent field scattered by a slab of scatterers can, in general, be written as

$$\langle \vec{E}^s(\vec{r}) \rangle = \bar{D} \cdot \vec{E}^i(\vec{r}) \tag{10}$$

where $\bar{D}$ is the scattering tensor of the slab and depends on the scattering properties of the individual scatterers and their random distribution in position, size, shape, and orientation angle. Specifically, for the single scattering case

$$\bar{D} = \bar{I} - j\frac{2\pi}{k_o} \int_{z_1,\omega} \bar{f}(\omega)\, n(z_1, \omega)\, dz_1 d\omega \quad . \tag{11}$$

In the derivation of this result the assumption was made that the plane wave is scattered only once by the particles. This assumption is unrealistic, since the wave may be scattered several times by the particles before reaching the point R at position $\vec{r}$. When the scattering coefficients of the particles and the particle density are small, contributions to the scattered wave by second, third, and higher order scattering may be ignored. There are cases, however, where the scattering coefficients of the scatterer are large (e.g., for raindrops above 30 GHz), and the multiple scattering contributions cannot be ignored. Starting with the next section we will take into consideration multiple-scattering contributions.

First-order multiple scattering by a slab of scatterers

Under the first-order multiple scattering approximation, the slab of particles of length L is divided into n thin subslab's. In each individual subslab the single approximation is assumed to hold. The coherent field at point R is then given by

$$\langle \vec{E}(\vec{r}) \rangle = \bar{D}_1 \cdot \bar{D}_2 \cdot \ldots \bar{D}_n \cdot \vec{E}^i(\vec{r}) \qquad (12)$$

where $\bar{D}_i$ is the scattering tensor of the i^{th} subslab and is defined by (11). This first-order multiple scattering approach has been used by a number of researchers in different areas of wave propagation. In radio wave propagation through precipitation, for example, Persinger et al. [1980] have used a computerized code to evaluate (12) in order to calculate attenuation and isolation of a wave propagating through a medium consisting of ice-particles and rain.

5.3 Multiple Scattering

Single scattering holds only when the scattering coefficients and the density of the particles are small. First-order multiple scattering holds for any forward scattering propagation situation provided that the thickness of each subslab is kept small. As shown in (12), the coherent field in this case contains the dot products of a large number of

tensors and its evaluation can be performed only by fast digital machines.

In order to include both forward and backward multiple scattering, we will use an approach first introduced by Foldy [1945] and developed further by Lax [1951] and Twersky [1962]. In our formulation we will assume that the medium is anisotropic, and we will derive the Dyson equation for the coherent vector electric field in terms of the scattering tensor of the individual scatterers and their distribution in location, size, shape and orientation.

Derivation of the general multiple scattering integral equation

Let N scatterers be randomly distributed in space, and have random size, shape, and orientation. The medium between any two scatterers is free space. (See Fig. 2) The vector electric field $\vec{E}(\vec{r})$ between the scatterers satisfies the Helmholtz equation

$$(\nabla^2 + k_o^2)\ \vec{E}(\vec{r}) = 0 \quad , \tag{13}$$

where k_o is the free space propagation constant.

The incident field $\vec{E}^a$ at the point $\vec{r}_a$ is the sum of the incident electric field $\vec{E}_i{}^a$ in the absence of the scatterers and the field scattered by the N scatterers, spe-

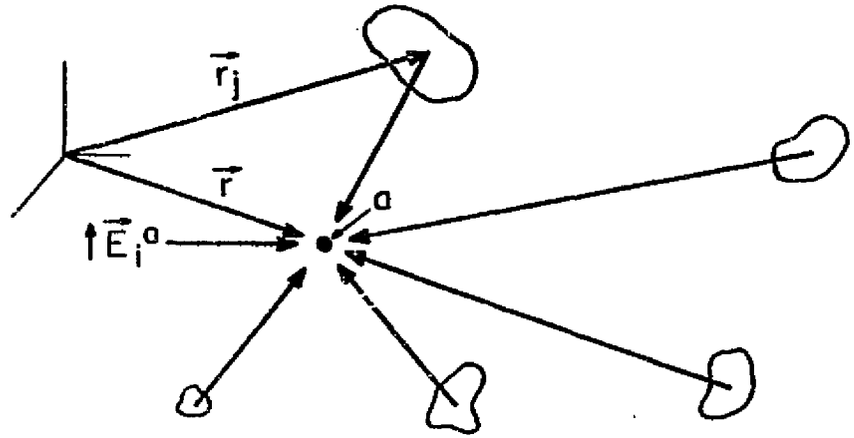

Figure 2. Geometry for multiple scattering. The total field at point a, $\vec{E}^a$, is the sum of the incident field in the absence of scatterers, $\vec{E}_i^a$, plus the fields scattered from all other particles.

cifically, we have

$$\vec{E}^a = \vec{E}_i^a + \sum_{j=1}^{N} \vec{G}_j^a \quad , \tag{14}$$

where $\vec{G}_j^a$ is the field at position $\vec{r}$ that is scattered by the j^{th} scatterer. The latter is a function of the scattering properties of the j^{th} scatterer at position $\vec{r}_j$ and the location $\vec{r}$. We can define a tensor $\bar{g}_j^a$ such that

$$\vec{G}_j^a = \bar{g}_j^a \cdot \vec{E}^j \quad . \tag{15}$$

The field incident on the jth particle is

$$\vec{E}^j = \vec{E}_i^j + \sum_{k=1,k\neq j}^{N} \vec{G}_k^j \quad . \tag{16}$$

Substituting (16) into (15) we obtain

$$\vec{G}^j = \bar{g}_j^a \cdot [\vec{E}_i^j + \sum_{k=1,k\neq j}^{N} \vec{G}_k^j] \quad . \tag{17}$$

Using (17) and (14), we have

$$\vec{E}^a = \vec{E}_i^a + \sum_{j=1}^{N} \bar{g}_j^a \cdot \vec{E}_i^j + \sum_{j=1}^{N} \sum_{k=1,k\neq j}^{N} \bar{g}_j^a \cdot \bar{g}_k^j \cdot \vec{E}^k \quad . \tag{18}$$

By iterating the above process it follows that

$$\vec{E}^a = \vec{E}_i^a + \sum_{j=1}^{N} \bar{g}_j^a \cdot \vec{E}_i^j + \sum_{j=1}^{N} \sum_{k=1,k\neq j}^{N} \bar{g}_j^a \cdot \bar{g}_k^j \cdot \vec{E}_i^k$$

$$+ \sum_{j=1}^{N} \sum_{k=1,k\neq j}^{N} \sum_{\ell=1,\ell\neq k}^{N} \bar{g}_j^a \cdot \bar{g}_k^j \cdot \bar{g}_\ell^k \cdot E_i^\ell + \ldots . \quad (19)$$

The triple summation in (19) may be written as

$$\sum_{j=1}^{N} \sum_{k=1,k\neq j}^{N} \sum_{\ell=1,\ell\neq k}^{N} \bar{g}_j^a \cdot \bar{g}_k^j \cdot \bar{g}_\ell^k \cdot \vec{E}_i^\ell$$

$$= \sum_{j=1}^{N} \sum_{k=1,k\neq j}^{N} \sum_{\ell=1,\ell=k,\ell\neq j}^{N} \bar{g}_j^a \cdot \bar{g}_k^j \cdot \bar{g}_\ell^k \cdot \vec{E}_i^\ell$$

$$+ \sum_{j=1}^{N} \sum_{k=1}^{N} \bar{g}_j^a \cdot \bar{g}_k^j \cdot \bar{g}_j^k \cdot \vec{E}_i^j \quad . \quad (20)$$

Assuming that backscattering is smaller than forward scattering, the second summation in (20) may be ignored, and (19) may be written as

$$\vec{E}^a = \vec{E}_i^a + \sum_{j=1}^{N} \bar{g}_j^a \cdot \vec{E}_i^j + \sum_{j=1}^{N} \sum_{k=1,k\neq j}^{N} \bar{g}_j^a \cdot \bar{g}_k^a \cdot \vec{E}_i^k$$

$$+ \sum_{j=1}^{N} \sum_{k=1,k\neq j}^{N} \sum_{\ell=1,\ell\neq k,\ell\neq j}^{N} \bar{g}_j^a \cdot \bar{g}_k^j \cdot \bar{g}_\ell^k \cdot \vec{E}_i^\ell + \ldots \quad . \quad (21)$$

Another way to state the significance of the approximation

involved in this equation is that we have ignored the following: triple scattering between two scatterers, fourth order scattering between three scatterers, and so on. The above procedure was first introduced by Twersky [1962] in order to obtain a closed form equation for the coherent field.

We next make the assumption, as in Section 2, that the scatterers have the same position, size, shape, and orientation distribution, and that there are no correlations between scatterers. The particle distribution may be defined as in (2). However, now N is the total number of particles in the entire volume. Taking the ensemble average of (21), we obtain an expression for the coherent field at point r:

$$\langle \vec{E}^a \rangle = \vec{E}_i^{\,a} + \sum_{j=1}^{N} \int_{\vec{\omega}_j} \bar{g}_j^{\,a} \cdot \vec{E}_i^{\,j} \frac{n(\vec{\omega}_j)}{N} d\vec{\omega}_j + \sum_{j=1}^{N} \sum_{k=1,k\neq j}^{N}$$

$$\int_{\vec{\omega}_j} \int_{\vec{\omega}_k} \bar{g}_j^{\,a} \cdot \bar{g}_k^{\,j} \cdot \vec{E}_i^{\,k} \frac{n(\vec{\omega}_j)n(\vec{\omega}_k)}{N^2} d\vec{\omega}_j\, d\vec{\omega}_k + \sum_{j=1}^{N} \sum_{k=1,k\neq j}^{N} \sum_{\ell=1,\ell\neq k,\ell\neq j}^{N}$$

$$\int_{\vec{\omega}_j} \int_{\vec{\omega}_k} \int_{\vec{\omega}_\ell} \bar{g}_j^{\,a} \cdot \bar{g}_k^{\,a} \cdot \bar{g}_\ell^{\,k} \cdot \vec{E}_i^{\,\ell} \frac{n(\vec{\omega}_j)n(\vec{\omega}_k)n(\vec{\omega}_\ell)}{N^3} d\vec{\omega}_j\, d\vec{\omega}_k\, d\vec{\omega}_\ell + \ldots \tag{22}$$

or

$$\langle \vec{E}^a \rangle = \vec{E}_i{}^a + \int_{\vec{\omega}_j} \bar{g}_j{}^a \cdot \vec{E}_i{}^j \, n(\vec{\omega}_j) \, d\vec{\omega}_j + \frac{N-1}{N} \int_{\vec{\omega}_j, \vec{\omega}_k} \bar{g}_j{}^a \cdot \bar{g}_k{}^j \cdot \vec{E}_i{}^k$$

$$n(\vec{\omega}_j) n(\vec{\omega}_k) d\vec{\omega}_j \, d\vec{\omega}_k + \frac{N-2}{N} \int_{\vec{\omega}_j, \vec{\omega}_k, \vec{\omega}_\ell} \bar{g}_j{}^a \cdot \bar{g}_k{}^j \cdot \bar{g}_\ell{}^k \cdot \vec{E}_i{}^\ell$$

$$n(\vec{\omega}_j) n(\vec{\omega}_k) n(\vec{\omega}_\ell) \, d\vec{\omega}_j \, d\vec{\omega}_k \, d\vec{\omega}_\ell + \ldots . \qquad (23)$$

By letting N tend to infinity, the ratios $\frac{N-1}{N}$, $\frac{N-2}{N}$, etc., tend to unity, and the infinite summation in (23) can be represented by the integral equation

$$\langle \vec{E}^a \rangle = \vec{E}_i{}^a + \int_{\vec{\omega}_j} \bar{g}_j{}^a \cdot \langle \vec{E}^j \rangle \, n(\vec{\omega}_j) \, d\vec{\omega}_j \quad . \qquad (24)$$

This is the Dyson equation for the coherent field in an ensemble of randomly distributed scatterers, and it is often called the Foldy-Lax-Twersky equation. It has been derived on the basis of the Twersky procedure. The same equation may also be obtained using Lax's polycrystaline approximation [Lax, 1951].

The Dyson equation, (24), is more general than the equations for the coherent field derived by the single scattering or first-order multiple scattering approximations; it includes backscattering. Evaluation of (24) is very difficult and depends on the complexity of the operator $\bar{g}_j{}^a$. If the medium is tenuous (the average distance d between any

two arbitrary scatterers much greater than the free space wavelength, i.e., $k_o d >> 1$), then each scatterer is in the far zone of all other scatterers, and $\bar{g}_j^a$ may be replaced by

$$\bar{g}_j^a = \frac{e^{-jk_o|\vec{r} - \vec{r}_j|}}{|\vec{r} - \vec{r}_j|} \bar{f} \quad , \tag{25}$$

where $\bar{f}$ is the scattering tensor for the scatterer.

Evaluation of multiple scattering for plane wave incidence

Most practical situations (such as in communications applications) are well approximated by a plane wave incident normally on a slab of scatterers as described in the previous section. Let a plane wave be propagating in the z-direction with electric field

$$\vec{E}_i = \vec{E}_o e^{-jk_o z} \quad .$$

The average field $\langle\vec{E}\rangle$ inside the slab obeys the vector Foldy-Lax-Twersky integral equation of (24). The medium of the scatterers is assumed to be tenuous, so that the scattering operator $\bar{g}_j^a$ can take the form shown in (25). Substituting (25) into (24) and evaluating at the observation point a with position vector $\vec{r}$,

$$\langle\vec{E}(\vec{r})\rangle = \vec{E}_o e^{-jk_o z} + \int_{\vec{\omega}_j} \bar{f}_j(\hat{z}, \vec{r}-\vec{r}_j)\langle\vec{E}^j\rangle \frac{e^{-jk_o|\vec{r}-\vec{r}_j|}}{|\vec{r} - \vec{r}_j|} n(\vec{\omega}_j)\, d\vec{\omega}_j \tag{26}$$

where $|\vec{r}-\vec{r}_j| = [(x-x_j)^2 + (y-y_j)^2 + (z-z_j)^2]^{1/2}$ and $\omega_j = (\vec{r}_j\ a_j,\ s_j,\ \theta_j)$. The medium is assumed to vary only in the z-direction and, therefore, the fields will also. Evaluation of (26) then proceeds by noting that the medium is assumed to be homogeneous in the x,y-plane and employing the method of stationary phase to reduce the integral giving

$$\langle\vec{E}(z)\rangle = \vec{E}_o\ e^{-jk_o z} + \frac{2\pi j}{k_o}\int_\omega \bar{f}\ \langle\vec{E}(z')\rangle\ e^{-jk_o(z-z')}\ n(\omega)\ d\omega \qquad (27)$$

where $\omega = (z',\ a,\ s,\ \theta)$ and $\bar{f}$ is the single-particle forward scattering tensor. The sclution to this integral equation in matrix form is

$$\langle\underline{E}(z)\rangle = e^{-j\underline{k}}\ E_o\ e^{-jk_o z} \qquad (28a)$$

where

$$\underline{k} = \frac{2\pi j}{k_o}\int_\omega \underline{f}\ n(\omega)\ d\omega \qquad (28b)$$

A similar solution has been reported [Oguchi, 1981] in the case where the medium was uniform in the z-direction.

Note that (28) is the same as (9). Thus, the exponential approximation to the derived single-scattering formula in (7) is justified on the basis that it really includes multiple scattering effects.

The equations derived in this section for the coherent vector electric field can be used to study radio wave propagation through precipitation media which vary in composition along the direction of propagation. This is explored in the next section.

5.4 Applications to Rain Media

The results of the derivation in the previous section can be applied to precipitation media. Here we consider rain. The formulation has the following features: it includes multiple scattering effects; it allows for direct inclusion of distributions of raindrop sizes, shapes, and canting angles; and it allows for a nonuniform rain rate along the propagation path. Most models used to make actual calculations for rain do not have such flexibility. Quite frequently the rain is assumed to be of uniform rate over some path length, the canting angle distribution is omitted or is included by modifying a constant canting angle result, and/or all drop shapes are alike.

Persinger et al. [1980] presented a first-order multiple scattering model that included a nonuniform spatial rain rate variation as well as raindrop canting angle and shape distributions. In this section we use the ideas of Persinger et al. together with the multiple scattering model to make calculations for rain media.

The scattering matrix for single raindrops

The equivolumetric radius of the raindrops varies from 0.1 to 4.0 mm. At millimeter wave frequencies the raindrop radius is comparable with the free space wavelength and the Rayleigh scattering approximation is not adequate for the calculation of the raindrop scattering matrix. It is necessary then to use one of the available numerical methods [Oguchi, 1981] to calculate the raindrop scattering coefficients. In our computations we will use values of scattering coefficients published by Uzunoglu et al. [1977]. These results have been computed using the Fredholm integral equation method. We will assume that the raindrops are either spherical or oblate spheroids.

Let θ be the canting angle of the oblate raindrop. The single raindrop scattering matrix is given by

$$\underline{f} = \frac{1}{2}\begin{bmatrix} f_V(a)+f_H(a)+\cos 2\theta[f_H(a)-f_V(a)] & [f_V(a)-f_H(a)]\sin 2\theta \\ [f_V(a)-f_H(a)]\sin 2\theta & f_V(a)+f_H(a)+\cos 2\theta[f_V(a)-f_H(a)] \end{bmatrix} \quad (2a)$$

In this expression, a is the equivolumetric radius of the oblate raindrop, and $f_V(a)$, $f_H(a)$, are the scattering coefficients for the incident electric field aligned with the minor and major axes, respectively. The quantities $f_V(a)$, $f_H(a)$ are expressed in terms of powers of the

equivolumetric radius of the raindrop; specifically,

$$f_H V(a) = \sum_{i=0}^{5} \alpha_i \, {}_H V \, a^i \qquad (30)$$

Values of $\alpha_i {}_H V$ are obtained by curve fitting published tabular results in terms of size, at a specific elevation angle.

Rain medium computations

The rain medium is represented by a slab of raindrops of extent L. With plane wave incidence the coherent field propagating inside the rain medium obeys (28), where the single drop scattering matrix $\underline{f}$ is given by (29). In $n(z', \omega)$ $n(\omega)$ of (28), z' is the distance along the direction of propagation into the rain slab, a is the equivolumetric radius for the individual raindrops, s is the shape of the raindrop (spherical or oblate speroidal), and θ is the raindrop canting angle. In the distribution density function $n(\omega)$ of (28b) θ and s are assumed to be statistically independent; i.e.

$$n(\omega) = n_o(z', a) \; p_1(\theta) \; p_2(s) \quad . \qquad (31)$$

$p_2(s)$ is a discrete shape distribution density function in which F_o is the fraction of drops that are oblate spheroidal and the remaining fraction $1 - F_o$ are spherical. The canting angle distribution is Gaussian with mean $\langle\theta\rangle$ and

standard deviation σ_θ:

$$p_1(\theta) = \frac{1}{\sqrt{2\pi}\,\sigma_\theta} e^{-(\theta-<\theta>)^2/2\sigma_\theta^2} \qquad (32)$$

For $n_o(z, a)$ we use the drop size distribution of Marshall and Palmer [1948] with rain rate as a function of position:

$$n_o(z, a) = 16{,}000\, e^{-8.2[R(z)^{-0.21}]a} \quad m^{-3}\,mm^{-1} \quad . \qquad (33)$$

The rain rate spatial variation used in the examples to follow is piecewise uniform as introduced by Persinger et al. [1980], where

$$R(z) = \begin{cases} R_o \left[\frac{R_o}{10}\right]^{-0.66} & 0 \leq z \leq 0.2L \\ R_o & 0.2\,L \leq z \leq L \end{cases} \qquad (34)$$

in which R_o is the point rainfall rate at the receiving station ($z = L$).

Evaluation of $\underline{k}$ in (28b) can proceed after substituting in the above stated information on the distributions:

$$\underline{k} = \frac{2\pi}{k_o} \int_o^L dz' \int_o^\infty da \int d\theta \, \{(1-F_o)\, \underline{f}^{SPH}(a) + F_o\, \underline{f}^{OBL}(a,\theta)\} n_o(z', a) \Gamma_1(\theta) \quad . \qquad (35)$$

The integral over the angle θ may be performed by first

evaluating the expressions

$$\langle \sin 2\theta \rangle = \int_{\langle\theta\rangle-\alpha}^{\langle\theta\rangle+\alpha} d\theta \sin 2\theta \; p_1(\theta) \;, \quad \langle \cos 2\theta \rangle = \int_{\langle\theta\rangle-\alpha}^{\langle\theta\rangle+\alpha} d\theta \cos 2\theta \; p_1(\theta) \tag{36}$$

where α is the maximum variation of the canting angle. It can be shown that (36) is approximated by

$$\langle \sin 2\theta \rangle = \exp(-2\sigma_\theta{}^2) \sin 2\langle\theta\rangle \tag{37}$$

and, similarly,

$$\langle \cos 2\theta \rangle = \exp(-2\sigma_\theta{}^2) \cos 2\langle\theta\rangle \quad . \tag{38}$$

With these approximations the average scattering matrix $\underline{k}$ becomes

$$\underline{k} = \frac{2\pi}{k_o} \int_0^L dz' \int_0^\infty da\{(1-F_o)\underline{f}^{SPH}(a) + F_o\langle \underline{f}^{OBL}(a)\rangle\} n_o(z,a) \tag{39}$$

where $\langle \underline{f}^{OBL}(a)\rangle$ is the average of $\underline{f}^{OBL}(a, \theta)$ with respect to θ, and is obtained from $\underline{f}(a, \theta)$ by replacing $\sin 2\theta$, $\cos 2\theta$ with $\langle \sin 2\theta \rangle$ and $\langle \cos 2\theta \rangle$, respectively.

The scattering coefficients $f^{SPH}(a)$, $f_{V,H}^{OBL}(a)$ are expressed, as in (30), in terms of powers of a up to the fifth order. Then the final evaluation of (39) follows

after performing the indefinite integral

$$I = \int_o^L dz' \int da\ \underline{f}(a)\ n_o(z', a)$$

$$= \sum_{n=0}^{5} c_n \int_o^L dz' \int da\ a^n\ e^{-\gamma(z)a} \qquad (40)$$

where $\gamma(z') = -8.2\ R(z')^{-0.21}$ and c_n are the expansion coefficients as in (30). Integrating over a and substituting in the rain rate variation of (34) and performing the final integration gives

$$I = \sum_{i=1}^{2} \ell_i \sum_{n=0}^{5} c_n \left[\sum_{m=1}^{n} \frac{n!}{(n-m)!} \frac{(a)^{n-m}}{\gamma_i^{m+1}} (-1)^m + \frac{a^n}{\gamma_i} \right] \qquad (41)$$

where $\ell_1 = 0.2L$, $\ell_2 = 0.8L$, and $\gamma_i = \gamma(\ell_i)$.

The elements of the matrix $\underline{k}$ have been evaluated explicity with (39) and (41). The depolarization matrix $e^{-j\underline{k}}$ of (28a) is then evaluated using eigenvalue-eigenvector methods. After the depolarization matrix is evaluated for the rain medium, attenuation and channel isolation on a dual-polarized system can be calculated for a wave passing through the rain slab [Cox, 1981].

Comparison of multiple and first-order multiple scattering results

The multiple scattering model as presented in Section 5.3 has been computer programmed. Program inputs include frequency, elevation angle, mean and standard deviation of

canting angles, rain rate at the receiver, fraction of oblate raindrops, rain medium length, and incident wave and receive antenna polarization parameters.

Calculations have been performed to test the model and to examine the frequency dependence of multiple scattering effects. To facilitate comparison, as frequency is varied over 11, 20, and 30 GHz the rain medium parameters are fixed with a 5 km length, a uniform rain rate along the entire path, and a shape mixture of 60% oblate and 40% spherical raindrops. The oblate raindrops have a Gaussian canting angle distribution with a mean of 0 degrees and a standard deviation of 12 degrees. The incident wave polarization is linear with a 45 degree tilt angle. The elevation angle is 45 degrees. Attenuation and isolation as a function of rain rate were computed using both the first-order multiple scattering and complete multiple scattering models. The results are plotted in Fig. 3 for 30 GHz. Note that there are only slight differences between the values computed for the two models. At lower frequencies the differences were negligible. From these calculations it can be concluded that higher-order multiple scattering effects in rain begin to appear in the range of 30 GHz. However, results using the single scattering formulation of Section 5.2 would deviate noticeably.

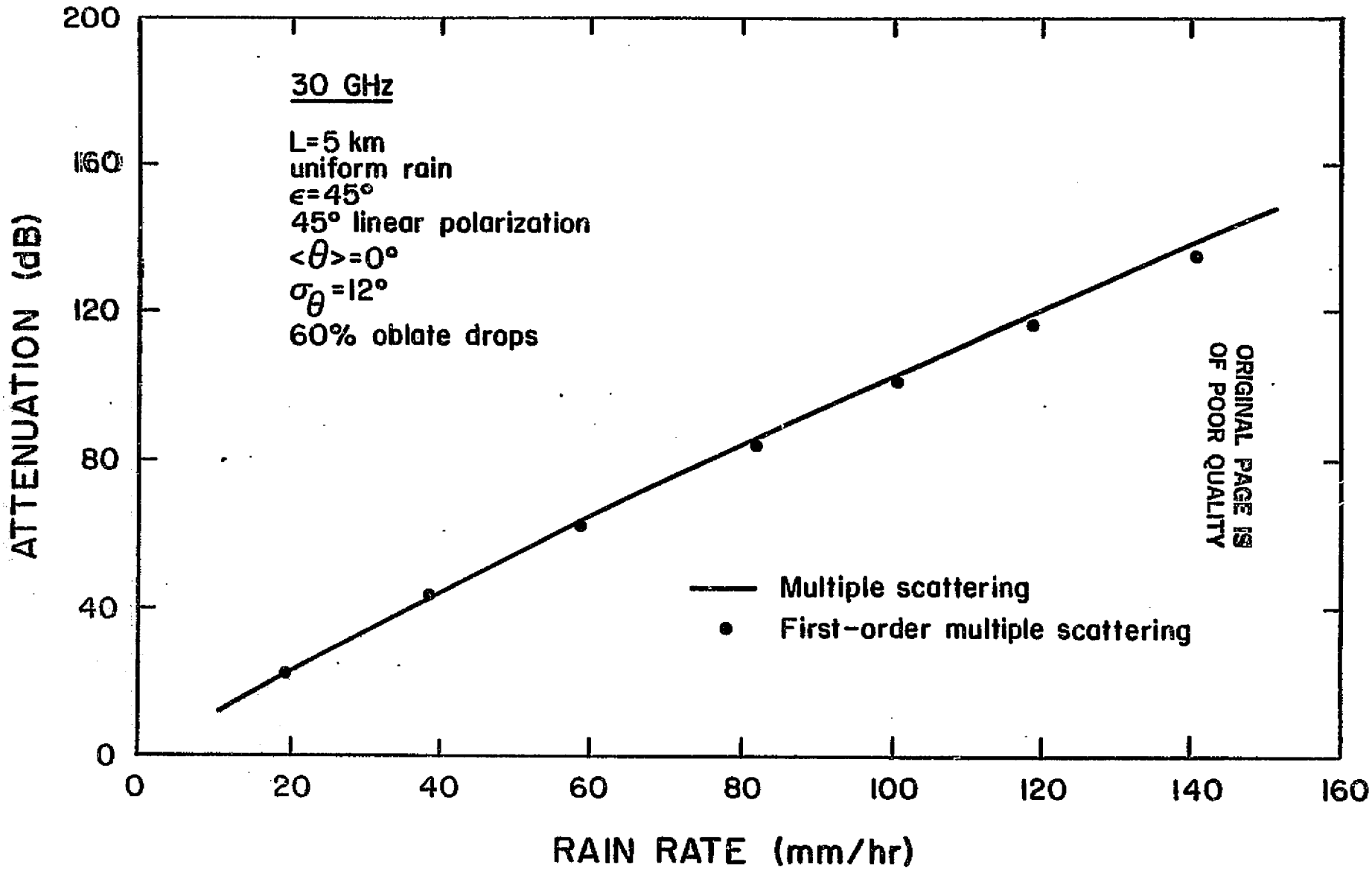

Figure 3a. Comparison of multiple scattering and first-order multiple scattering rain attenuation calculations at 30 GHz.

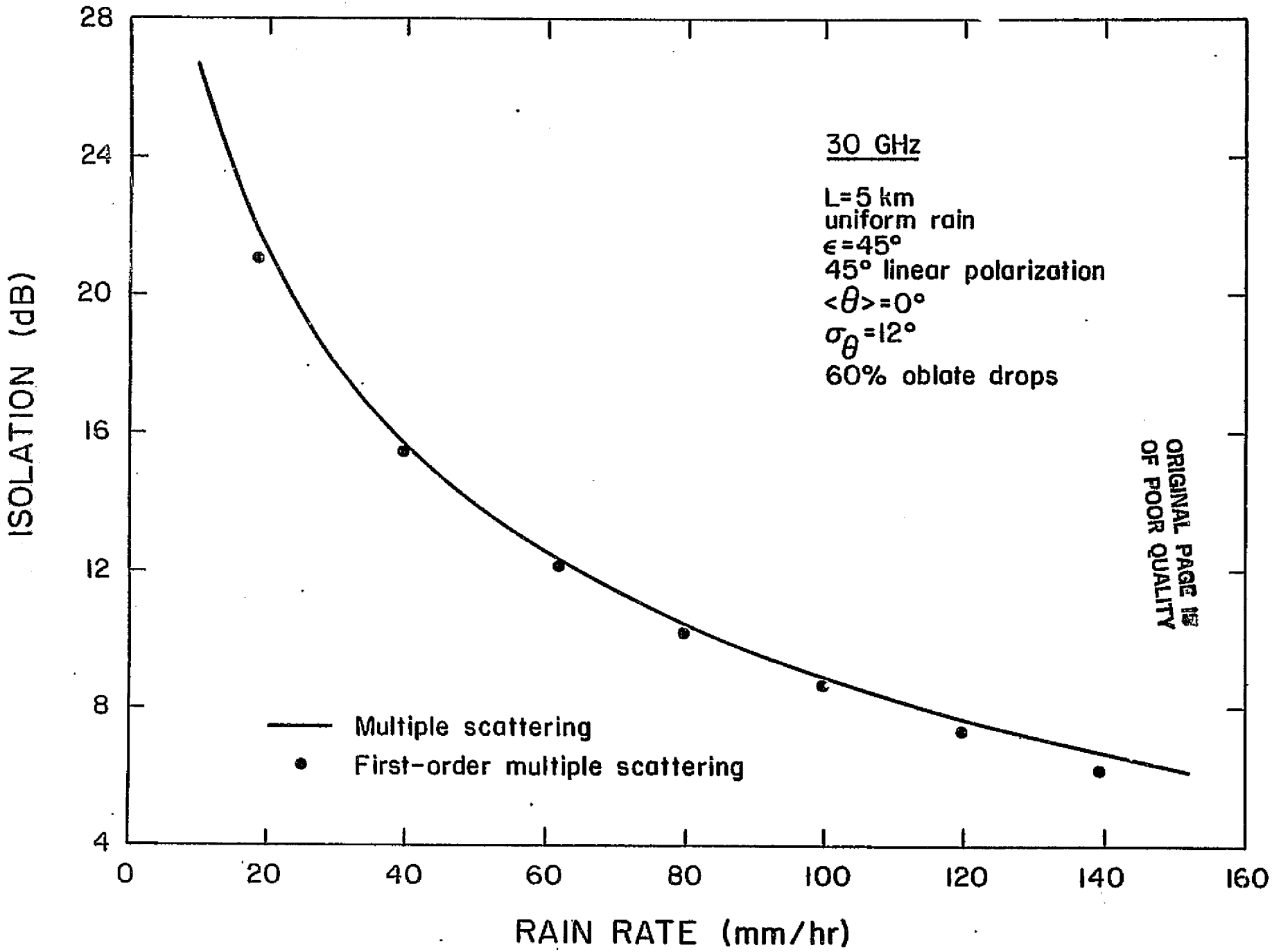

Figure 3b. Comparison of multiple scattering and first-order multiple scattering rain-induced isolation calculations at 30 GHz.

. To further justify the claim that higher-order multiple scattering effects of rain are negligible on communication links operating below 30 GHz, the calculated attenuation and isolation are plotted in Fig. 4 for parameters matching those of the VPI&SU COMSTAR D2 satellite, earth terminal. To more realistically represent rain, the piecewise uniform rain distribution of (34) was used. Note the nearly identical results with and without higher-order multiple scattering included.

5.5 Conclusions

In this paper formulations were presented for computing the effects of electromagnetic scattering from tenuous particulate media. The formulations were for single, first-order multiple, and complete multiple scattering. Each included the distributions of particle sizes, shapes, and orientation angles.

The multiple scattering formulation as presented here offers several features for calculation of millimeter wave propagation through precipitation media. These features are as follows. (a) The formulation is vector in nature and easily accomodates arbitrary polarization states for the input wave and receiving antenna. (b) Complete medium depo-

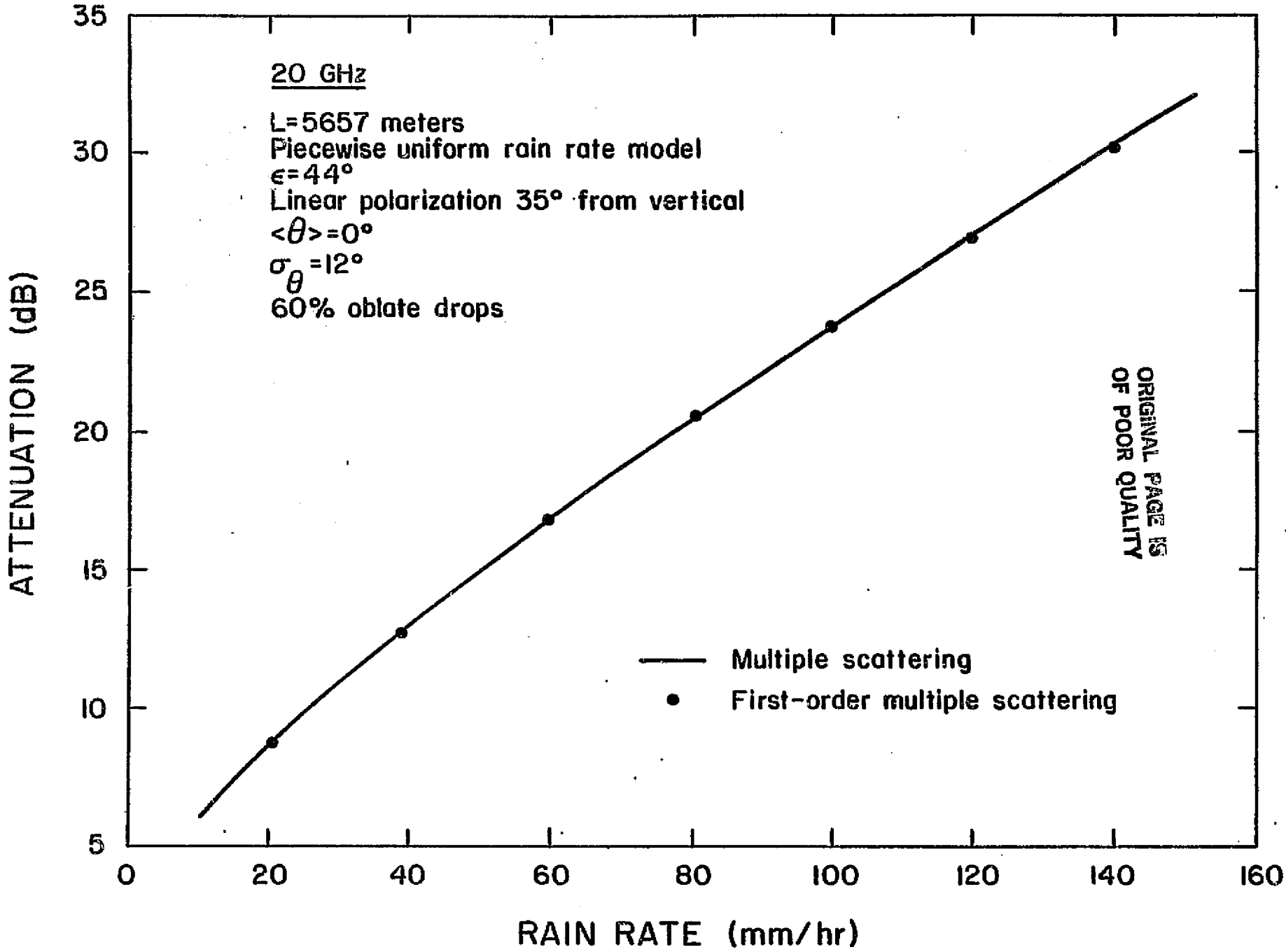

Figure 4a. Comparison of multiple scattering and first-order multiple scattering rain attenuation calculations for the Comstar satellite at 20 GHz.

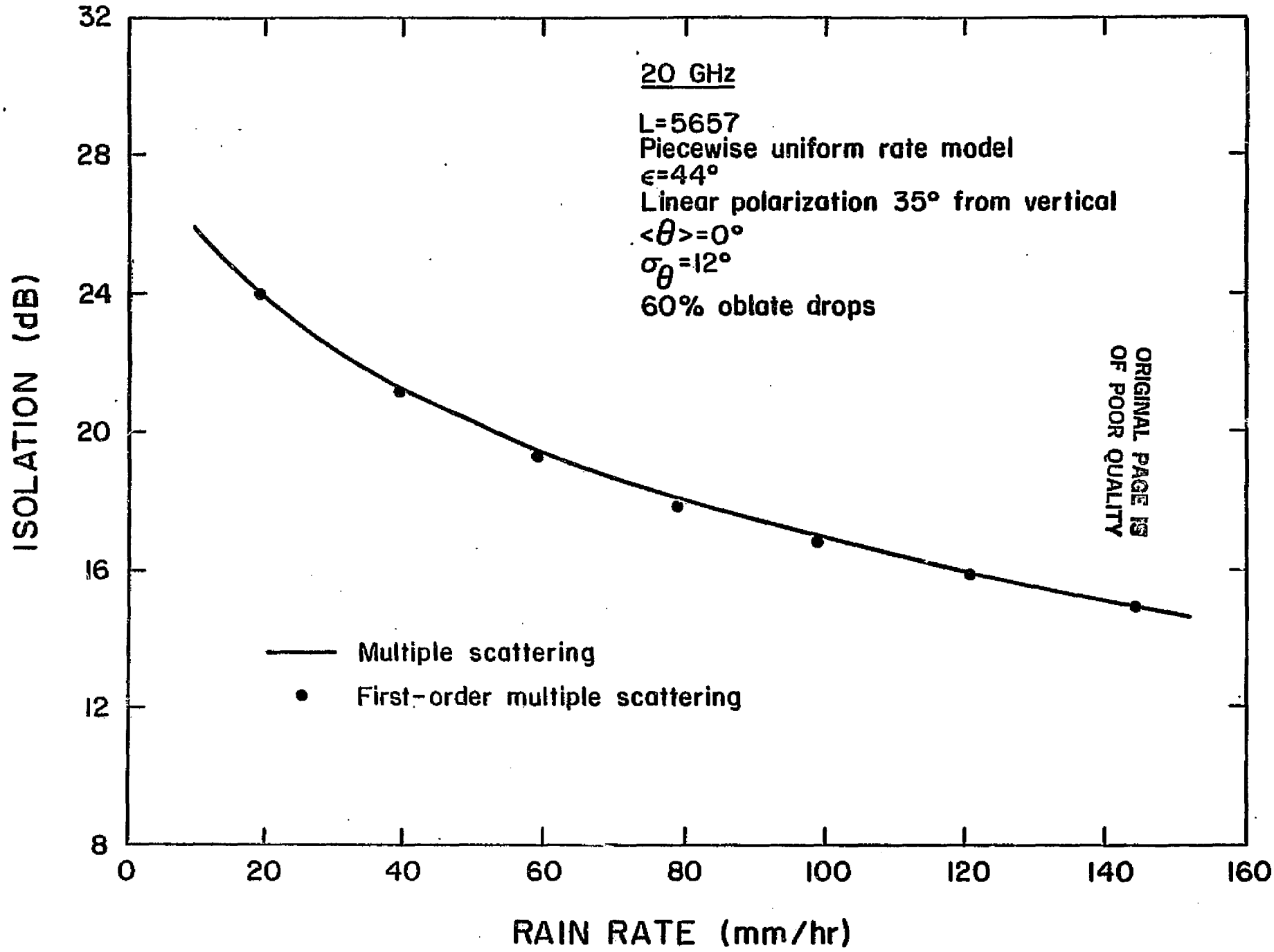

Figure 4b. Comparison of multiple scattering and first-order multiple scattering rain-induced isolation calculations for the Comstar satellite at 20 GHz.

larization effects can be calculated (i.e., attenuation, isolation, and phase shift). (c) Scattering particle distributions of particle size, shape, and orientation angle are directly included into the model. (d) Varying medium density along the propagation path (such as rain rate) can be accomodated. (e) Ice as well as rain hydrometeors can be included. (f) The multiple scattering formulation is numerically efficient. For typical communication link calculations the computer solution executes at least 30 times faster than the first-order multiple scattering version. (g) The multiple scattering model will give accurate results for systems operating above 30 GHz.

The multiple scattering model was used to calculate communication link performance for rain along earth-space paths. It was shown that higher-order multiple scattering effects only begin to become important in the 30 GHz frequency range.

5.6 References

Cox, D.C. (1981), Depolarization of radio waves by atmospheric hydrometeros in earth-space paths: A review, 16(5), 781-812.

Foldy, L.L. (1945), The multiple scattering of waves, Physical Review, 67(3&4), 107-121.

Ishimaru, A. (1977), Theory and application of wave propagation and scattering in random media, Proc. IEEE, 65(7), 1030-1061.

Ishimaru. A. (1978), Wave Propagation and Scattering in Random Media, Vol. 2, Academic Press, New York, Chapter 14.

Lax, M. (1951), Multiple scattering of waves, Reviews of Modern Physics, 23(4), 287-310.

Marshall, J.S., and W.M. Palmer (1948), The distribution of raindrops with size, J. Meteorology, 5, 165-166.

Oguchi, T. (1981), Scattering from hydrometeors: A survey, Radio Science, 16(5), 691-730.

Olsen, R.L. (1982), A review of theories of coherent radio wave propagation through precipitation media of randomly oriented scatterers, and the role of multiple scattering, Radio Science, to be published.

Persinger, R.R., W.L. Stutzman, R.E. Castle, and C.W. Bostian (1980), Millimeter wave attenuation prediction using a piecewise uniform rain rate model, IEEE Trans. on Ant. and Prop., AP-28(2), 149-153.

Rayleigh, Lord (1871), On the light from the sky, its polarization and colour, Phil. Mag., 41(107), 274.

Tsolakis, A. T. (1982), Multiple Scattering of Waves by Distributions of Particles with Applications to Radio Wave Propagation Through Precipitation, Ph.D. Dissertation, Virginia Tech (EE Dept. Blacksburg, VA), January, 1982.

Twersky, V. (1962), On scattering of waves by random distributions. I. Freespace formalism, J. Math. Phys., 3, 700-715.

Uzunoglu, N.K., B.G. Evans, and A.R. Holt (1977), Scattering of electromagnetic radiation by precipitation particles and propagation characteristics of terrestrial and space communication systems, Proc. IEE, 124(5), 417-424.

Van de Hulst, H.C. (1957), Light Scattering by Small Particles, John Wiley, New York.

Chapter 6

APPENDIX: COMPUTER PROGRAMS

In this section three computer programs are presented. They correspond to the following: the simple attenuation model of Chapter 3, the single rain drop scattering coefficient derivation of Chapter 4, and the multiple scattering model for rain of Chapter 5.

6.1 SIMPLE ATTENUATION MODEL PROGRAM

The statement listing of the Simple Attenuation Model (SAM) follows.

```
C*************************************************************************
C*                                                                       *
C*                        SIMPLE ATTENUATION MODEL                       *
C*                                                                       *
C*************************************************************************
C*                                                                       *
C*       THIS PROGRAM CALCULATES THE SLANT-PATH ATTENUATION DUE TO       *
C*       A POINT RAIN RATE AT AN EARTH STATION.                          *
C*                                                                       *
C*       THIS PROGRAM WAS DEVELOPED BY THE SATELLITE COMMUNICATIONS      *
C*       GROUP AT VIRGINIA POLYTECHNIC INSTITUTE AND STATE UNIVERSITY    *
C*       AND WAS SUPPORTED BY NASA UNDER JPL CONTRACT NO. 955954         *
C*                                                                       *
C*       ASSUMPTIONS: SPECIFIC ATTENUATION FROM OLSEN, ROGERS,           *
C*                    AND HODGE (1978).                                  *
C*                    POINT RAIN RATE DISTRIBUTION FROM CCIR             *
C*                    DOC. 5/5049-E (DRAFT RPT. 563-1, 1981)             *
C*                                                                       *
C*       INPUT PARAMETERS:                                               *
C*                                                                       *
C*            FREQ = FREQUENCY (GHZ)                                     *
C*            ELEV = ELEVATION ANGLE OF SLANT PATH                       *
C*            LAT = LATITUDE OF EARTH STATION                            *
C*            HO = ALTITUDE OF EARTH STATION (METERS)                    *
C*            REGION = RAIN CLIMATE REGION                               *
C*              1=A     5=E     9=J    13=N                              *
C*              2=B     6=F    10=K    14=P                              *
C*              3=C     7=G    11=L                                      *
C*              4=D     8=H    12=M                                      *
C*            LABEL = OPTIONAL ALPHANUMERIC STRING (22 CHAR. MAX.)       *
C*                                                                       *
C*************************************************************************
C
      DIMENSION T(7),RAIN(7,14),LABEL(6)
      REAL LAT,L
      INTEGER REGION
C* INITIALIZE RAINRATE EXCEEDANCE DATA (FROM CCIR DOC. 5/5049-E TABLE I)
      DATA T/.001,.003,.01,.03,0.1,0.3,1.0/
      DATA RAIN/22.,14.,8.,5.,2.,1.,0.,
     $          32.,21.,12.,6.,3.,2.,1.,
     $          42.,26.,15.,9.,5.,3.,0.,
     $          42.,29.,19.,13.,8.,5.,3.,
     $          70.,41.,22.,12.,6.,3.,1.,
     $          78.,54.,28.,15.,8.,4.,2.,
     $          65.,45.,30.,20.,12.,7.,0.,
     $          83.,55.,32.,18.,10.,4.,0.,
     $          55.,45.,35.,28.,20.,13.,0.,
     $         100.,70.,42.,23.,12.,6.,2.,
     $         150.,105.,60.,33.,15.,7.,0.,
     $         120.,95.,63.,40.,22.,11.,4.,
     $         180.,140.,95.,65.,35.,15.,5.,
     $         250.,200.,145.,105.,65.,34.,12./
C* READ THE INPUT DATA VALUES
      READ (5,5) FREQ,ELEV,LAT,HO,REGION,LABEL
    5 FORMAT(4F10.3,1X,I2,7X,5A4,A2)
```

```
C* CALCULATE SPECIFIC ATTENUATION COEFFICIENTS
      IF(FREQ.GE.1. .AND. FREQ.LE.1000.) GO TO 20
      WRITE(6,10) FREQ
 10   FORMAT(1H1,' FREQUENCY=',F10.4,' IS OUT OF PERMITTED RANGE',
     $ ' - - PROGRAM STOP')
      GO TO 999
 20   A1=6.39E-9*FREQ**2.03
      IF(FREQ.GE.2.9) A1=4.21E-5*FREQ**2.42
      IF(FREQ.GE.54.0) A1=0.0409*FREQ**0.699
      IF(FREQ.GE.180.) A1=3.38*FREQ**(-0.151)
      B1=0.851*FREQ**0.158
      IF(FREQ.GE.8.5) B1=1.41*FREQ**(-0.0779)
      IF(FREQ.GE.25.0) B1=2.63*FREQ**(-0.272)
      IF(FREQ.GE.164.0) B1=0.616*FREQ**0.0126
C* INITIALIZE RAIN DISTRIBUTION PARAMETERS
      GAMMA=1./22.0
C  CALCULATE AVERAGE ZERO-DEGREE ISOTHERM HEIGHT
      HI=4.8
      IF(LAT.GT.30.) HI=7.8-0.1*LAT
C  SUBTRACT EARTH STATION ELEVATION
      HI=HI-(HO/1000.0)
      ELEVR=ELEV*3.14159265/180.
C* PRINT OUTPUT HEADER
      WRITE(6,25) LABEL
  25  FORMAT(1H1,///,11X,'SAM - - SIMPLE ATTENUATION MODEL'//,5X,5A4,A2)
      WRITE(6,30) FREQ,ELEV,LAT,HO,REGION
  30  FORMAT('0',4X,'FREQUENCY: ',F5.2,' GHZ'/,5X,'ELEVATION: ',F5.2,
     $' DEGREES'/,5X,' LATITUDE: ',F5.2,' DEGREES',/,
     $5X,' ALTITUDE: ',F5.1,' METERS'/5X,'RAIN CLIMATE REGION: ',I2)
      WRITE(6,35) A1,B1
  35  FORMAT('0',4X,'SPECIFIC ATTENUATION COEFFICIENTS: A1=',F8.5,/,
     $40X,'B1=',F8.5)
      WRITE(6,40)
  40  FORMAT(1HO,7X,'PERCENT',/,9X,'TIME     RAINRATE   ATTENUATION'/)
C* CALCULATE ATTENUATION
      DO 70 J=1,7
      N=8-J
      R=RAIN(N,REGION)
      HE=HI
      IF(R.GT.10.) HE=HI+ALOG10(R/10.)
      L=HE/SIN(ELEVR)
      ALPHA=A1*R**B1
      IF(R.GT.10.) GO TO 45
      A=ALPHA*L
      GO TO 50
 45   ARG=GAMMA*B1*ALOG(R/10.)*COS(ELEVR)
      A=ALPHA*(1.-EXP(-ARG*L))/ARG
 50   WRITE(6,55) T(N),R,A
 55   FORMAT(9X,F5.3,5X,F5.1,7X,F6.2)
 70   CONTINUE
999   STOP
      END
```

6.2 SINGLE RAINDROP SCATTERING PROGRAM

The COEFF program was written based on the algorithm developed in Section 4.2. It computes the scattering coefficients of a raindrop. In this section we will describe the main subroutines of the program.

1. Subroutine GENLGP.

This subroutine calculates the associated Lengendre polynomials. It uses the recurrence formulas

$$P_o^o(x) = 1.0 \qquad P_1^o(x) = x \tag{1}$$

$$P_n^m(x) = \frac{(2n-1)\, P_{n-1}^m(x)\, x - (n+m-1)\, P_{n-2}^m(x)}{n-m} \qquad m < n \tag{2}$$

$$P_n^n(x) = \frac{(2n)!}{2^m\, m!} \left(1-x^2\right)^m \tag{3}$$

$$P_n^m(x) = 0 \qquad m > n \tag{4}$$

2. Subroutine SHPBES.

This subroutine calculates the spherical Bessel functions of first and second kind. Quadratic precision is necessary in order to match results

published in literature.(1) First we compute the P and Q polynomials, then we compute the spherical Bessel functions and $h_n^1(x)$. P and Q are given by

$$P(n + 1/2, x) = \sum_{k=0}^{[1/2\, n]} (-1)^k Q(n + 1/2, k)\ (2x)^{-2k} \qquad (5)$$

$$Q(n + 1/2, x) = \sum^{[1/2(n-1)]} (-1)^k\ (n + 1/2, 2k + 1)\ (2x)^{-2k-1} \qquad (6)$$

where

$$(n + 1/2, k) = \frac{(n + k)!}{k!\ \Gamma(n - k + 1)} \qquad (7)$$

Then $j_n(x)$, $y_n(x)$ are given by

$$j_n(x) = x^{-1}[P(n + 1/2, x)\ \sin(x - \tfrac{n\pi}{2}) + Q(n + 1/2, x)\ \cos(x - \tfrac{n\pi}{2})] \qquad (8)$$

$$y_n(x) = (-1)^{n+1}\ x^{-1}[P(n + 1/2, x)\ \cos(x + \tfrac{n\pi}{2}) - Q(n + 1/2, x)\ \sin(x + \tfrac{n\pi}{2})] \qquad (9)$$

---

(1)Abramowitz, M., Stegun, I.A., Handbook of Mathematical Functions, Doven Publications, New York, 1965.

Then

$$h_n^1(x) = j_n(x) + j\, y_n(x) \tag{10}$$

3. Subroutine GENGEN.

This subroutine calculates Gegenbauer polynomials using the recurrence formula

$$C_0^1(x) = 1.0 \tag{11}$$

$$C_1^1(x) = 2. * x \tag{12}$$

$$C_n^1(x) = C_1^1(x) * C_{n-1}^1(x) - C_{n-2}^1(x) \tag{13}$$

4. Subroutine VMATR.

This subroutine calculates $V(\vec{k}_1, \vec{k}_2)$ as

$$V(k_1, k_2) = 4\pi abc\ \gamma \frac{\sin|\vec{k}_1 - \vec{k}_2| - \cos|\vec{k}_1 - \vec{k}_2|}{|\vec{k}_1 - \vec{k}_2|^2} \tag{14}$$

Note when $\vec{k}_1 = \vec{k}_2$ we divide by 0 so we must take the limit $\vec{k}_2 \to \vec{k}_1$ giving

$$U(\vec{k}_1, \vec{k}_1) = \frac{4}{3}\pi\, abc\ \gamma \quad . \tag{15}$$

5. Subroutine ZMATR.

This subroutine calculates the integrand of (27).

6. Subroutine KNTGR.

This routine performs a numerical integration over x in (27) using a Clensaw-Curtis quadrature. Then it calculates matrix $\underline{K}(\vec{k}_1, \vec{k}_2)$

$$\underline{K} = \varepsilon_r \underline{\underline{I}} V(\vec{k}_1, \vec{k}_2) - \underline{\underline{Z}}(\vec{k}_1, \vec{k}_2) \qquad (16)$$

The seven point Clensahw-Curtis quadrature is given as:

$$\int_{-1}^{1} f(x)\, dx = \sum_{n=1}^{7} c_n f(x_n) \qquad (17)$$

where:

$$c_1 = 1/35 = c_7 \quad c_2 = c_6 = 16/63 \quad c_3 = c_5 = 16/35 \quad c_4 = 164/135 \qquad (18)$$

$$x_1 = -1\ ,\ x_2 = -\sqrt{3}/2\ ,\ x_3 = -0.5\ ,\ x_4 = 0.0\ ,\ x_5 = 0.5\ , \qquad (19)$$

$$x_6 = \sqrt{3}/2\ ,\ x_7 = 1$$

In the main program we develop the matrix equations to solve for $[\underline{\underline{C}}(\vec{k}_i)]$ and then calculate for the scattering tensor $\underline{\underline{f}}(\vec{k}_i, \vec{k}_s)$.

Inputs to the program are: the equivolumetric radius of the raindrop, the length of the major axis, frequency of incident wave, relative dielectric constant of raindrop, and the directions of the incident and scattering waves. The output is the scattering matrix of the rain drop. The listing of the program follows.

```
C$JOB
CCCCCCCCCCCCCCCCCCCCCCCCCCCCCCCCCCCCCCCCCCCCCCCCCCCCCCCCCCCCCCCCCCCCCCCCC
C
C
C     THIS PROGRAM CALCULATES THE SCATERING TENSOR OF A DIELECTRIC
C     SPHEROID. THE VARIABLES ARRE AS FOLLOWS:
C
C     THEI,PHII : THE DIRECTIONS OF THE INCIDENT WAVE
C     THES,PHIS : THE DIRECTIONS OF THE SCATERED WAVE
C     ABAR:THE EQUIVOLUMETRIC RADIUS OF THE SHEROID
C     AKO : THE WAVE NUMBER OF THE INCIDENT PLANE WAVE
C     CEPSIL : THE DIELECTRIC CONSTANT OF THE DIELECTRIC
C     THE PROGRAM IS AN APPLICATION TO A THEORETICAL
C     MODEL ESTABLISHED BY HOLT ET ALL.
C     THE PROGRAM WAS WRITTEN BY ANASTASIOS TSOLAKIS.
C     THIS PROJECT WAS SUPERVISED BY DR. W. L. STUTZMAN
C
CCCCCCCCCCCCCCCCCCCCCCCCCCCCCCCCCCCCCCCCCCCCCCCCCCCCCCCCCCCCCCCCCCCC
C
C
ISN 0002        IMPLICIT REAL*8(A-B,E-H,O-Z),COMPLEX*16(C)
ISN 0003        COMPLEX DKK(60,60),DUNIT(60,3)
ISN 0004        REAL*16 FACT(20),FACT1
ISN 0005        REAL DWA(60)
ISN 0006        DIMENSION CKMATR(3,3),CAJ(3,3)
               C,CF(3,3),AFACT(20),CSUM(3,3),AJ(3,3)
ISN 0007        COMMON/ACT/ AFACT,FACT
ISN 0008        COMMON/WEIGH/ CW(7),YY(7)
ISN 0009        COMMON/PAR/ A,AC,CGAM,PI,CEPSIL
ISN 0010        PI=3.14159265358979
C
C     NX  IS THE NUMBER OF THE INTERVALS USED FOR THE INTEGRATION
C     IN THE X DIRECTION
C
C     NPH  IS THE NUMBER OF THE INTERVALS USED FOR THE INTEGRATION
C     IN THE PHI VARIABLE
C
C     N  IS THE ORDER THAT THE INFINITE SUMMATION WAS TRUNCATED
C
ISN 0011        NX=5
ISN 0012        NPH=4
ISN 0013        I1=1
ISN 0014        N=9
C
C     READ THE VARAIBLES
C
ISN 0015        READ (5,99) ABAR,A,FO,CNO
ISN 0016     99 FORMAT(2F8.6,5X,F6.2,2(5X,F5.3))
ISN 0017        WRITE(6,99) ABAR,A,FO,CNO
ISN 0018        READ(5,101) PHII,THEI,PHIS,THES
ISN 0019    101 FORMAT(4F10.5)
ISN 0020        WRITE(6,101) PHII,THEI,PHIS,THES
ISN 0021        ALOC=3.0D-01
```

```
ISN 0022              AC=(ABAR**3)/(A**2)
ISN 0023              AC=AC/100.
ISN 0024              A=A/100.
ISN 0025              AKO=2.*PI*FO/VELOC
ISN 0026              PHII=PHII*PI/180.
ISN 0027              THEI=THEI*PI/180.
ISN 0028              PHIS=PHIS*PI/180.
ISN 0029              THES=THES*PI/180.
ISN 0030              CEPSIL=CNO**2
ISN 0031              RTHE1=3.0D+00
ISN 0032              RSQ=DSQRT(RTHE1)
ISN 0033              ONE=1.0D+00
ISN 0034              CONE=(1.0,0.0)
ISN 0035              YY(1)=-ONE
ISN 0036              YY(3)=-ONE/2.
ISN 0037              YY(2)=-ONE*RSQ/2.
ISN 0038              YY(4)=ONE*0.0
ISN 0039              YY(5)=-YY(3)
ISN 0040              YY(6)=-YY(2)
ISN 0041              YY(7)=ONE
ISN 0042              CW(1)=CONE/35.
ISN 0043              CW(7)=CW(1)
ISN 0044              CW(2)=CONE*16/63.
ISN 0045              CW(6)=CW(2)
ISN 0046              CW(3)=CONE*16./35.
ISN 0047              CW(5)=CW(3)
ISN 0048              CW(4)=CONE*104./315.
ISN 0049              CCAM=(AKO**2)*(CEPSIL-1.)
ISN 0050              CAK1=AKO*CNO
ISN 0051              CAK2=AKO*CNO
ISN 0052              CAKO=CONE*AKO
ISN 0053              N2=2*N+2
ISN 0054              DO 5 I=1,N2
ISN 0055              FACT(I)=FACT1(I-1)
ISN 0056            5 AFACT(I)=AFACT1(I-1)

CCCC  CALCULATE THE JAI TENSOR IN THE DIRECTION OF THE INCIDENT
      WAVE

ISN 0057              CALL AJMA(PHII,THEI,AJ)
ISN 0058              ICOUN1=-3
ISN 0059              ICOUN2=-3

CCCC  ESTABLISH THE MATRIX EQUATIONS THAT THE TWO COUPLED INTEGRAL
      COUPLED EQUATIONS HAVE BEEN REDUCED
      THE DIMENSION OF THE DKK MATRIX IS NX*NPH*49*3

ISN 0060              DO 10 I=1,NPH
ISN 0061              PH1=PI*(I-1.)/(NPH-1.)
ISN 0062              DO 10 J=1,NX
ISN 0063              X1=-1.+(J-1.)*2./(NX-1.)
ISN 0064              ICOUN1=ICOUN1+3
ISN 0065              DO 20 K=1,NPH
ISN 0066              PH2=PI*(K-1.)/(NPH-1.)
ISN 0067              DO 20 L=1,NX
ISN 0068              X2=-1.+(L-1.)*2./(NX-1.)
ISN 0069              ICOUN2=ICOUN2+3
ISN 0070              CALL MATGF(NX1,CAK1,CAK2,PH1,PH2,X1,X2,CAKO,N,CKMATR)
```

```
ISN 0071              DO 30 IK=1,3
ISN 0072              DO 30 IJ=1,3
ISN 0073           30 DKK(ICOUN1+IK,ICOUN2+IJ)=CKMATR(IK,IJ)
C          30 DKK(ICOUN2+IK,ICOUN1+IJ)=CKMATR(IK,IJ)
ISN 0074           20 CONTINUE
ISN 0075              WRITE(6,600)
ISN 0076          600 FORMAT(5X,5HKNTGR)
ISN 0077              ICOUN2=-3
ISN 0078              TH1=DARCOS(X1)
ISN 0079              CALL DMATR(CAK1,PH1,TH1,CAK0,PHI1,THEI,CU)
ISN 0080              CALL CMULT(AJ,3,3,CU,CAJ)
ISN 0081              DO 50 IK1=1,3
ISN 0082              DO 50 IJI=1,3
ISN 0083           50 DUNIT(ICOUN1+IK1,IJI)=CAJ(IK1,IJI)
ISN 0084           10 CONTINUE
ISN 0085              JM=NX*NPH*3
                   C
                   CCC   SOLVE FOR THE C(K) MATRIX AND THEN CALCULATE THE CF(3,3)
                   CCC   SCATERING TENSOR IN THE DIRECTION OF THE SCATERED WAVE
                   C
ISN 0086              WRITE(6,700)
ISN 0087          700 FORMAT(5X,6HLEQT1C)
ISN 0088              CALL LEQT1C(DKK,NM,NN,DUNIT,3,3,0,DWA,IER)
ISN 0089              WRITE(6,128) IER
ISN 0090          128 FORMAT(5X,'THE TER IS',I5)
ISN 0091              WRITE(6,700)
ISN 0092              DO 65 I=1,3
ISN 0093              DO 65 J=1,3
ISN 0094           65 CSUM(I,J)=(0.0,0.0)
ISN 0095              ICOUN=-3
ISN 0096              DO 70 I=1,NPH
ISN 0097              PH1=PI*(I-1.)/(NPH-1.)
ISN 0098              DO 70 J=1,NX
ISN 0099              X1=-1.+(J-1.)*2./(NX-1.)
ISN 0100              DO 80 K=1,3
ISN 0101              DO 80 L=1,3
ISN 0102           80 CAJ(K,L)=DUNIT(ICOUN+K,L)
ISN 0103              THE1=DARCOS(X1)
ISN 0104              CALL DMATR(CAK0,PHIS,THES,CAK1,PH1,THE1,CU)
ISN 0105              CALL CCMULT(CAJ,3,3,CU)
ISN 0106              CALL CCSUM(CSUM,3,3,CAJ)
ISN 0107           70 CONTINUE
ISN 0108              CALL AJOA(PHIS,THES,AJ)
ISN 0109              CALL CMULT(AJ,3,3,CAJ,3,CF)
ISN 0110              DO 100 I=1,3
ISN 0111              DO 100  J=1,3
ISN 0112          100 WRITE(6,102) CF(I,J)
ISN 0113          102 FORMAT(5X,3(E12.4,3X,E12.4,2X))
ISN 0114              STOP
ISN 0115              END
```

```
ISN 0002              SUBROUTINE ZMATRX(PH1,X1,PH2,X2,CAK1,CAK2,CAKO,X,N,CZ)
                C
                CCC   THIS SUBROUTINE CALCULATES THE ZI MATRIX
                C
ISN 0003              IMPLICIT REAL*8(A-B,D-H,O-Z),COMPLEX*16(C)
ISN 0004              REAL*16 FAC1(20)
ISN 0005              DIMENSION CZ(3,3),CAK1J(10),CAK2J(10),CYKOY(10),CYKOJ(10)
                     C,CSUM(3,3)
ISN 0006              DIMENSION SUM(3,3),PCH(10,10),PCH1(10,10),PCH2(10,10)
                     C,GEN(10),Q(3,3),AFACT(20)
ISN 0007              COMMON/ACI/ AFACT,FACT
ISN 0008              COMMON/PAR/ A,AC,CGAM,PI,CEPSIL
ISN 0009              CUA1=(0.0,1.0)
ISN 0010              SA=A**2
ISN 0011              ACSA=AC**2-A**2
ISN 0012              DO 5 IK=1,3
ISN 0013              DO 5 IJ=1,3
ISN 0014            5 CZ(IK,IJ)=(0.0,0.0)
ISN 0015              ACH=AC*X/DSQRT(SA+ACSA*(X**2))
ISN 0016               IF(DABS(ACH).EQ.1.0) RETURN
ISN 0018              ACH1=AC*X1/DSQRT(SA+ACSA*(X1**2))
ISN 0019              IF(DABS(ACH1).EQ.1.0) RETURN
ISN 0021              ACH2=AC*X2/DSQRT(SA+ACSA*(X2**2))
ISN 0022              IF(DABS(ACH2).EQ.1.0) RETURN
ISN 0024              CAKK1=CAK1*DSQRT(SA*(1.-X1**2)+(AC*X1)**2)
ISN 0025              CAKK2=CAK2*DSQRT(SA*(1.-X2**2)+(AC*X2)**2)
ISN 0026              Y=DSQRT(SA*(1.-X**2)+(AC*X)**2)
ISN 0027              CYKO=CAKO*Y
                C
                CCCC  CALCULATE THE LEGENDRE FUNCTION AND THE SHERICAL
                      BESSEL FUNCTIONS OF ORDER N+1
                C
ISN 0028              NN=N+1
ISN 0029              CALL GENLGP(PCH,ACH,NN)
ISN 0030              CALL GENLGP(PCH1,ACH1,NN)
ISN 0031              CALL GENLGP(PCH2,ACH2,NN)
ISN 0032              CALL SPHBES(CAKK1,NN,CAK1J,CYKOY)
ISN 0033              CALL SPHBES(CAKK2,NN,CAK2J,CYKOY)
ISN 0034              CALL SPHBES(CYKO,NN,CYKOJ,CYKOY)
                C     WRITE(6,300) NN
ISN 0035            300 FORMAT(5X,'THE ORDER IS  ',I3)
ISN 0036              PH12=PH1-PH2
                C
                CCC   CALCULATE THE GEGENBAUER POLYNOMIALS
                C
ISN 0037               CALL GEGEN(GEN,DCOS(PH12),N+1)
                C
                CCCC  INDICATE THE INFINITE SUMMATION TO ORDER N AND DO
                      ALL THE COMPUTATIONS TO FIND THE ZI MATRIX
                C
ISN 0038               I=N+1
ISN 0039              DO 10 I=1,II
ISN 0040              DO 10 J=1,II
```

```
ISN 0041              IN=I-1
ISN 0042              IM=J-1
ISN 0043              IF(((IN+IM)/2)*2.NE.IN+IM) GO TO 10
ISN 0045              DO 20 IK=1,3
ISN 0046              DO 20 IJ=1,3
ISN 0047           20 SUM(IK,IJ)=0.0
ISN 0048              DO 30 K=1,I
ISN 0049              DO 30 L=1,J
ISN 0050              KS=K-1
ISN 0051              LT=L-1
ISN 0052              ACON1=(KS+1)*AFACT(1+IN-KS)*(LT+1)*AFACT(1+IM-LT)/
                     C(AFACT(IN+KS+3)*AFACT(IM+LT+3))
ISN 0053              ACON2=ACON1*PCH(IN+1,KS+1)*PCH(IM+1,LT+1)
                     C*PCH1(IN+1,KS+1)*PCH2(IM+1,LT+1)
ISN 0054              IF(KS.GE.LT) PHB=PH1
ISN 0056              IF(KS.LT.LT) PHB=PH2
ISN 0058              MIN=MIN0(KS,LT)
ISN 0059              G=2.*PI*GEN(IN+IM+1)
                C
                CCC   EVALUATE THE I1,I2,...,I6 INTEGRALS DEPENDIG ON THE SUM KS,LT
                CCC   BEING EVEN OR ODD
                C
ISN 0060              IF(((KS+LT)/2)*2.NE.(KS+KT)) GO TO 100
ISN 0062              AI1=G
ISN 0063              AI2=0.0
ISN 0064              AI3=0.0
ISN 0065              AI4=G*(DSIN(PHB)**2)
ISN 0066              AI5=G*DSIN(PHB)*DCOS(PHB)
ISN 0067              AI6=G*(DCOS(PHB)**2)
ISN 0068              IF(KS.NE.LT) GO TO 200
ISN 0070              AI4=AI4+PI*DCOS(KS*PH12+2.*PH1)
ISN 0071              AI5=AI5-PI*DSIN(KS*PH12+2.*PH1)
ISN 0072              AI6=AI6-PI*DCOS(KS*PH12+2.*PH1)
ISN 0073              GO TO 200
ISN 0074          100 AI1=0.0
ISN 0075              AI4=0.0
ISN 0076              AI5=0.0
ISN 0077              AI6=0.0
ISN 0078              AI2=G*DSIN(PHB)
ISN 0079              AI3=G*DCOS(PHB)
ISN 0080          200 SY=1-X**2
ISN 0081              SQRY=DSQRT(SY)
                C
                CCC   CALCULATE THE Q(S,T) MATRIX
                C
ISN 0082              Q(1,1)=AI1-SY*AI6
ISN 0083              Q(2,1)=-SY*AI5
ISN 0084              Q(3,1)=-X*SQRY*AI3
ISN 0085              Q(1,2)=-SY*AI5
ISN 0086              Q(2,2)=AI1-SY*AI4
ISN 0087              Q(3,2)=-X*SQRY*AI2
ISN 0088              Q(1,3)=-X*SQRY*AI3
ISN 0089              Q(2,3)=-X*SQRY*AI2
ISN 0090              Q(3,3)=SY*AI1
ISN 0091              CALL AULIC(Q,3,3,ACON2)
ISN 0092              CALL ASUM(SUM,3,3,Q)
ISN 0093           30 CONTINUE
ISN 0094              I=A(I+1)+
```

```
ISN 0095            IMIN=MINO(IM,IN)+1
ISN 0096            CON1=(2.*IN+3.)*(2.*IM+3)*(CAK1J(IN+1)/CAKK1)*
                   C(CAK2J(IM+1)/CAKK2)*CYKOJ(IMAX)*(CYKOJ(IMIN)+CJAI*CYKOY(IMIN))
ISN 0097            CALL CMULT(SUM,3,3,CON1,CSUM)
ISN 0098            CALL MCSUM(CZ,3,3,CSUM)
ISN 0099         10 CONTINUE
ISN 0100            CONY=CJAI/(Y**2)
ISN 0101            CALL CCMULT(CZ,3,3,CONY)
ISN 0102            RETURN
ISN 0103            END



ISN 0002            SUBROUTINE GENLGP(P,X,N)
CCC
CCC   THIS SUBROUTINE CALCULATES THE LENGENDRE FUNCTIONS
CCC
ISN 0003            IMPLICIT REAL*8(A-H,O-Z)
ISN 0004            REAL *16 FACT(20)
ISN 0005            DIMENSION P(N,N),AFACT(20)
ISN 0006            COMMON/ACT/ AFACT,FACT
ISN 0007            ASIN=DSQRT(1.-X**2)
ISN 0008            DO 5 I=1,N
ISN 0009            DO 5 J=1,N
ISN 0010         5  P(I,J)=0.0
ISN 0011            IF(ASIN.EQ.0.0) RETURN
ISN 0013            P(1,1)=1.0/ASIN
ISN 0014            P(2,1)=X/ASIN
ISN 0015            DO 10 I=2,N
ISN 0016            DO 10 J=1,I
ISN 0017            IF(I.EQ.2.AND.J.EQ.1) GO TO 10
ISN 0019            IF(I.NE.J) GO TO 20
ISN 0021            P(I,I)=AFACT(1+2*(I-1))*ASIN**(I-2)/((2**(I-1))*AFACT(I))
ISN 0022            GO TO 10
ISN 0023         20 P(I,J)=((2.*I-3)*X*P(I-1,J)-(I+J-3)*P(I-2,J))
                   C/(I-J)
ISN 0024         10 CONTINUE
ISN 0025            RETURN
ISN 0026            END
```

```
ISN 0095              IMIN=MINO(IM,IN)+1
ISN 0096              CON1=(2.*IN+3.)*(2.*IM+3)*(CAK1J(IN+1)/CAKK1)*
                     C(CAK2J(IM+1)/CAKK2)*CYKOJ(IMAX)*(CYKOJ(IMIN)+CJAI*CYKOY(IMIN))
ISN 0097              CALL CMULT(SUM,3,3,CON1,CSUM)
ISN 0098              CALL MCSUM(CZ,3,3,CSUM)
ISN 0099           10 CONTINUE
ISN 0100              CONY=CJAI/(Y**2)
ISN 0101              CALL CCMULT(CZ,3,3,CONY)
ISN 0102              RETURN
ISN 0103              END
```

```
ISN 0002              SUBROUTINE GENLGP(P,X,N)
CCC
CCC     THIS SUBROUTINE CALCULATES THE LENGENDRE FUNCTIONS
CCC
ISN 0003              IMPLICIT REAL*8(A-H,O-Z)
ISN 0004              REAL *16 FACT(20)
ISN 0005              DIMENSION P(N,N),AFACT(20)
ISN 0006              COMMON/ACT/ AFACT,FACT
ISN 0007              ASIN=DSQRT(1.-X**2)
ISN 0008              DO 5 I=1,N
ISN 0009              DO 5 J=1,N
ISN 0010            5 P(I,J)=0.0
ISN 0011              IF(ASIN.EQ.0.0) RETURN
ISN 0013              P(1,1)=1.0/ASIN
ISN 0014              P(2,1)=X/ASIN
ISN 0015              DO 10 I=2,N
ISN 0016              DO 10 J=1,I
ISN 0017              IF(I.EQ.2.AND.J.EQ.1) GO TO 10
ISN 0019              IF(I.NE.J) GO TO 20
ISN 0021              P(I,I)=AFACT(1+2*(I-1))*ASIN**(I-2)/((2**(I-1))*AFACT(I))
ISN 0022              GO TO 10
ISN 0023           20 P(I,J)=((2.*I-3)*X*P(I-1,J)-(I+J-3)*P(I-2,J))
                     C/(I-J)
ISN 0024           10 CONTINUE
ISN 0025              RETURN
ISN 0026              END
```

```
ISN 0002          SUBROUTINE SHPBES(OARG,N,OJSH,OYSH)
C
CCC   THIS SUPROUTINE CALCULATES THE SPHERICAL BESSEL FUNCTIONS
CCC   THE METHOD USED IS THE ONE DISCRIBED IN THE ABRAMOVITZ,STEGUN
CCC   HANDBOOK OF MATHEMATICAL FUNCTIONS.  QUADRATIC PRECISION IS
CCC   NECESSARY
C
ISN 0003          IMPLICIT REAL *16(A-B,D-H,P-Z),COMPLEX*32(C),COMPLEX*16(O)
ISN 0004          REAL*8 AFACT(20)
ISN 0005          DIMENSION  OJSH(N),OYSH(N),FACT(20)
ISN 0006          COMMON/ACT/ AFACT,FACT
ISN 0007          CARG=OARG
ISN 0008          DO 20 I=1,N
ISN 0009          CP=(0.0,0.0)
ISN 0010          CQ=(0.0,0.0)
ISN 0011          M1=I/2+1
ISN 0012          M2=(I-1)/2+1
ISN 0013          DO 25 J=1,M1
ISN 0014          AK=J-1
ISN 0015          K=J-1
ISN 0016          CP1=((-1.)**K)*FACT(1+I+2*K)/(FACT(1+2*K)
                 C*FACT(1+I-2*K))
ISN 0017          CP=CP+CP1/((2.*CARG)**(2*K))
ISN 0018       25 CONTINUE
ISN 0019          DO 30 J=1,M2
ISN 0020          AK=J-1
ISN 0021          K=J-1
ISN 0022          CQ1=((-1.)**K)*FACT(I+2*K+2)/(FACT(2*K+2)
                 C*FACT(I-2*K))
ISN 0023          CQ=CQ+CQ1/((2.*CARG)**(2*K+1))
ISN 0024       30 CONTINUE
ISN 0025          AM=I/4.
ISN 0026            B=I/4.
ISN 0027          IF(AM.EQ.B+0.25) GO TO 60
ISN 0029          IF(AM.EQ.B+0.5) GO TO 70
ISN 0031          IF(AM.EQ.B+0.75) GO TO 80
ISN 0033          CSHP=(CP*COSIN(CARG)+CQ*COCOS(CARG))/CARG
ISN 0034          CYSH=((-1.)**(I+1))*(CP*COCOS(CARG)-CQ*COSIN(CARG))/CARG
ISN 0035          GO TO 90
ISN 0036       60 CSHP=(-CP*COCOS(CARG)+CQ*COSIN(CARG))/CARG
ISN 0037          CYSH=((-1.)**(I+1))*(CP*COSIN(CARG)+CQ*COCOS(CARG))/CARG
ISN 0038          GO TO 90
ISN 0039       70 CSHP=(-CP*COSIN(CARG)-CQ*COCOS(CARG))/CARG
ISN 0040          CYSH=((-1.)**(I+1))*(-CP*COCOS(CARG)+CQ*COSIN(CARG))/CARG
ISN 0041          GO TO 90
ISN 0042       80 CSHP=(CP*COCOS(CARG)-CQ*COSIN(CARG))/CARG
ISN 0043          CYSH=((-1.)**(I+1))*(-CP*COSIN(CARG)-CQ*COCOS(CARG))/CARG
ISN 0044       90 CONTINUE
ISN 0045          OJSH(I)=CSHP
ISN 0046          OYSH(I)=CYSH
ISN 0047       20 CONTINUE
ISN 0048          RETURN
ISN 0049          END
```

```
ISN 0002          REAL  FUNCTION AFACT1*8(N)
C
C     THIS SUBROUTINE CALCULATES THE N  FACTORIAL USING DOUBLE
C     PRECISION
C
ISN 0003          AFACT1=1.0D+00
ISN 0004          IF(N.EQ.0.) RETURN
ISN 0005          DO 10 I=1,N
ISN 0006       10 AFACT1=AFACT1*I
ISN 0007          RETURN
ISN 0008          END
```

```
ISN 0002          REAL FUNCTION FACT1*16(N)
C
C     THIS SUBROUTINE CALCULATES THE N FACTORIAL USING
C     QUADRATIC PRECISION.
C
ISN 0003          FACT1=1.0
ISN 0004          IF(N.EQ.0) RETURN
ISN 0005          DO 10 I=1,N
ISN 0006          FACT1=FACT1*I
ISN 0007       10 CONTINUE
ISN 0008          RETURN
ISN 0009          END
```

```
ISN 0002          SUBROUTINE GEGEN(C,CARG,N)
C
C     THIS SUBROUTINE CALCULATES THE GEGENBAUER POLYNOMIALS
C     USING THE RECURRENCE FORMULAS.
C
ISN 0003          IMPLICIT REAL*8 (A-H,O-Z)
ISN 0004          DIMENSION C(1)
ISN 0005          C(1)=1.0D+00
ISN 0006          C(2)=2.*CARG
ISN 0007          DO 10 I=3,N
ISN 0008       10 C(I)=C(2)*C(I-1)-C(I-2)
ISN 0009          RETURN
ISN 0010          END
```

```
ISN 0002              SUBROUTINE MULT(AJ,N,M,CAJ,M1,CF)
                C
                C     THIS SUBROUTINE MULTIPLIES A REAL MATRIX WITH A COMLEX ONE
                C
ISN 0003              IMPLICIT COMPLEX *16(B-H,O-Z)
ISN 0004              DIMENSION CAJ(M,M1),CF(N,M1)
ISN 0005              DIMENSION  AJ(N,M)
ISN 0006              DO 20 I=1,N
ISN 0007              DO 20 J=1,M1
ISN 0008              CSUM=(0.0,0.0)
ISN 0009              DO 10 K=1,M
ISN 0010           10 CSUM=CSUM+AJ(I,K)*CAJ(K,J)
ISN 0011              CF(I,J)=CSUM
ISN 0012           20 CONTINUE
ISN 0013              RETURN
ISN 0014              END
```

```
ISN 0002              SUBROUTINE SUB(CKMATR,N,M,CIZ)
                C
                C     THIS SUBROUTINE SUBTRACTS TWO COMPLEX MATRICES.
                C
ISN 0003              IMPLICIT COMPLEX*16(C)
ISN 0004              DIMENSION CKMATR(N,M),CIZ(N,M)
ISN 0005              DO 10 I=1,3
ISN 0006              DO 10 J=1,3
ISN 0007           10 CKMATR(I,J)=CKMATR(I,J)-CIZ(I,J)
ISN 0008              RETURN
ISN 0009              END
```

```
ISN 0002              SUBROUTINE MCSUM(CZ,N,M,CSUM)
                C
                C     THIS SUBROUTINE ADDS TWO COMPLEX MATRICES.
                C
ISN 0003              COMPLEX*16 CZ(N,M),CSUM(N,M)
ISN 0004              DO 10 J=1,3
ISN 0005              DO 10 I=1,3
ISN 0006           10 CZ(I,J)=CZ(I,J)+CSUM(I,J)
ISN 0007              RETURN
ISN 0008              END
```

```
ISN 0002          SUBROUTINE MULTC(Q,N,M,A)
C
C     THIS SUBROUTINE MULTIPLIES A REAL MATRIX WITH A REAL
C     CONSTANT.
C
ISN 0003          IMPLICIT REAL*8(A-H,O-Z)
ISN 0004          DIMENSION Q(N,M)
ISN 0005          DO 10 I=1,N
ISN 0006          DO 10 J=1,M
ISN 0007       10 Q(I,J)=Q(I,J)*A
ISN 0008          RETURN
ISN 0009          END
```

```
ISN 0002          SUBROUTINE CMULT(SUM,N,M,CON,CSUM)
C
C     THIS SUBROUTINE MULTIPLIES A REAL AMTRIX WITH A
C     COMPLEX CONSTANT.
C
ISN 0003          COMPLEX*16 CON,CSUM(N,M)
ISN 0004          REAL*8 SUM(N,M)
ISN 0005          DO 10 I=1,N
ISN 0006          DO 10 J=1,M
ISN 0007       10 CSUM(I,J)=CON*SUM(I,J)
ISN 0008          RETURN
ISN 0009          END
```

```
ISN 0002          SUBROUTINE MSUM(SUM,N,M,Q)
C
C     THIS SUBROUTINE ADDS TWO REAL MATRICES.
C
ISN 0003          IMPLICIT REAL*8 (A-H,O-Z)
ISN 0004          DIMENSION SUM(N,M),Q(N,M)
ISN 0005          DO 10 I=1,N
ISN 0006          DO 10 J=1,M
ISN 0007       10 SUM(I,J)=SUM(I,J)+Q(I,J)
ISN 0008          RETURN
ISN 0009          END
```

```
ISN 0002          SUBROUTINE CCMULT(CZ,N,M,CY)
C
C     THIS SUBROUTIONE MULTIPLIES A COMPLEX MATRIX WITH
C     A COMPLEX CONSTANT.
C
ISN 0003          COMPLEX*16 CY,CZ(N,M)
ISN 0004          DO 10 I=1,N
ISN 0005          DO 10 J=1,M
ISN 0006       10 CZ(I,J)=CZ(I,J)*CY
ISN 0007          RETURN
ISN 0008          END
```

```
ISN 0002          SUBROUTINE AJMA(PHI,THE,AJ)
C
C     THIS SUBROUTINE CALCULATES THE JAI TENSOR IN THE
C     DIRECTION PHI,THETA.
C
ISN 0003          IMPLICIT REAL *8 (A-H,O-Z)
ISN 0004          DIMENSION AJ(3,3)
ISN 0005          X=DCOS(THE)
ISN 0006          Y=DSQRT(1.-X**2)
ISN 0007          SY=Y**2
ISN 0008          AJ(1,1)=1.-SY*(DCOS(PHI)**2)
ISN 0009          AJ(2,1)=-SY*(DCOS(PHI)*DSIN(PHI))
ISN 0010          AJ(3,1)=-Y*X*DCOS(PHI)
ISN 0011          AJ(1,2)=-SY*DCOS(PHI)*DSIN(PHI)
ISN 0012          AJ(2,2)=1.-SY*(DSIN(PHI)**2)
ISN 0013          AJ(3,2)=-X*Y*DSIN(PHI)
ISN 0014          AJ(1,3)=-X*Y*DCOS(PHI)
ISN 0015          AJ(2,3)=-X*Y*DSIN(PHI)
ISN 0016          AJ(3,3)=SY
ISN 0017          RETURN
ISN 0018          END
```

```
      SUBROUTINE KNTGR(NX,CAK1,CAK2,PH1,PH2,X1,X2,CAKO,N,CUNIT)
C
CC    THIS SUBROUTINE CALCULATES THE KAI MATRIX.
C
      IMPLICIT COMPLEX*16(C),REAL*8(A-B,D-H,O-Z)
      DIMENSION CIZ(3,3),CZ(3,3),CUNIT(3,3)
      COMMON/WEIGH/ CW(7),YY(7)
      COMMON/PAR/ A,AC,CGAM,PI,CEPSIL
      DO 10 I=1,3
      DO 10 J=1,3
   10 CIZ(I,J)=(0.0,0.0)
      DO 20 I=1,NX
      AA=(I-1)*1./NX
      BB=I*1./NX
      DO 20 J=1,7
      X=((BB+AA)/2.+((BB-AA)/2.)*YY(J)
      CALL ZMATRX(PH1,X1,PH2,X2,CAK1,CAK2,CAKO,X,N,CZ)
C     WRITE(6,300)
  300 FORMAT(5X,6HZMATRX)
      CALL CCMULT(CZ,3,3,CW(J))
   20 CALL MCSUM(CIZ,3,3,CZ)
      WRITE(6,100) CZ(3,3)
  100 FORMAT(5X,'THE C IS',2F15.8)
C     WRITE(6,400)
  400 FORMAT(5X,6HSKAIAA)
      CON1=8.*PI*(A**4)*(AC**2)*(CGAM**2)/CAKO
      CALL CCMULT(CIZ,3,3,CON1)
      DO 30 I=1,3
      DO 30 J=1,3
      CUNIT(I,J)=(0.0,0.0)
      IF(I.EQ.J) CUNIT(I,I)=(1.0,0.0)
   30 CONTINUE
      TH1=DARCOS(X1)
      TH2=DARCOS(X2)
      CALL UMATR(CAK1,PH1,TH1,CAK2,PH2,TH2,CU)
      CU=CU*CEPSIL
      CALL CCMULT(CUNIT,3,3,CU)
      CALL SUB(CUNIT,3,3,CIZ)
      RETURN
      END


      SUBROUTINE UMATR(CAK1,PH1,TH1,CAK2,PH2,TH2,CU)
C
CC    THIS SUBROUTINE CALCULATES THE U(K1,K2)
C
      IMPLICIT REAL*8(A-B,D-H,O-Z),COMPLEX*16(C)
      COMMON/PAR/ A,AC,CGAM,PI,CEPSIL
      CX=CDSQRT((A**2)*((CAK1*DSIN(TH1)*DCOS(PH1)-CAK2*DSIN(TH2)*DCOS(
     C PH2))**2+(CAK1*DSIN(TH1)*DSIN(PH1)-CAK2*DSIN(TH2)*DSIN(PH2))**2)
     C+(AC*(CAK1*DCOS(TH1)-CAK2*DCOS(TH2)))**2)
      IF(CDABS(CX).EQ.0.0) GO TO 10
      CU=4.*PI*(A**2)*AC*CGAM*(CDSIN(CX)-CDCOS(CX))/(CX**2)
      RETURN
   10 CU=4./3.*PI*(A**2)*AC*CGAM
      RETURN
      END
```

6.3 MULTIPLE SCATTERING RAIN PROPAGATION PROGRAM

The multiple scattering formulation for the rain problem as developed in Chapter 5 has been coded into Fortran. The block diagram of the Rain Multiple Scattering Program (RMP) is shown in Fig. 1. The correspnding analytical development and examples of computer results are discussed in Section 5.3.

The statement listing of the program follows.

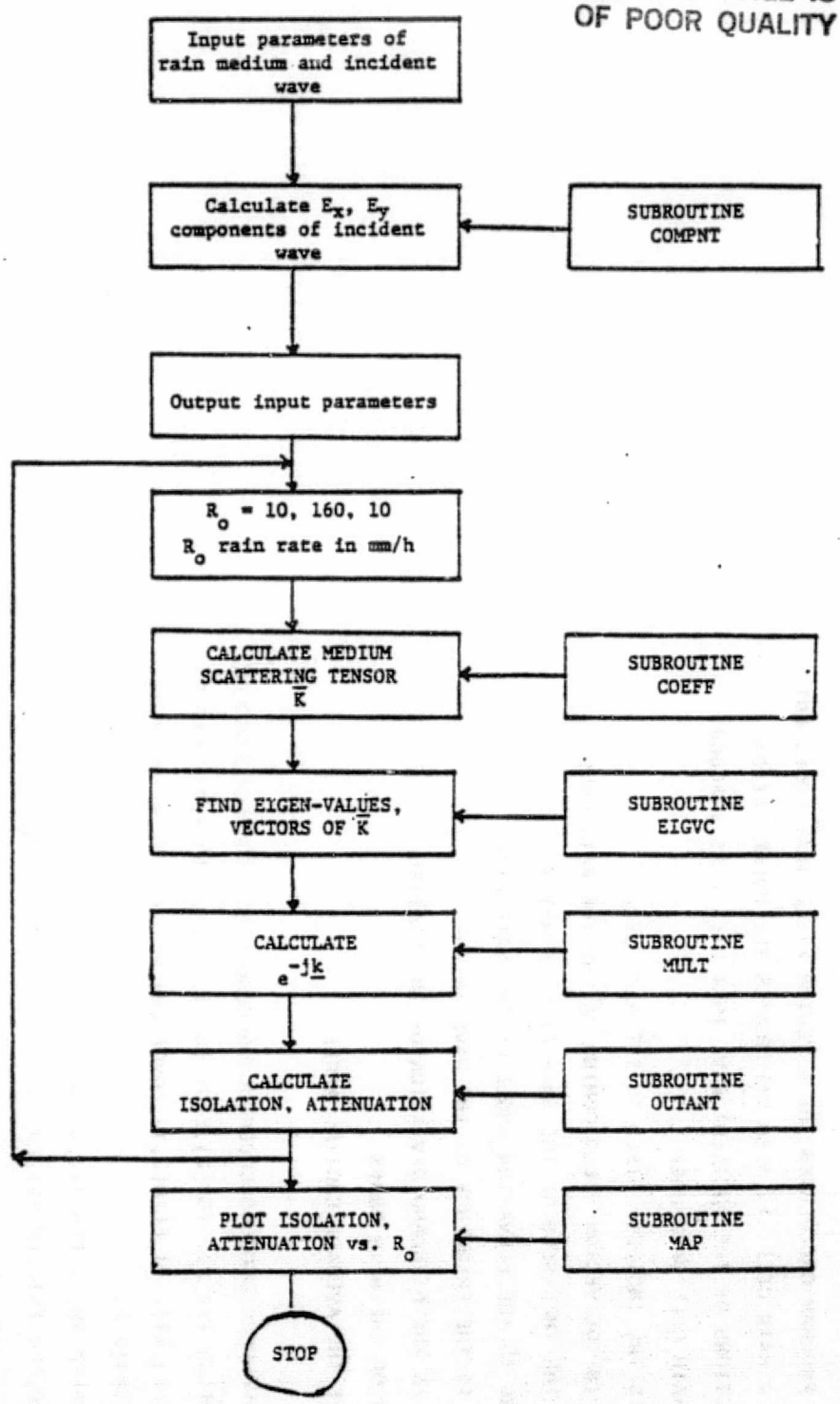

Figure 1. Block diagram of RMP program.

```
CCCCCCCCCCCCCCCCCCCCCCCCCCCCCCCCCCCCCCCCCCCCCCCCCCCCCCCCCCCCCCCCCCC
C
C   THIS PROGRAM CALCULATES THE E VECTOR FIELD THAT COMES OUT
C   FROM A RAIN CELL. IT ALSO CALCULATES THE POLARIZATION
C   DIRECTIONS OF THE INCIDENT WAVE THAT WILL PASS THROUGH
C   THE RAIN CELL UNCHANGED.
C   EI  IS THE INCIDENT FIELD TO THE RAIN CELL
C   IFIV IS THE VECTOR FIELD COMING OUT OF THE RAIN CELL
C   L IS THE THICKNESS OF THE RAIN CELL IN METERS
C   LOKANG IS THE ELEVATION ANGLE OF THE SATELLITE
C   FREQ IS THE FREQUENCY OF THE WAVE IN GHZ
C   SIGM IS THE STANDARD DEVIATION OF THE CANTING
C   ANGLE OF THE RAIN DROPS
C   THE IS THE AVERAGE CANTING ANGLE
C
CCCCCCCCCCCCCCCCCCCCCCCCCCCCCCCCCCCCCCCCCCCCCCCCCCCCCCCCCCCCCCCCCCC
      COMPLEX F(2,2),EIGV(2),EIGVC(2,2),WK(2),DIAG(2,2),UNIT(2,2)
     C,WA(2),EI(2,1),EFIN(2,1),EGVC(2,2),MATR1(2,2),MATR2(2,2)
     C,MATR3(2,2)
      COMPLEX FH,FV,FSH,JAI,SCTHE,DIFF,ER1,ISOL,ATT
     C,ERO,ELO,FV1,FV2,FH1,FH2,DIFF1,DIFF2,FSH1,FSH2
     C,MINUSJ,EXC,EYC,EXX,EYX
```

```
      REAL NO,KO,LOKANG,L,LAM,ISOLDB,ISD(52),RATE(52)
     C,AMODE(6),ATTD(52)
      DATA AMODE/0.0,0.25,1.0,2.0,2.5,3.5/
      COMMON/VAR/ ISD,RATE,ATTD
       COMMON/BLOC1/ MINUSJ,CONV
      COMMON/BLOC2/ VWACM
       MINUSJ=(0.0,-1.0)
      PI=3.1415927
      CONV=PI/180.0
      JAI=(0.0,1.0)
      P1=0.4
      P2=0.6
C
C   READ IN THE VARIABLES OF THE MAIN CELL
C
   15 READ(5,999) LOKANG,THE1,SIGM1,L,NO,FREQ
      IF(LOKANG.EQ.0.) GO TO 88
      READ(5,977) EPSW,TAUW,EPSC,TAUC,EPSX,TAUX
  977 FORMAT(6F10.0)
      WRITE(6,93)
      WRITE(6,92) THE1,SIGM1,L
C
C   READ THE INCIDENT VECTOR FIELD
```

```
C
C     READ(5,91) (EI(J,1),J=1,2),ISTAT
C  91 FORMAT(4(F4.1,1X),1X,I1)
      LOKANG=LOKANG*PI/180.


      THE=THE1*PI/180.
      SIGM=SIGM1*PI/180.
      LAM=0.3/FREQ
      KO=2.*PI/LAM
      CALL COMPNT(EPSW,TAUW,EI(1,1),EI(2,1))
      CALL COMPNT(EPSC,TAUC,EXC,EYC)
      CALL COMPNT(EPSX,TAUX,EXX,EYX)
      EYC=CONJG(EYC)
      EYX=CONJG(EYX)
      VWACM=CABS(EXC*EI(1,1)+EYC*EI(2,1))
      CALL ERROR(SIGM,ER1,2.)
      SCTHE=CEXP(JAI*2.*THE)*ER1*EXP(-2.*(SIGM**2))/2.
C
C   CALCULATE THE AVERAGE OF COS(2.0*THETA) , SIN(2.*THETA)
C
```

```
      CTHE=REAL(SCTHE)
      CTHE=AIMAG(SCTHE)
      STHE=0.0
      CTHE=EXP(-2.*(SIGM**2))
      WRITE(6,777) CTHE
  777 FORMAT(1X,F15.5)
      IK=9
      DO 50 IJK=1,50
      RO=10.+145.*(IJK-1)/50.
      IK=IK+1
      DO 66 I=1,2
      DO 66 J=1,2
   66 F(I,J)=(0.0,0.0)
      DO 65 J=1,2
      AL=0.8*L
      R=RO*((RO/10.)**(-0.66))
      IF(J.EQ.2) AL=L*0.2
      IF(J.EQ.2) R=RO
      DO 65 I=1,5
      AMODE1=AMODE(I)+0.001
      AMODE2=AMODE(I+1)
      CALL COEF(FREQ,AMODE1,FV1,FH1,FSH1,DIFF1,LOKANG,R)
```

```
      CALL COEF(FREQ,AMODE2,FV2,FH2,FSH2,DIFF2,LOKANG,R)
      FV=FV2-FV1
      FH=FH2-FH1
      FSH=FSH2-FSH1
      DIFF=DIFF2-DIFF1
      F(1,1)=F(1,1)+(P1*FSH+P2*((FH+FV)/2.-DIFF
     C*CTHE/2.))*AL*NO
      F(2,2)=F(2,2)+(P1*FSH+P2*((FV+FH)/2.+DIFF
     C*CTHE/2.))*AL*NO
      F(1,2)=F(1,2)+(P2*DIFF )*AL*NO*STHE/2.
      F(2,1)=F(1,2)
   65 CONTINUE
      F(1,1)=2.*PI*F(1,1)/KO
      F(2,2)=2.*PI*F(2,2)/KO
      F(2,1)=2.*PI*F(2,1)/KO
      F(1,2)=F(2,1)
C
C   FIND THE EIGENVALUES AND EIGENVECTORS OF THEPROPAGATION


C   TENSOR F
C
```

```
      CALL EIGCC(F,2,2,1,EIGV,EIGVC,2,WK,IER1)
      DIAG(1,1)=CEXP(-JAI*EIGV(1))
C     DIAG(1,1)=1.-JAI*EIGV(1)
C     DIAG(2,2)=1.-JAI*EIGV(2)
      DIAG(2,2)=CEXP(-JAI*EIGV(2))
      DO 10 I=1,2
      DO 10 J=1,2
      IF(I.EQ.J) GO TO 10
      DIAG(I,J)=(0.0,0.0)
   10 CONTINUE
      DO 20 I=1,2
      DO 20 J=1,2
      UNIT(I,J)=(0.0,0.0)
      IF(I.EQ.J) UNIT(I,J)=(1.0,0.0)
   20 CONTINUE
      DO 30 I=1,2
      DO 30 J=1,2
   30 EGVC(I,J)=EIGVC(I,J)
C
C   FIND THE INVERSE OF THE MATRIX OF EIGENVECTORS
C   AND THEN CALCULATE EXP(F*L) * INCIDENT VECTOR FIELD
C
```

```
      CALL LEQT1C(EIGVC,2,2,UNIT,2,2,0,WA,IER)
      CALL MULT(EGVC,2,2,DIAG,2,MATR1)
      CALL MULT(MATR1,2,2,UNIT,2,MATR3)
      CALL MULT(MATR3,2,2,EI,1,EFIN)
      IF(IK.LT.10) GO TO 150
      WRITE(6,97)  RO,FREQ
   97 FORMAT(1X,/,'FOR RAIN RATE',F5.1,'MM /HR AND FREQUENCY',F5.1,
     C' GHZ THE UNDEPOLARIZED POLARIZATION DIRECTIONS ARE:')
      DO 55 J=1,2
      WRITE(6,96) (UNIT(I,J),I=1,2)
   96 FORMAT(1X,'(',F5.2,'+JA ',F5.2,') XO  +  (',F5.2,
     C'+JAI',F5.2,') YO')
   55 CONTINUE
      IK=0
  150 CONTINUE
      CALL OUTANT(EFIN(1,1),EFIN(2,1),EXC,EYC,EXX,EYX,ISOLDB,ATTDB
     C,PHAS)
      ISD(IJK)=ISOLDB
      ATTD(IJK)=ATTDB
      RATE(IJK)=RO
   50 CONTINUE
      CALL MAP
```

```
      WRITE(6,8) (ISD(J),ATTD(J),RATE(J),J=1,20)
    8 FORMAT(5X,3F10.3)
      GO TO 15
  999 FORMAT(3F5.2,F8.2,F12.3,F6.3)
   92 FORMAT(5X,'THE AVERAGE CANTING ANGLE:',F5.2,5X,
     C'THE STANDARD DEV. OF THE CANTING ANGLE:',F5.2,/,
     C5X, 'HE EFFECTIVE LENGTH',F8.2)
   93 FORMAT(1HO,15X,'THE VARAIBLESS OF THE RAIN CLOUD ARE'//)
   88 STOP


      END
C
C
      SUBROUTINE  MULT(A,N,M,B,M1,C)
C
C   THIS SUBROUTINE MULTIPLIES TWO COMPLEX MATRICES
C
      COMPLEX A(N,M),B(M,M1),C(N,M1),SUM
      DO 10 I=1,N
      DO 10 J=1,M1
```

```
      SUM=(0.0,0.0)
      DO 20 IJ=1,M
   20 SUM=SUM+A(I,IJ)*B(IJ,J)
   10 C(I,J)=SUM
      RETURN
      END
C
C
      SUBROUTINE ERROR(SIGM,ER,ALFA)
C
C   THIS SUBROUTINE CALCULATES THE ERROR FUNCTION OF
C   A COMPLEX VARIABLE AND IT USES THESE RESULTS TO
C   CALCULATE THE COMPLEX COEFFICIENTS OF THE AVERAGE
C   COS(ALFA* PHI) AND SIN(ALFA* PHI) WHERE PHI IS
C   A RANDOM VARIABLE WITH NORMAL DISTRIBUTION (0,SIGM)
C
      COMPLEX ER,JAI,Z1,Z2,Z,ZS,W1,W2,X3
      JAI=(0.0,1.0)
      Z1=3.3553-JAI*ALFA*SIGM/SQRT(2.)
      Z2=-3.3553-JAI*ALFA*SIGM/SQRT(2.)
      Z=JAI*Z1
      ZS=Z*Z
```

```
      W1=-Z1*((0.4613135/(ZS-0.1901635))+(0.09999216/(ZS-
     C1.7844927))+(0.002883894/(ZS-5.5253437)))
      W2=2.*CEXP(JAI*5.*ALFA*SIGM)
      X3=JAI*AIMAG(Z2*Z2)
      ER=W2*CEXP(-X3)-CONJG(W1)*CEXP(-Z2*Z2)-W1*CEXP(-Z1*Z1)
      RETURN
      END
C
C
      SUBROUTINE MAP
C
C   THIS SUBROUTINE PLOTS ATTENUATION AND
C   ISOLATION VERSUS RAIN RATE
C
      REAL ISD(52),RATE(52),ATTD(52)
      COMMON/VAR/ ISD,RATE,ATTD
      CALL PLOTS(0,0,50)
      CALL SCALE(RATE,8.0,50,1)
      CALL SCALE(ISD,6.0,50,1)
      CALL SCALE(ATTD,6.0,50,1)
      CALL PLOT(2.0,2.0,-3)
      CALL AXIS(0.0,0.0,9HRAIN RATE,-9,8.0,0.0,RATE(51),RATE(52))
```

```
      CALL AXIS(0.0,0.0,9HISOLATION,9,6.0,90.0,ISD(51),ISD(52))



      CALL LINE(RATE,ISD,50,1,0,0)
      CALL PLOT(0.0,0.0,+999)
      CALL PLOTS(0,0,50)
      CALL PLOT(2.0,2.0,-3)
      CALL AXIS(0.0,0.0,9HRAIN RATE,-9,8.0,0.0,RATE(51),RATE(52))
      CALL AXIS(0.0,0.0,11HATTENUATION,11,6.0,90.0,ATTD(51),ATTD(52))
      CALL LINE(RATE,ATTD,50,1,0,0)
      CALL PLOT(0.0,0.0,+999)
      RETURN
      END
C
C
      SUBROUTINE COEF(FREQ,AMODE,FV,FH,FSPH,DIFF,LOKANG,R)
C
C     THIS SUBROUTINE RETURNS TO THE CALLING PROGRAM THE SCATTERING
C     COEFFICIENTS FOR SPHERICAL AND OBLATE RAIN DROPS.
C     THE COEFFICIENTS ARE A FUNCTION OF FREQUENCY AND DROP SIZE
C     AND ELEVATION ANGLE.  THE COEFFICIENTS USED ARE THOSE OF UZUNOGLU,
C     EVANS AND HOLT. THIS IS A MODIFIED VERSION OF THE
```

```
C     SUBROUTINE DEVELOPED BY PRESINGER AND STUTZMAN.
C
      COMPLEX CMPLX
      REAL LOKANG
C
      COMPLEX FV,FH,FSPH,DIFF
      DOUBLE PRECISION U22,U33,U44,U55,AK1,AK2,AK3,AK4,AK5
      AK=-8.2*(R**(-0.21))
      AK1=EXP(AK*AMODE)/AK
C
      IF(AMODE.LT.0.25) AMODE=0.25
      IF(AMODE.LE.0.25) GO TO 100
      IF((INT(FREQ).EQ.11).AND.(AMODE.GT.3.5)) AMODE=3.5
      IF((INT(FREQ).EQ.14).AND.(AMODE.GT.3.5)) AMODE=3.5
      IF((INT(FREQ).EQ.20).AND.(AMODE.GT.3.0)) AMODE=3.0
      IF((INT(FREQ).EQ.30).AND.(AMODE.GT.3.0)) AMODE=3.0
      IF((INT(FREQ).EQ.20).AND.(AMODE.GT.3.0)) GO TO 100
      IF((INT(FREQ).EQ.30).AND.(AMODE.GT.3.0)) GO TO 100
C
      U11=AMODE
      U22=AMODE**2
      U33=AMODE**3
```

```
      U44=AMODE**4
      U55=AMODE**5
      AK2=AK**2
      AK3=AK**3
      AK4=AK**4
      AK5=AK**5
      U1=(U11-1./AK)
      U2=(U22-2.*U11/AK+2.0/AK2)
      U3=(U33-3.*U22/AK+6.*U11/AK2
     C-6.0/AK3)
      U4=(U44-4.*U33/AK+12.*U22/AK2-
     C24.*U11/AK3+24./AK4)
      U5=(U55-5.*U44/AK+20.*U33/AK2
     C-60.*U22/AK3+120.*U11/AK4-120./AK5)


      GO TO 101
  100 U1=AMODE
      U2=(AMODE**2)
      U3=(AMODE**3)
      U4=(AMODE**4)
```

```
      U5=(AMODE**5)
  101 CONTINUE
C
C
C
C     11.0 GHZ COEFFICIENTS
C
      IF(INT(FREQ).NE.11) GO TO 1
C
C     SPHERICAL DROP COEFFICIENTS
C
      IF(AMODE.GT.1.00) GO TO 10
C
      EOR=-0.0020548+0.01638947*U1-0.0417568*U2+0.08832213*U3
      EOI=-0.0025154+0.01928553*U1-0.0456816*U2+0.03655147*U3
      GO TO 11
   10 CONTINUE
C
      EOR=-1.28155706+2.83287718*U1-2.07399678*U2+0.60190887*U3
     1-0.00984194*U4-0.01096165*U5
      EOI=2.60278025-7.52434662*U1+8.14691632*U2-4.12133971*U3
     1+0.99089467*U4-0.08731788*U5
C
```

```
      GO TO 12
   11 CONTINUE
C
C     OBLATE DROP COEFFICIENTS
C
      EV90R=-0.001322+0.01036867*U1-0.025372*U2+0.07072533*U3
      EV90I=-0.0024306+0.01861967*U1-0.0440232*U2+0.03507413*U3
      EH90R=-0.0023684+0.01878307*U1-0.0473704*U2+0.09255573*U3
      EH90I=-0.0030366+0.02320527*U1-0.0546296*U2+0.04299093*U3
      DIFFR=-0.0010464+0.0084144*U1-0.0219984*U2+0.0218304*U3
      DIFFI=-0.000606+0.0045856*U1-0.0106064*U2+0.0079168*U3
C
      GO TO 1000
   12 CONTINUE
C
      EV90R=-0.3653892+0.32540943*U1+0.45280976*U2-0.53907398*U3
     1+0.20309215*U4-0.02432204*U5
      EV90I=2.20618555-6.19251766*U1+6.43873903*U2-3.090414*U3
     1+0.70600211*U4-0.0607173*U5
      EH90R=2.09022706-7.07345119*U1+9.03639726*U2-5.33156215*U3
     1+1.49716423*U4-0.15747063*U5
      EH90I=3.28654422-9.68217951*U1+10.71102231*U2-5.5491184*U3
```

```
     1+1.36694565*U4-0.12512466*U5
      DIFFI=1.08034369-3.48962081*U1+4.2722407*U2-2.45868344*U3
     1+0.66093861*U4-0.06440692*U5
C
      IF(AMODE.GT.2.0) GO TO 120
C
      DIFFR=-0.32599997+0.7531995*U1-0.57039996*U2+0.15039999*U3
      GO TO 1000
C
  120 CONTINUE
C
      DIFFR=11.94200847-14.59334299*U1+5.80600359*U2-0.7346671*U3
C
      GO TO 1000
C
    1 CONTINUE
C
C     14 GHZ COEFFICIENTS
C
```

```
      IF(INT(FREQ).NE.14) GO TO 2
C
C     SPHERICAL DROP COEFFECIENTS
C
      IF(AMODE.GT.1.00) GO TO 20
C
      EOR=-0.001376+0.012776*U1-0.040136*U2+0.128736*U3
      EOI=-0.008796+0.06731467*U1-0.1588*U2+0.12418133*U3
C
      GO TO 21
   20 CONTINUE
C
      EOR=-12.13707993+34.85683676*U1-37.84887378*U2+19.48995359*U3
     1-4.69149894*U4+0.42548477*U5
      EOI=-8.4550178+22.97909617*U1-23.38444001*U2+11.09553161*U3
     1-2.41694538*U4+0.19907664*U5
C
      GO TO 22
   21 CONTINUE
C
C     OBLATE DROP COEFFICIENTS
C
```

```
      EV90R=-0.000248+0.00335467*U1-0.013928*U2+0.10002133*U3
      EV90I=-0.008436+0.06455867*U1-0.152256*U2+0.11893333*U3
      EH90R=-0.000656+0.007656*U1-0.029656*U2+0.122656*U3
      EH90I=-0.010366+0.079154*U1-0.18596*U2+0.143872*U3
      DIFFR=-0.000408+0.00430133*U1-0.015728*U2+0.02263467*U3
      DIFFI=-0.00193+0.01459533*U1-0.033704*U2+0.02493867*U3
C
      GO TO 1000
   22 CONTINUE
C
      EV90R=-4.48493663+12.45481829*U1-12.90182271*U2+6.32901913*U3
     1-1.42805671*U4+0.11875301*U5
      EV90I=-0.1923376+0.3425132*U1-0.196242*U2+0.07468968*U3
C
      IF(AMODE.GT.2.5) GO TO 24
C
      EH90I=1.10278458-3.74696237*U1+4.48042001*U2-2.22964317*U3
     1+0.42010037*U4
      DIFFR=-0.15268404+0.39830845*U1-0.3527577*U2+0.11767014*U3
```

```
      DIFFI=-1.29960041+2.93303524*U1-2.15255009*U2+0.5206384*U3
C
      IF(AMODE.GT.2.00) GO TO 25
C
      EH90R=-1.02599992+2.30733317*U1-1.60799988*U2+0.4266664*U3
C
      GO TO 1000
   24 CONTINUE
C
      EH90I=2.51000033-2.03000022*U1+0.62000004*U2
      DIFFR=-15.85152202+18.27189723*U1-6.68140666*U2+0.79411153*U3
      DIFFI=22.32321586-44.48681458*U1+30.17926125*U2-8.46925565*U3
     1+0.85300427*U4
C
      GO TO 1000
   25 CONTINUE
C
      EH90R=-19.65+20.6567*U1-6.66*U2+0.6933*U3
C
      GO TO 1000
    2 CONTINUE
C
C     20 GHZ COEFFICIENTS
C
```

```
      IF(INT(FREQ).NE.20) GO TO 3
C
C     SPHERICAL DROP COEFFICIENTS
C
      IF(AMODE.GT.1.0) GO TO 30
C
      EOR=0.020295-0.145276*U1+0.297656*U2+0.008224*U3
C
      EOI=-0.015488+0.12709133*U1-0.334568*U2+0.30583467*U3
C
      GO TO 31
   30 CONTINUE
C
      EOR=3.35567152-8.61818659*U1+7.8157989*U2-2.68217917*U3
     1+0.3108073*U4
      EOI=1.85636463-3.70750898*U1+2.19599302*U2-0.25148145*U3
C
      GO TO 32
   31 CONTINUE
C
C     OBLATE COEFFICIENTS
C
```

```
      EV90R=0.02454800-0.17912133*U1+0.384448*U2-0.07447467*U3
      EV90I=-0.013492+0.11190533*U1-0.299032*U2+0.27853867*U3
      EH90R=0.02282-0.16596667*U1+0.34976*U2-0.03061333*U3
      EH90I=-0.015178+0.12623933*U1-0.33848*U2+0.31533867*U3
      DIFFR=0.000072+0.00175467*U1-0.015488*U2+0.03426133*U3
      DIFFI=-0.001686+0.014334*U1-0.039448*U2+0.0368*U3
C
      GO TO 1000
   32 CONTINUE


C
      EV90R=1.56037246-3.97019757*U1+3.66524972*U2-1.24458239*U3
     1+0.14526662*U4
      EV90I=4.77376463-13.63610787*U1+14.83397997*U2
     1-7.66136891*U3+1.96881573*U4-0.19749381*U5
      EH90R=4.63026679-11.97374109*U1+11.0254653*U2
     1-4.0050613*U3+0.50244373*U4
      EH90I=-1.5390057+6.3417866*U1-9.35328879*U2+6.20987895*U3
     1-1.74544867*U4+0.17820925*U5
      DIFFR=3.06989428-8.00354339*U1+7.36021547*U2
```

```
     1-2.76047886*U3+0.3571771*U4
      DIFFI=-6.31274803+19.97783334*U1-24.1872053*U2+13.8712166*U3
     1-3.71425705*U4+0.3757024*U5
C
      GO TO 1000
    3 CONTINUE
C
      IF(INT(FREQ).NE.30) GO TO 2000
C
C     30 GHZ COEFFICIENTS
C
C     SPHERICAL DROP COEFFICIENTS
C
      IF(AMODE.GT.1.0) GO TO 40
C
      EOR=0.028004-0.221564*U1+0.530744*U2+0.022816*U3
      EOI=-0.007072+0.09329866*U1-0.390112*U2+0.55688533*U3
C
      GO TO 41
   40 CONTINUE
C
      EOR=-1.95096901+3.4107597*U1-0.82790307*U2-0.39982485*U3
```

```
     1+0.1291964*U4
      EOI=5.77798866-16.3876166*U1+16.10102407*U2-6.06482662*U3
     1+0.82747918*U4
C
      GO TO 42
   41 CONTINUE
C
C     OBLATE DROP COEFFICIENTS
C
      EV90R=0.03542-0.2838733*U1+0.7038*U2-0.15834666*U3
      EV90I=0.013876-0.064756*U1-0.026904*U2+0.290784*U3
      EH90R=0.031652-0.252652*U1+0.614952*U2-0.049952*U3
      EH90I=-0.000532+0.04746533*U1-0.299512*U2+0.50957867*U3
      DIFFR=-0.003768+0.03122133*U1-0.088848*U2+0.10839467*U3
      DIFFI=-0.014408+0.11222133*U1-0.272608*U2+0.21879467*U3
C
      GO TO 1000
   42 CONTINUE
C
      EV90R=3.93161268-10.97208846*U1+11.43870068*U2
     1-4.78953064*U3+0.69447892*U4
      EV90I=3.12729055-9.08249632*U1+9.16246329*U2
```

```
     1-3.47227982*U3+0.47789632*U4



      EH90R=-6.97583584+16.79179963*U1-13.53607686*U2
     1+4.63811854*U3-0.57535653*U4
      EH90I=-1.39373246+1.72736066*U1-0.14076091*U2+0.05474057*U3
      DIFFR=-10.90744851+27.76388807*U1-24.97477753*U2
     1+9.42764918*U3-1.26983545*U4
      DIFFI=5.33984552-17.20920477*U1+20.7812541*U2
     1-11.64360435*U3+3.07942984*U4-0.30370378*U5
C
 1000 CONTINUE
C
      ALPH=1.576796-LOKANG
      CSLA=0.001*COS(ALPH)**2
      SNLA=0.001*SIN(ALPH)**2
      FVR=CSLA*EOR+SNLA*EV90R
      FVI=-CSLA*EOI-SNLA*EV90I
      FHR=CSLA*EOR+SNLA*EH90R
      FHI=-CSLA*EOI-SNLA*EH90I
      DIFFR=-SNLA*DIFFR
```

```
      DIFFI=SNLA*DIFFI
      EOR=0.001*EOR
      EOI=-0.001*EOI
C
      FV=CMPLX(FVR,FVI)*AK1
      FH=CMPLX(FHR,FHI)*AK1
      FSPH=CMPLX(EOR,EOI)*AK1
      DIFF=CMPLX(DIFFR,DIFFI)*AK1
C
      GO TO 3000
C
 2000 WRITE(6,2001)
 2001 FORMAT(//,3X,'FREQUENCY NOT ALLOWED, ONLY 11,14,20,30 GHZ ALLOWED'
     1)
C
      STOP
 3000 CONTINUE
C
      RETURN
      END
C
C
```

```
      SUBROUTINE OUTANT(EXN,EYN,EXC,EYC,EXX,EYX,ISOL1,ATTEN1,PHASE1)
C
C     THIS SUBROUTINE TAKES THE X AND Y COMPONENTS OF THE WAVE EXITING
C     THE RAIN CELL (EXN,EYN) AND USES THE COMPLEX VECTOR METHOD
C     TO COMPUTE VALUES FOR ATTENUATION, ISOLATION, AND PHASE AS A
C     RESULT OF THE RAIN MEDIUM AND POLARIZATION MISMATCH EFFECTS OF THE
C     RECEIVE ANTENNA
C     THIS DATA IS STORED IN PROGRAM MEMORY FOR LATER OUTPUT
C     THIS SUBROUTINE WAS WRITTEN BY PRESINGER.
C
      REAL ISOL1
      COMMON/BLOC1/MINUSJ,CONV
      COMMON/BLOC2/ VWACM
      COMPLEX MINUSJ
      COMPLEX  EXC,EYC,EXX,EYX


      COMPLEX  VWPAC,VWPAX
      COMPLEX  EXN,EYN
      REAL  VWPACM,VWPAXM
C
```

```
      VWPAC=EXN*EXC + EYN*EYC
      VWPAX=EXN*EXX + EYN*EYX
C
C
      VWPACR=REAL(VWPAC)
      VWPACI=AIMAG(VWPAC)
      VWPACM=CABS(VWPAC)
      VWPACR=ATAN2(VWPACI,VWPACR)
      VWPACP=VWPACR/CONV
C
      VWPAXR=REAL(VWPAX)
      VWPAXI=AIMAG(VWPAX)
      VWPAXM=CABS(VWPAX)
      IF(VWPAXM.EQ.0.0) GO TO 10
      VWPAXR=ATAN2(VWPAXI,VWPAXR)
      VWPAXP=VWPAXR/CONV
      IF(VWPAXM.LE.0.000001) VWPAXP=0.0
C
      ISOL1=20.*ALOG10(VWPACM/VWPAXM)
      GO TO 11
   10 CONTINUE
      VWPAXP=0.0
```

```
      ISOL1=999.99
   11 CONTINUE
C
      PHASE1=VWPAXP-VWPACP
C
      IF(PHASE1.LT.0.0) PHASE1=PHASE1+360.0
C
      ATTEN1=20.*ALOG10(VWACM/VWPACM)
C
      RETURN
      END
C
C
      SUBROUTINE COMPNT(EPS,TAU,EX,EY)
C
C     THIS SUBROUTINE RETURNS THE X AND Y COMPONENTS GIVEN AN EPSILON
C     AND TAU (IN DEGREES) DESCRIBING AN ARBITRARY POLARIZATION STATE
C
      COMPLEX  EX,EY
      COMPLEX MINUSJ
      COMMON/BLOC1/MINUSJ,CONV
C
```

```
      EPSR=EPS*CONV
      TAUR=TAU*CONV
C
      IF(ABS(EPSR).EQ.(45.*CONV)) GO TO 1
      IF(EPSR.EQ.0.) GO TO 2
      IF(TAUR.EQ.0.) GO TO 3
      IF(TAUR.EQ.(90.*CONV)) GO TO 4


C
      T1=TAN(2.*EPSR)
      T2=SIN(2.*TAUR)
      DELTR=ATAN2(T1,T2)
      GAMR=0.5*ARCOS(COS(2*EPSR)*COS(2*TAUR))
      GO TO 100
    1 DELTR=2.*EPSR
      GAMR=45.*CONV
      GO TO 100
    2 DELTR=0.
      GAMR=TAUR
      GO TO 100
```

```
    3 DELTR=SIGN(1.,EPSR)*90.*CONV
      GAMR=ABS(EPSR)
      GO TO 100
    4 DELTR=SIGN(1.,EPSR)*90.*CONV
      GAMR=90.*CONV-ABS(EPSR)
  100 CONTINUE
C
      EX=COS(GAMR)
      EY=SIN(GAMR)*CEXP(-MINUSJ*DELTR)
C
      RETURN
      END
```